Abstract

Title of Ph.D. Dissertation: NEAR QUANTUM LIMITED MEASUREMENT IN NANOELECTROMECHANICAL SYSTEMS

Akshay Naik

Research directed by: Prof. Keith Schwab

Nanoelectromechanical systems have many potential applications in nanoelectronics as well as in fundamental studies of quantum mechanics in mesoscopic systems. Nanoelectromechanical systems have been touted as an extension of microelectromechanical systems which would operate at higher frequencies and consume far less power due their higher quality factors. Since these systems can be cooled close to their ground states with existing cryogenic techniques, they are useful tools to study the quantum effects like backaction, coherent states and superposition in mesoscopic mechanical systems. Also there have been proposals to use these systems as qubits and buses in quantum computing.

In this thesis I discuss the effects of the backaction of a superconducting single electron transistor that measures the position of a radio frequency nanomechanical resonator. One of the novel effects of this backaction is the cooling of the nanomechanical resonator. The fact that a system can be cooled by merely coupling it to noisy non-equilibrium device is a counterintuitive phenomenon. Although backaction effects have been used to produce ultra-cold atoms, our results are the first

demonstration of this cooling effect in a mesoscopic system. For a linear continuous position detection scheme, quantum mechanics places a lower limit on the product of position shot noise, S_x, and the backaction force noise, S_F, which is given by,

$$\sqrt{S_x S_F} \geq \frac{\hbar}{2}$$

As part of this work we demonstrate that our detection scheme is only 15 times away from this limit and only 4 times away from quantum limit for position sensitivity.

NEAR QUANTUM LIMITED MEASUREMENT IN NANOELECTROMECHANICAL SYSTEMS

by

Akshay Naik

Dissertation submitted to the Faculty of the Graduate School of the
University of Maryland, College Park in partial fulfillment
of the requirements for the degree of
Doctor of Philosophy
2006

Advisory Committee:
Professor Raymond Phaneuf, Advisor
Professor Keith Schwab, Advisor
Professor Julius Goldhar
Professor P. S. Krishnaprasad
Professor J. R. Anderson

© Copyright by

Akshay Naik

2006

DEDICATION

To my family ..

ACKNOWLEDGMENTS

This thesis was as much my effort as it was due to sacrifices and support of my family. I would like to thank my parents for their support and encouragement in everything that I pursued. They have put our education above everything else. This thesis is the result of their love and blessings. My wife has been the source of encouragement through out my Ph.D. and has taken everything in her stride with a smile on her face. She has been a calming influence during all these years. I cannot thank her enough for everything she has done and endured during these years to make things easier for me. I would also like to thank my brothers, Ashwin and Aditya, for their encouragement and support.

I would not have completed the Ph.D. had it not been for encouragement and sound advice of my advisor, Prof. Keith Schwab. He has given a lot of freedom and very insightful advice during the course of this work. I would like to thank him for everything that I have learned from him from research to life in general.

I would like to thank Prof. Phaneuf for accepting the responsibilities of the dissertation chair and his willingness to discuss my research. I would also like to thank Prof. Goldhar, Prof. Krishnaprasad and Prof. Anderson for being on my committee and discuss my research time and again.

I would like to thank Dr. Olivier Buu for his invaluable contribution to this research. His knowledge about the low temperature physics and the research has

made this research possible. I would also like to thank Dr. Clerk, Dr. Armour and Dr. Blencowe for their insights into the theoretical analysis of the research. I would like to thank Dr. Carlos Sanchez for teaching me everything from fabrication to low temperature measurements. I would like to thank Dr. Benjamin Palmer for helpful advice about research. He has been very supportive during some very tough times during my Ph.D. I would like to thank Benedetta Camarotta for helping us during our measurements and giving us advice about making samples. I would like to thank Jared Hertzberg for some very good advice about making devices close to each other and also reading through my thesis and suggesting corrections. I would like to thank Dr. Matt LaHaye for giving insights into making samples and helping with the measurements. I would like to thank my lab mates Harish, Patrick and Emrah for useful conversation about measurements, results and life in general. I would also like to thank other QC labmates for their useful advice and conversation over the years.

I would like to thank Dr. Bruce Kane, Dr. Barry Barker and Dr. Marc Manheimer for providing an excellent environment for doing research and all the support over the years. I would like to thank Les Lorentz for his willingness to machine pieces for us at short notices. If it were not for him we would be a few years behind schedule. I would also like to thank J.B, George and Pete for their help in machining parts for us. I would like to thank Butch for bringing helium and letting me order helium a few times even after the deadline.

I would like to thank my friends Ayesh, Jita, Karthik, Kapil, Mani, Rakesh, Ragu and Vishnu for their friendship and support over the years. Life would have

been dull without you!

TABLE OF CONTENTS

List of Tables x

List of Figures xi

List of Symbols xvi

1 Introduction 1

1.1 Motivation 1

1.2 Quantum Effects in Devices 3

1.3 Thesis 4

2 Fabrication 6

2.1 Photolithography for Bond Pads and Tank Circuit 6

2.2 SSET and the Mask for NR 10

2.3 Etching Free the Nanomechanical Resonator 17

3 Measurement Scheme 21

3.1 Single Electron Transistor and Principle of Operation 21

3.2 Nanomechanical resonator 28

3.3 Position Detection of NR using SSET 30

3.4 Radio Frequency Single Electron Transistor 32

4 Position Sensitivity and Backaction 34

4.1 Forward Coupled Noise 36

4.1.1 Shot Noise 36

4.1.2 Noise floor of amplifier 37

4.2 Backaction 38

4.2.1 Linear response theory 39

4.3 Position Sensitivity 48

5 Methods 51

5.1 Resonator Characterization 51

5.1.1 Frequency and the quality factor 51

5.1.2 Spring constant 55

5.2 SET Parameter Characterization 59

5.2.1 Capacitance of the device 60

5.2.2 Charging energy of the SSET 62

5.2.3 Superconducting gap of the SSET 64

5.2.4 Resistance of the SSET 64

5.2.5 Estimates of Josephson energy of the junctions 64

5.3 Characterize RFSET 66

5.3.1 Center frequency and bandwidth 66

5.3.2 Gain and noise temperature 66

5.3.3 Reference signal calibration 70

5.3.4 Sensitivity 73

5.4 Method for Backaction Measurement 75

5.4.1 Measuring spectra for the backaction 76

5.5 Optimizing the RFSET for backaction measurements 80

6 Results and Future Work 81

6.1 Effects of the intrinsic bath 81

6.1.1 Frequency 81

6.1.2 Damping 84

6.1.3 Temperature of the resonator 85

6.2 Effect of coupling the NR to SSET 86

6.2.1 Effect on the resonant frequency 87

6.2.2 Effect on the damping of the resonator 89

6.2.3 Effect on the temperature of the resonator 91

6.3 Effect of Changing the SSET Bias Point 93

6.3.1 Effect on resonant frequency 96

6.3.2 Effect on the damping of the NR 96

6.3.3 Effect on the Temperature of the NR 101

6.4 Backaction Effects near DJQP 103

6.5 Effect of NR motion on the SSET 104

6.6 Limits of our device 108

6.7 Conclusion 111

6.8 Future Work 111

A Theoretical Calculations 113

B Femlab Calculations 120

Bibliography 122

LIST OF TABLES

2.1 Dose levels for SSET and NR fabrication 12

2.2 Dimension of various parts of the device design pattern 15

5.1 Capacitance values of the device 63

LIST OF FIGURES

2.1 Design pattern of each die. Each die has multiple bond pads, which are used to make wire bond connections to the outside electronics, and two tank circuits for making two RFSETs. The dimension of each die is about 4mm $\times$ 4mm The magnified image of the area around the tank circuit is shown in fig 2.2. 7

2.2 Design pattern of tank circuit and SEM writing area.The SEM writing area is about $100\mu m \times 100\mu m$ and is used to make the SSET and the NR using a e-beam lithography. 8

2.3 Design pattern of electron beam lithography. The outer cross marks are at the vertices of a $80\mu m \times 80\mu m$ square. The electron beam dose for various structures is given in table 2.1 13

2.4 Close up of the design pattern for electron beam writing showing the SSET and the NR. The dimensions of the device parts are given in table 2.2 14

2.5 Schematics of second layer of lithography 16

2.6 Schematics of third layer of lithography 18

2.7 Colorised SEM photo of the sample 19

3.1 Schematic of SET and the heuristic arguments for conduction mechanism. The energy levels of the island are separated by $2E_C$. For $eV_{DS} < 2E_C$, gate voltage can be adjusted such that energy levels of island either allow or impede the tunneling of electrons through the SET. 22

3.2 Current through SET as a function of V_{DS} and V_G. 24

3.3 $I - V_{DS} - V_G$ map of SET 25

3.4 $I - V_{DS} - V_G$ map of SSET. The asymmetry in the $I - V_{DS} - V_G$ map is due to the asymmetric junctions of the SSET. 27

3.5 Schematics of a doubly clamped beam 28

3.6 Simplified schematics of measurement using RFSET 32

4.1 Schematics of DJQP process 47

4.2 Schematics of JQP process 47

4.3 Position resolution of the device as a function of coupling voltage . . 50

5.1 Circuit diagram for magnetomotive measurement 52

5.2 Amplitude (red line) and phase (black line) of the resonator as a function of frequency of current through the NR at a magnetic field of 6T 53

5.3 Quality factor of the resonator as a function of the magnetic field . . 55

5.4 Simplified circuit diagram to drive the beam and measure its response 57

5.5 Response of the resonator as a function of drive frequency 59

5.6 Current modulation of the SSET as a function of the SSET gate voltage 60

5.7 Current modulation of the SSET as a function of the NR gate voltage 61

5.8 Current modulation of the SSET as a function of the NR voltage . . 62

5.9 Current map of the SSET as a function of drain source voltage and gate voltage 63

5.10 Plot of drain source current against the drain source voltage. The slope of the plot at V_{DS} much larger than the 4Δ gives the value of $1/R_{\Sigma}$. 65

5.11 Simplified circuit for measuring frequency, bandwidth, gain and noise temperature of the measurement system 67

5.12 Plot of noise spectra with zero current and $0.2\mu A$ through the SSET. 68

5.13 Plot of noise spectra shot noise of the RFSET 69

5.14 Plot of noise as a function of current through the RFSET 70

5.15 Typical coulomb blockade that is suitable for reference signal calibration 71

5.16 Circuit diagram for Bessel function calibration of the gate charge signal figure7. 72

5.17 Plot of output amplitude as a function of RMS amplitude at the source. The red lines shows the Bessel fit to the data 73

5.18 Simplified circuit to measure the charge sensitivity of the RFSET . . 74

5.19 Circuit diagram for measuring the spectra 77

5.20 Mechanical noise spectrum and the Lorentzian fitting 79

5.21 Amplitude of the microwave for optimal working of RFSET and for measuring backaction 80

6.1 $I - V_{DS} - V_G$ map showing the bias point for evaluating the effect of coupling between the SSET and NR. Point 1 is near one of the JQP resonance and 2 and 3 are near DJQP 82

6.2 Plot of the resonant frequency as a function of bath temperature with SSET biased at different points at a coupling voltage, $V_{NR} = 1V$ . . . 83

6.3 Intrinsic frequency of the resonator 84

6.4 Intrinsic damping of the resonator 85

6.5 Power of the resonator 86

6.6 Plot of resonant frequency of the resonator as a function of the coupling voltage 88

6.7 Expected damping of the SSET as a function of the coupling voltage 90

6.8 Damping of the NR as a function of the coupling voltage. Note that damping due to the bath has temperature dependence and we have shown just one of those γ_{Bath} lines for clarity 91

6.9 Temperature of the resonator as function of bath temperature for different couplings 92

6.10 The measured value and theoretical prediction for the current as we sweep across the two JQP peaks 94

6.11 The measured value and theoretical prediction for the frequency shift as we sweep across the two JQP peaks 95

6.12 Plot of current as a function of gate voltage showing regions of positive and negative damping 98

6.13 The measured value and theoretical prediction for the damping of the resonator as we sweep across the two JQP peaks 99

6.14 The measured value and theoretical prediction for the absolute value of damping of the resonator as we sweep across the two JQP peaks . 100

6.15 The measured value and theoretical prediction for the temperature of the resonator as we sweep across the two JQP peaks 101

6.16 The measured value and theoretical prediction for the absolute value of temperature of the resonator as we sweep across the two JQP peaks 102

6.17 Backaction effects on NR with SSET biased near DJQP resonance . . 105

6.18 Distortion of the IV curve near JQP resonance due to coupling to the NR 106

6.19 Distortion of the IV curve near DJQP resonance due to coupling to the NR 107

6.20 Position resolution of the device as a function of the coupling voltage 110

LIST OF SYMBOLS

Symbol	Definition
Al	Aluminum
Au	Gold
B	Magnitude of the magnetic field
C_{Ji}	Individual SET junction capacitances
C_{GB}	Capacitance between the NR and the NR gate
C_{GNR}	Capacitance between the gate of the NR and the SET island
C_G	Capacitance between the SSET island and the SSET gate
C_{NR}	Capacitance of resonator to SET island
CHF_3	Triflouromethane
C_{Tank}	Tank circuit capacitance
C_Σ	Total SET island capacitance
$\delta_A$and δ_B	detuning energies of the two cooper pair resonances of DJQP
Δ	superconducting gap energy of SET leads and islands
Δf	Bandwidth of the measurement circuit
Δx	Uncertainty in position
Δp	Uncertainty in momentum

Symbol	Definition
d	Spatial separation between SET island and the NR
d_{GB}	Spatial separation between NR gate and NR
DJQP	Double Josephson Quasiparticle Resonance
DI	Deionized water
e	magnitude of electron charge
E	Young's Modulus of resonator
E_C	Charging energy of SET
E_J	Josephson energy of SET junctions
f_{avg}	Average backaction force
δf_0	Fluctuations in the equilibrium force
δf_{avg}	Fluctuations in the backaction force
ΔF	Backaction force due to detector
$\bar{F}_L$	Lorentz force
Γ_a and Γ_b	Tunneling rate of quasiparticles through the SET
γ_{NR}	Total damping of the resonator
γ_{Bath}	Intrinsic damping of the resonator
γ_{SSET}	Damping due to the SSET
G	Gain of measurement circuit including pre-amplifiers and loss
$\hbar$	Planck's constant divided by 2π

Symbol	Definition
h	Planck's constant
HF	Hydrogen Fluoride
HDMS	Hexamethyldisilazane
I	Bending Moment of inertia of the resonator
I_{DS}	SET drain source current
I_{RF}	RF current through the resonator
IPA	IsoPropyl Alcohol
JQP	Josephson Quasiparticle Resonance
k	Spring constant of resonator
k_B	Boltzmann's constant
λ	Gain of the detector
L	Length of NR
LIGO	Laser Interferometer Gravitational-Wave Observatory
L_{Tank}	Inductance of the tank circuit of the RFSET
m	Geometric mass of the resonator
m_{eff}	Effective mass of resonator with respect to mid-point motion for the fundamental mode
MIBK	MethylIsoButyl Ketone
MMA	Methyl Methacrylate
η	Fano factor

Symbol	Definition
NR	Nanomechanical resonator
N_{th}	Thermal occupation number of resonator's fundamental mode
OPD4262	Tetramethyl ammonium hydroxide
PMMA	Poly-Methyl Methacrylate
q	charge on the island of the SSET
q_G	Polarization charge on SET gate electrode
Δq_G	Charge modulation on SET gate
Q_0	Quality factor of the resonator
Q_L	Effective quality factor of the NR due to intrinsic dissipation and due to the loading of the magnetomotive measurement circuit
Q_{NR}	Effective quality factor of the NR
$RFSET$	Radio Frequency Single-Electron Transistor
ρ	Mass density of resonator
R_i	Individual SET junction resistances
R_Q	Resistance quantum
R_m	Electromechanical resistance
RPM	Revolutions per minute
R_Σ	Total resistance of SET junctions at large V_{DS}
SEM	Scanning Electron Microscope
SET	Single-Electron Transistor

Symbol	Definition
SSET	Superconducting Single-Electron Transistor
SF_6	Sulfur Hexafluoride
S_F	Symmetrized back action force noise spectral density of linear detector
S_x^{BA}	Back action contribution to the symmetrized spectral displacement sensitivity
S_I	Symmetrized current spectral noise density of SSET due to shot noise
S_x^{th}	Spectral density of displacement due to thermal motion
S_x	Shot noise contribution to the symmetrized spectral displacement sensitivity
S_q	Spectral density of charge noise
S_{xtotal}	Total spectral displacement sensitivity
τ	Coherence time
T	Temperature of the fridge
t	Thickness of resonator
T_{Bath}	Temperature of the thermal bath i.e. the dilution refrigerator
T_{eff}	Effective temperature of the detector
T_{NR}	Total effective temperature of the resonator due to contact to thermal bath and the detector
T_n	Noise temperature contribution of measurement circuit including pre-amplifier and circuit loss

Symbol	Definition
T_{SSET}	Effective temperature of the SSET
V_G	Gate voltage of the SSET
V_{NR}	Bias voltage on the resonator i.e. the coupling voltage
V_{DS}	SET drain-source bias
w	Width of resonator
ω	Frequency in rad/s
ω_{NR}	Resonator's fundamental mode frequency in rad/s
ω_T	Resonant Frequency of tank circuit in rad/s
Z_{ext}	Electromechanical impedance for magnetomotive detection circuit

Chapter 1

Introduction

As the size of electronic devices shrink, their quantum properties become increasingly important. It is important to understand the quantum properties of these devices to make the next generation of devices. Also, as we try to detect ever smaller quantities with extremely sensitive detectors; it is natural to ask what are the limitations posed by quantum mechanics? How is the process of measurement affecting the device itself? These answers are important in wide ranging fields from quantum computing to ultra sensitive force microscopy.

As part of my doctoral thesis work, I have tried to explore some of these avenues and some other interesting features that these effects give rise to.

1.1 Motivation

Nanoelectromechanical systems have received a lot attention in recent years in various fields from quantum computing to sensors. We list here a few interesting ones and discuss how this work might be relevant to these fields.

1. Quantum computing: Quantum computing would require measurements of qubits using quantum limited detectors. Also to fully control the system a complete knowledge of how the detector is influencing the qubit is important.

2. Quantum limited measurements : A whole range of measurements require using quantum limited detectors. It is important to be able to separate the

intrinsic effects of the device from the effects of the measurement itself. In LIGO(Laser Interferometer Gravitational Wave Observatory) [1] for instance the researchers are looking for gravitational waves using km long Fabry Perot interferometers.

3. Cooling of the device : As we'll show later, an important by product of back-action is the effect of cooling. By coupling a device to a noisy detector it is possible to cool (and heat) the device just by changing the bias conditions of the detector. It might be possible to use this cooling to produce ultra cold states of a sufficiently isolated resonator.

4. Ultra-sensitive force microscopy [2] where the cantilevers are used to detect the spins by looking at the change in frequency of the cantilever because of the magnetic forces. This technique has the potential of forming 3D images using the nuclear spin of the material. The work of this thesis might indicate how sensitive we can make these kinds of measurements and whether it is possible to get squeezed states which might be useful in doing such measurements.

5. Ultra low mass detection : The nanomechanical resonators have a very small mass. Any additional mass that is attached to the resonator alters the resonant frequency of the resonator. The quality factor of tens of thousands in these devices makes detecting even small changes in frequency possible. Devices with mass sensitivities of an attogram[3]and zeptogram[4] have recently been shown . With improvements in external amplifier noise properties, it is predicted that these nanomechanical devices would be able to reach sensitivities of a single

Dalton [5].

6. With resonant frequencies in the range of microwaves and high Q, these resonators can be used as highly selective filters. Since these devices have low dissipation, the devices made out a nanomechanical resonators would result in power dissipation which is orders of magnitude smaller than conventional electronic devices [6].

7. There have also been proposals about using these mechanical structures as qubits [7],[8] and as a data buses [9], [10] for quantum computing.

8. With resonant frequencies reaching GHz range, these devices can be cooled down to their ground state using dilution refrigerators, where the quantum behavior in mesoscopic mechanical devices can be studied.

1.2 Quantum Effects in Devices

As the sizes of electronic devices have decreased over the years, it has become clear that quantum effects would become important as we try to squeeze ever smaller devices into small places. These effects would dramatically change the way we have used the properties of the electronic devices. Even though quantum effects are an immediate hindrance to reducing the size of the devices, they present us an opportunity to explore the possibilities of using the quantum effects in devices to our advantage. Even as it closes a few doors, it opens up a lot of interesting academic and technological avenues. Using the quantum effects to our advantage would help

us make devices that are "in tune" with nature at the most fundamental levels. This is an interesting study where improvements in technology are pushing the boundary of basic science and this in turn is opening up new opportunities in technology.

Quantum information processing is one such field that seems to attract a lot of attention. Although this field is still in its infancy and is not quite clear whether we can build "quantum computers", quantum information processing does hold a lot of promise in solving the problems which "classical" computers would find daunting. It uses the "strange" quantum property of a bit being both 1 and 0 at the same time to improve the computational power. There has been a lot of theoretical work into the kinds of problems that such a computer could solve from factorizing large numbers[11] to searching[12]. On the experimental front the best that such a computer has achieved is factoring 15 into 5 and 3! [13]

1.3 Thesis

To study the nanoelectromechanical systems, we have used a device consisting of a superconducting single electron transistor (SSET) coupled to mechanical beam of submicron dimension and clamped at the two ends.

As part of my doctoral research work, the emphasis has been to determine the effects of backaction of a superconducting single electron transistor when it measures the position of a nanomechanical resonator. The superconducting single electron transistor has been touted as a near quantum limited detector[14]. LaHaye et. al [15] were able to reach a position noise level about 5 times away from the

quantum limit when continously monitoring the position of the nanomechanical resonator with a RFSET. Because of insufficient coupling between the resonator and the SSET, the position resolution in that measurement was limited to a regime where the effect of shot noise dominates. In this work we show a device which is strongly coupled and we are able to demonstrate the effects of the measurement backaction of the SSET on the resonator.

The structure of the thesis is as follows

Chapter 2 explains the details of the fabrication steps involved in the making of the device.

Chapter 3 explains the details of our measurement scheme. It briefly explains the RFSET technique that we use to detect the motion of the resonator.

Chapter 4 discusses the limits to the position sensitivity and the effects of the backaction of the SSET. We start out by discussing what the fundamental limits are for the continuous position detection scheme that we are using and discuss the origin of these effects. We then discuss how the backaction effects play a role into these limits. We then describe the effects of backaction that we should be able to see in our measurements.

Chapter 5 describes the methods we use to characterize our devices and do the backaction measurements.

Chapter 6 discusses the results and future directions that might be worth pursuing.

Chapter 2

Fabrication

The sample consists of a nanomechanical resonator(NR) coupled to a radio frequency single electron transistor (RFSET). The sample is fabricated on a Silicon substrate coated with 50nm of low stress Silicon Nitride (Si_3N_4). The sample is prepared in three distinct lithography steps.

2.1 Photolithography for Bond Pads and Tank Circuit

The tank circuit for RFSET and the bond pads was done commercially at MEMS Exchange. Figure 2.1 shows a single die pattern that is formed in this step. Each wafer has an array of these dies. The process involved

- **Deposit 500A^0 of low stress Silicon Nitride**: The wafer is cleaned using Piranha and then by 10:1 HF(hydrogen fluoride) dip. It is then deposited with 500A^0 of low stress Silicon Nitride layer using low pressure chemical vapor deposition.

- **Photolithography for bond pads, capacitor and inductor**: The wafer is then coated with HMDS(Hexamethyldisilazane) primer and Arch OiR 620-7i and soft baked to remove all the solvents. It is then exposed using a 5x stepper and the mask. It is then post baked and the resist is developed.

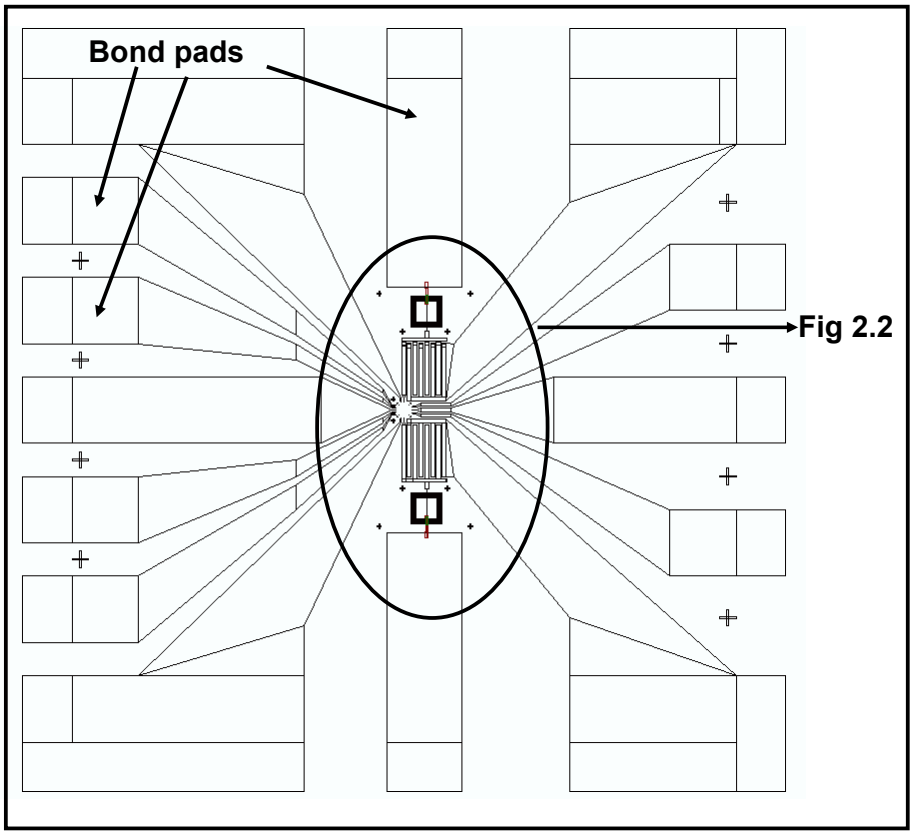

Figure 2.1: Design pattern of each die. Each die has multiple bond pads, which are used to make wire bond connections to the outside electronics, and two tank circuits for making two RFSETs. The dimension of each die is about 4mm × 4mm The magnified image of the area around the tank circuit is shown in fig 2.2.

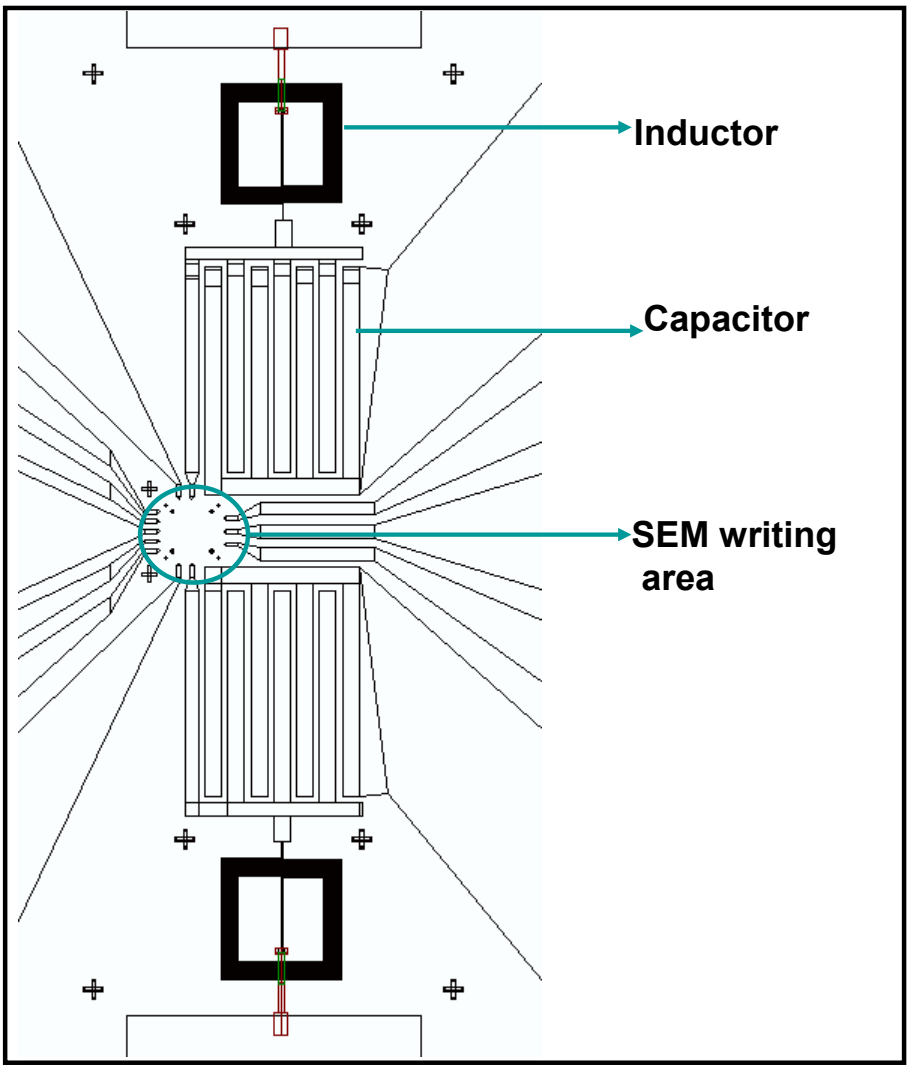

Figure 2.2: Design pattern of tank circuit and SEM writing area.The SEM writing area is about $100\mu m \times 100\mu m$ and is used to make the SSET and the NR using a e-beam lithography.

- **Silicon Nitride etch**: The exposed silicon nitride is then etched, so that the silicon underneath is exposed. This is done to ensure the metalization on silicon instead of on silicon nitride

- **Metalization**: The wafers are then coated with $500A^0$ of Aluminum, $200A^0$ of Titanium and $200A^0$ of gold. The thickness of the evaporated material is monitored using a quartz crystal monitor. The aluminum layer in the step insures that the inductor and the capacitor made in this step become superconducting at low temperatures. The gold layer is required to facilitate the wire bonding of the device to external circuitry. The titanium layer between the aluminum and gold prevents gold from diffusing into aluminum and destroying the superconductivity of aluminum.

- **Liftoff**: The wafers are then dipped into the acetone to liftoff the resist.

- **Photolithography for silicon oxide bridge on inductor lines**: The wafers are coated with HMDS and Arch OiR 620-7i and soft baked. They are then aligned and exposed using a 5x stepper. They are then post baked and the resist is developed.

- **Evaporation**: Silicon oxide is then evaporated using an electron-beam evaporator. The thickness of the silicon oxide is $2200\mathrm{A}^0$. This layer acts as an insulator for a crossover link from inductor to the bond pad.

- **Liftoff**: The wafers are then dipped in acetone to strip off the resist.

- **Photolithography for cross-over link**: The wafers are coated with HMDS primer and Arch OiR 620-7i and soft baked. Each wafer is then aligned and exposed using a 5x stepper. The wafers are then post baked and the resist is developed.

- **Evaporation**: The crossover link is then completed by evaporating 3300A^0 aluminum using electron-beam evaporator. This connects the innermost inductor turn to the bond pad.

- **Liftoff**: The resist is then stripped off using acetone.

- **Dicing**: The wafers are then coated with photoresist and diced into individual dies. The photoresist in this case is required to avoid silicon dust, due to dicing, from settling onto the device writing area.

These individual dies are used to make the RFSET and the nanomechanical resonator.

2.2 SSET and the Mask for NR

The second stage of lithography involves making superconducting single electron transistor(SSET) and the etch mask for the nanomechanical resonator(NR). The SSET is made using the double angle evaporation technique [23].

- The individual dies are cleaned by placing them in hot acetone to remove the leftover photoresist.

- The die is then coated with copolymer 8.5MMA(8.5% methacrylic acid mixed with PMMA(Poly methyl methacrylate)) EL (1:1) at 4000RPM for 1 minute. It is then baked on hot plate at 180^0C for 5 minutes. It is then spun coated with 950K PMMA A-4 (4% solution of PMMA in anisole) at 5000RPM for 1 minute. The chip is then baked on the hotplate at 180^0C for 5 minutes. The chip is then coated with a thin (50-100 A^0) layer of thermally evaporated Al to prevent charging up of the sample during electron beam lithography.

- The first layer of design pattern shown in figure 2.3 and 2.4 is then written using scanning electron microscope to make the superconducting single electron transistor and the etch mask for the NR. The dose levels used to write the pattern are given in table 2.1. The structures in black are from previous photolithography steps and are used here only for alignment purposes.

- The chip is rinsed in OPD 4262(tetramethylammonium hydroxide) for 1 minute to remove the Al anti charging layer. It is then rinsed in DI(deionized water) for 30 seconds and blown dry. The sample is then developed in MIBK:IPA(Methyl Iso Butyl Ketone:IsoPropyl Alcohol) (1:3) for 1 minute followed by rinsing in IPA and is then blown dry.

- The sample is then cleaned with oxygen plasma (50mW and 175mTorr) in reactive ion etching for 12 seconds.

- The sample is then loaded into a thermal evaporator. The sample is placed at an angle of 10^0 with respect to the source and 300A^0 of aluminum is evap-

orated at $5A^0$/sec. The chamber is then filled with dry oxygen to a pressure of 150mTorr for two minute. This procedure produces about $10A^0$ thick aluminum oxide layer which acts as barrier layer of the SET. The oxygen is then pumped out and the sample is placed at an angle of -10^0 and $600A^0$ of Al is evaporated at $6A^0$/sec.

- The sample is then soaked in hot acetone for 20 minutes to liftoff the resist.

The schematics for this step is shown in figure 2.5.

Device part	Design color	Dose
SET island area	Light Blue	350 μC/cm^2
SET leads	Blue	1.4nC/cm
Beam etch mask	Light Blue	350μC/cm^2
Undercut for SET	Green	160μC/cm^2
Lines to bond pads	Red	450μC/cm^2
Etch Area	Orange	400μC/cm^2

Table 2.1: Dose levels for SSET and NR fabrication

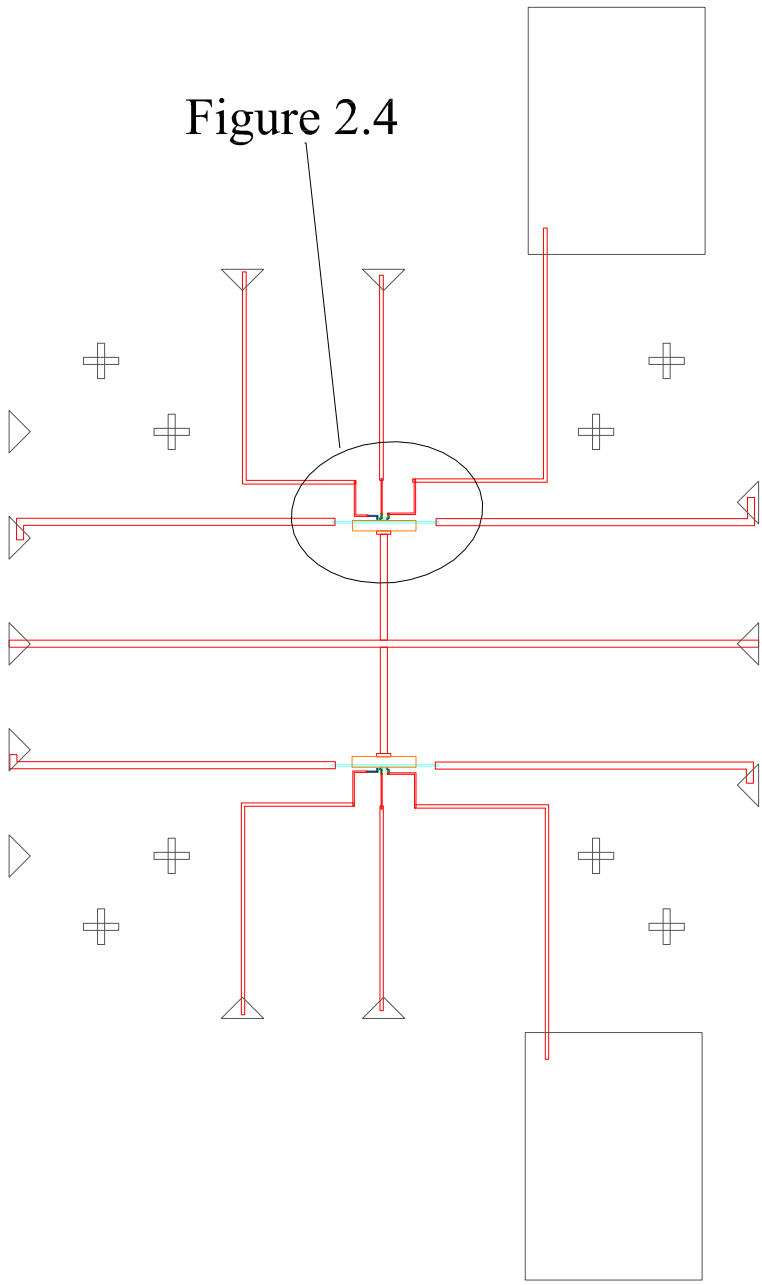

Figure 2.3: Design pattern of electron beam lithography. The outer cross marks are at the vertices of a $80\mu m \times 80\mu m$ square. The electron beam dose for various structures is given in table 2.1

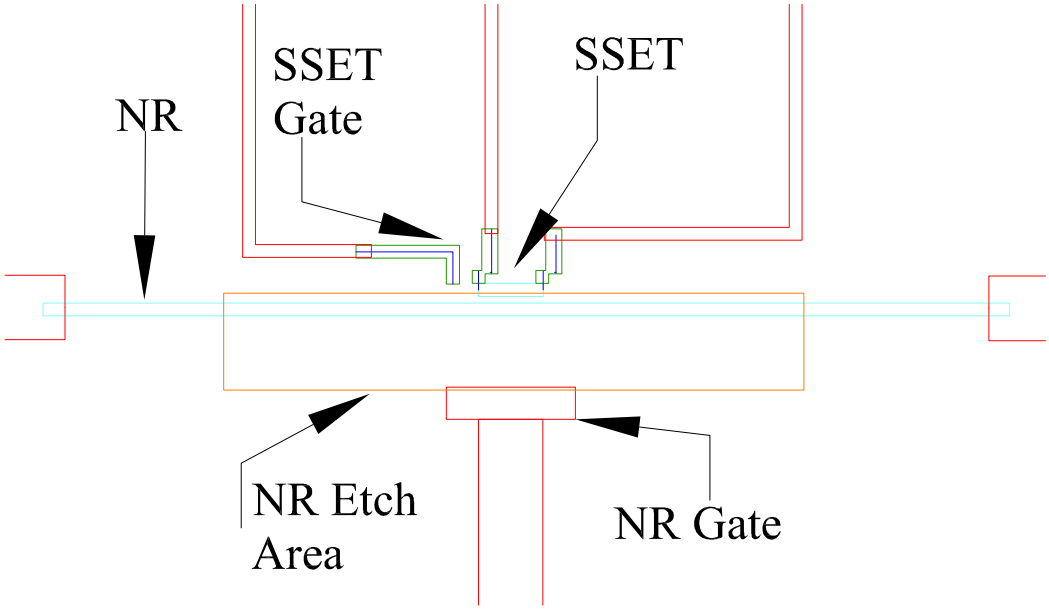

Figure 2.4: Close up of the design pattern for electron beam writing showing the SSET and the NR. The dimensions of the device parts are given in table 2.2

Device part	dimension
SET island	$1\mu m \times 200nm$
SET junction area	$80nm \times 60nm$
NR etch area	$9\mu m \times 1.5\mu m$
NR Gate length	$1.6\mu m$
Width of NR	$200nm$

Table 2.2: Dimension of various parts of the device design pattern

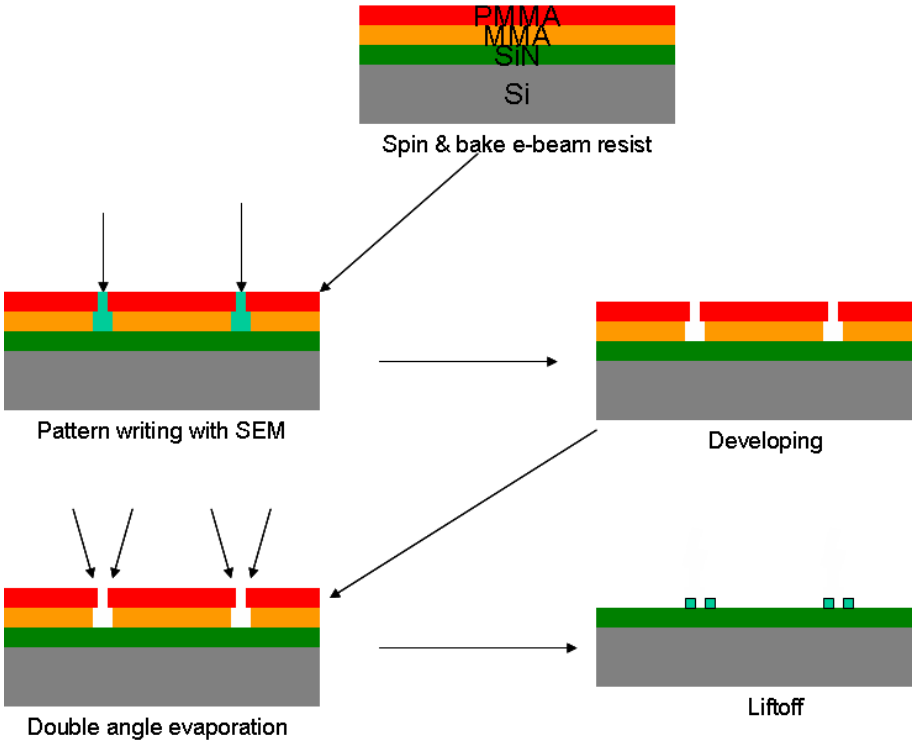

Figure 2.5: Schematics of second layer of lithography

2.3 Etching Free the Nanomechanical Resonator

The third stage of fabrication involves reactive ion etching to free the NR.

- The sample is first spun coated at 4000RPM for 1 minute with 950K PMMA A-7 (7% PMMA in anisole). It is then baked at 180^0C on hot plate for 5 minutes.

- The etch area, shown as orange colored structure in figure 2.4, is then defined using scanning electron microscope. The dose used is $400\mu C/cm^2$.

- It is then developed in MIBK:IPA(1:3) for 1 minute and rinsed in IPA for 30 seconds and blown dry.

- The sample is then etched in three steps. First the silicon nitride is anisotropically etched using a plasma of CHF_3(Trifluoromethane) and O_2.

- Next the silicon is isotropically etched using SF_6(Sulfur Hexafluoride) plasma to free the beam.

- Then the resist is etched away using oxygen plasma. Schematics of this stage of lithography is shown in figure 2.6.

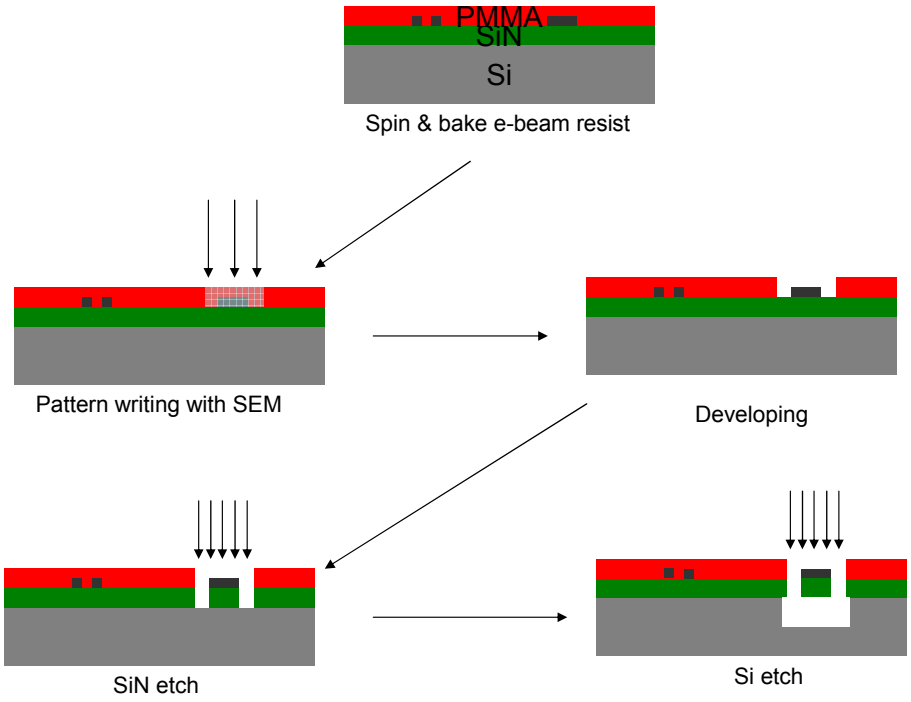

Figure 2.6: Schematics of third layer of lithography

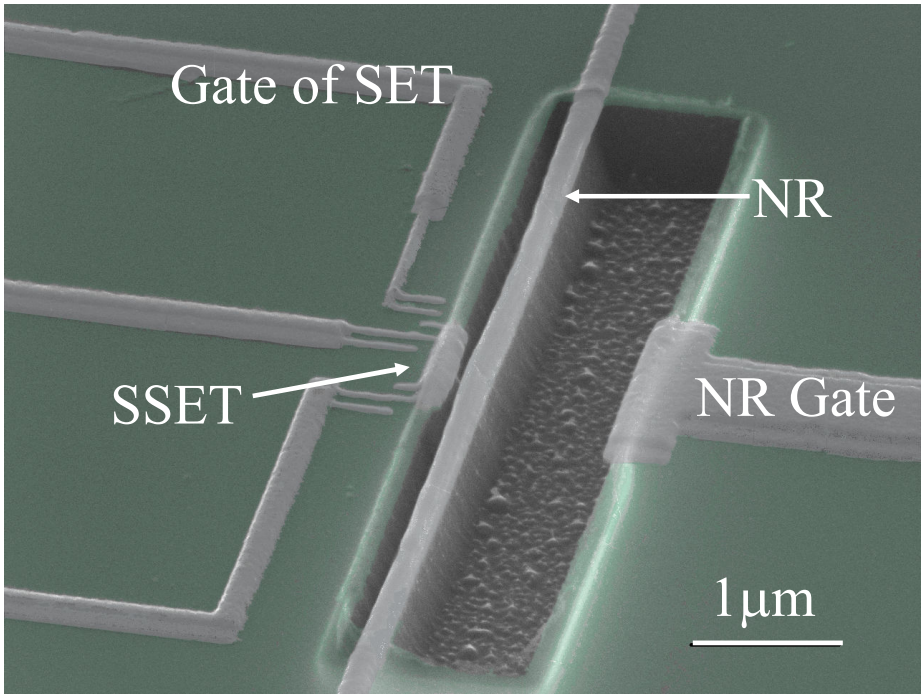

Figure 2.7: Colorised SEM photo of the sample

The fabrication of the devices with SSET coupled to NR has been developed by other students and post-doctoral researchers in the group. The RFSET fabrication has inputs from Matthew LaHaye, Benedetta Camarotta and Carlos Sanchez. The described NR fabrication process was developed by Jared Hertzberg. My contribution in the fabrication process was to develop a process wherein I can make SSET island very close to the NR ($\sim 100nm$). This required making both the SSET and the NR mask in the same step.

Chapter 3

Measurement Scheme

3.1 Single Electron Transistor and Principle of Operation

A single electron transistor (SET)[16] is a sensitive electrometer with charge sensitivities reaching the quantum limit[18]. It consists of two electrodes separated from the central island using two junctions with very small capacitances. The charge on the island is an integral multiple electronic charge when the tunnel junction resistance is much greater than the resistance quantum, $R_Q = h/e^2 \approx 26k\Omega$. If the energy provided by the environment is lower than the electrostatic energy required for the electrons to tunnel into or out of the island, the electrons are localized on the island. This electrostatic energy, also called charging energy, is determined by the total capacitance of the SET, which in our case is about 500aF, giving us a charging energy, E_C, of around $175\mu eV$. If the two reservoirs are grounded then the number of electrons on the island can be changed by changing the electrostatic potential on a nearby gate. When using this device as a single electron transistor a bias is applied across the two junctions which results in electrons tunneling on and off the island producing a finite current.

The current through the SET is controlled by the sequential tunneling of electrons. The rate of this tunneling, Γ, and hence the current, I_{DS}, depends on the

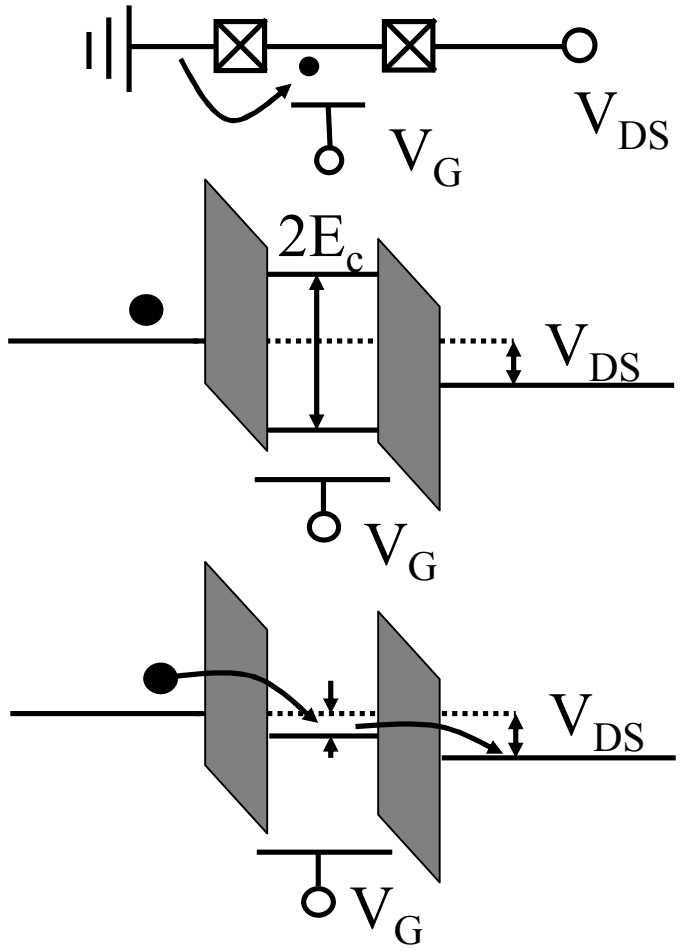

Figure 3.1: Schematic of SET and the heuristic arguments for conduction mechanism. The energy levels of the island are separated by $2E_C$. For $eV_{DS} < 2E_C$, gate voltage can be adjusted such that energy levels of island either allow or impede the tunneling of electrons through the SET.

free energy difference Δf before and after the tunneling and is given by,

$$I_{DS} \propto \frac{\Delta f}{e^{\Delta f} \pm 1} \tag{3.1}$$

The free energy calculations for these tunneling processes shows that the current through the SET can be modulated by changing the potential on the gate of the SET. As shown in figure 3.1, the charges hop on and off the island to produce current. This current flow is controlled by varying either the gate voltage, V_G, or the drain source voltage, V_{DS}.

At low temperatures i.e. $k_B T << E_C$, tunnel events take place only if they are energetically allowed, that is, $\Delta f < 0$. For $eV_{DS} < E_C$, the current therefore depends critically on the value of the gate voltage. If the gate voltage is adjusted such that there are an integer numbers of electrons on the island of the SET, tunneling events are not allowed. This phenomenon is called Coulomb blockade. If the gate voltage is adjusted such that the gate charge corresponds to half that of the electron then the tunneling is energetically allowed, and current flows through the SET. In practice, the current is not zero in the Coulomb blockade regime. This is because of the finite resistance of the SET i.e. junction resistances are not much larger than the quantum of resistance. This finite resistance gives rise to cotunneling events which utilize the virtual energy levels of the island to tunnel through the SET.

For $eV_{DS} < 2E_C$, the tunneling probability increase exponentially and the coulomb blockade oscillations change significantly. The variation in current through the SET as V_G and V_{DS} are changed is shown in figure 3.2. The combined map of $I - V_{DS} - V_G$ curves is shown in figure 3.3.

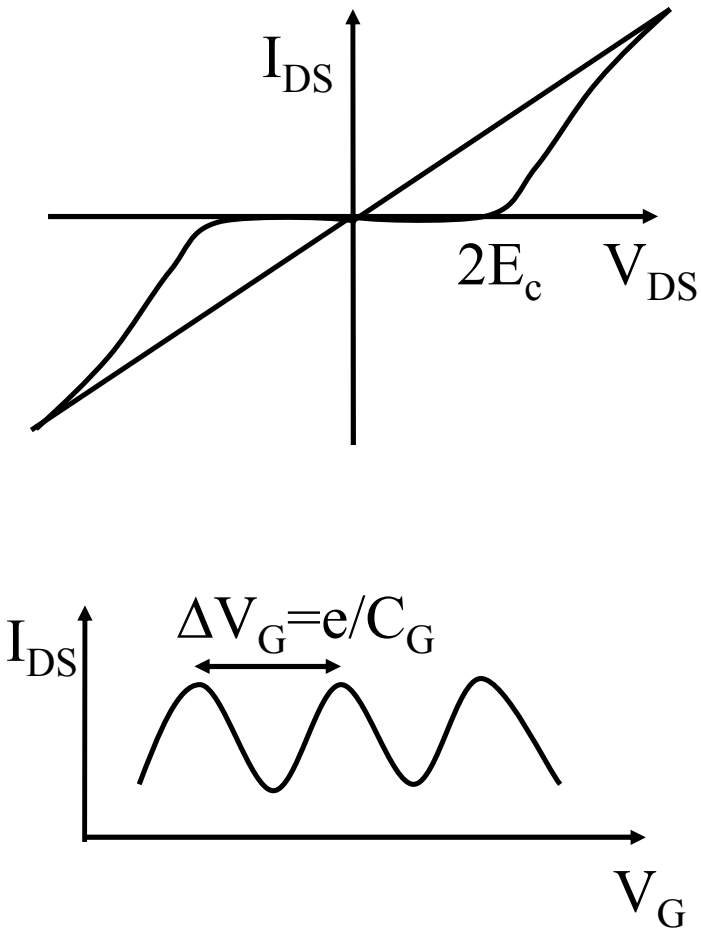

Figure 3.2: Current through SET as a function of V_{DS} and V_G.

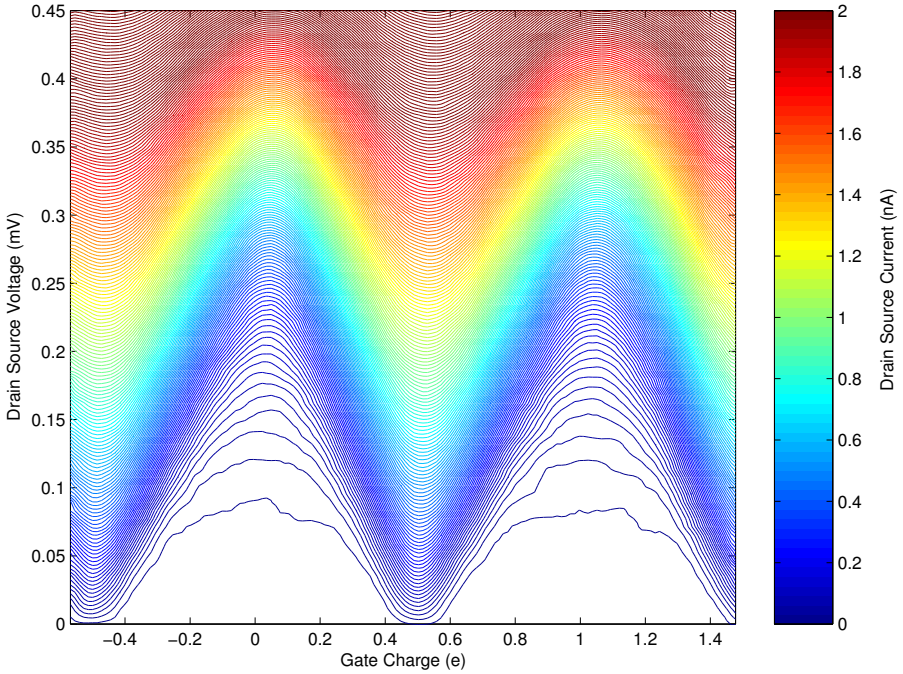

Figure 3.3: $I - V_{DS} - V_G$ map of SET

In a superconducting single electron transistor(SSET), the normal metal leads and island are replaced by superconducting materials. In SSET, the current is carried by both Cooper pairs(2e) and the quasiparticles(e). The bias conditions of the SSET determine the contribution of these charge particles to the current. The presence of the superconducting gap, Δ, produces certain features in $I - V_{DS} - V_G$ curves of a superconducting SET which are not there in normal state SET. The $I - V_{DS} - V_G$ map of a superconducting SET is shown in figure 3.4. This current map also shows features like Josephson quasiparticle peak (JQP), double Josephson quasiparticle peak (DJQP) and the onset of quasiparticle current. As is evident from the figure, the current through the SSET is a sensitive function of gate voltage. Since SSET current is sensitive to the changes in charge on the island, the gate voltage is usually expressed in terms of gate charge.

$$q_G = C_G V_G \tag{3.2}$$

In the coulomb blockade peaks, each period of current oscillation corresponds to changing the gate charge by one electron (see figure 3.2). We use this sensitivity of the SSET current to gate charge to detect the motion of the NR. This detection scheme is described in detail in section 3.3.

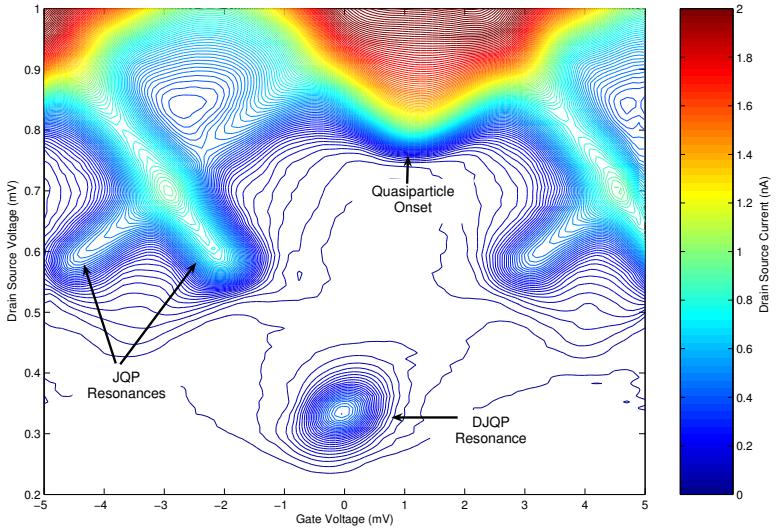

Figure 3.4: $I - V_{DS} - V_G$ map of SSET. The asymmetry in the $I - V_{DS} - V_G$ map is due to the asymmetric junctions of the SSET.

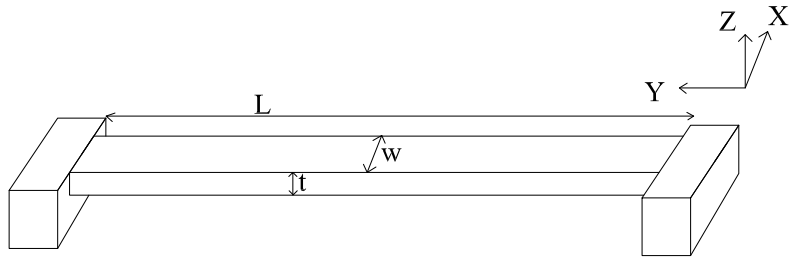

Figure 3.5: Schematics of a doubly clamped beam

In our work we are using aluminum as the superconducting material for the island and the leads and aluminum oxide as the junction material.

3.2 Nanomechanical resonator

Our nanomechanical resonator is a mechanical beam with nanometer size dimension which is clamped at the two ends. The behavior of a mechanical beam clamped at two ends and with aspect ratio $L/t >> 1$ can be described by Euler Bernoulli differential equation. For a beam oriented along the Y axis and transverse motion along X axis, as shown in figure 3.5, this equation is written as [31],

$$\rho wt \left(\frac{\partial^2}{\partial t^2} X\left(y,t\right) \right) = -\frac{\partial^2}{\partial y^2} EI \frac{\partial^2}{\partial y^2} X\left(y,t\right) \tag{3.3}$$

where,

ρ is the density of the material

E is the Young's modulus of the material of the beam

$I = wt^3/12$ is bending moment of inertia

Applying the boundary conditions,$X(y=0) = X(y=L) = 0$ and $\frac{dX(y=0)}{dt} = \frac{dX(y=L)}{dt} = 0$,it can be shown that the eigenfrequencies of this beam are given by,

$$\omega_n = \zeta_n \sqrt{\frac{E}{\rho}} \frac{w}{L^2} \tag{3.4}$$

where, ζ_n depends on the mode shape and is of the order of unity and

L is the length of the resonator

The quality factor of the resonator determines the amount of energy lost to the environment. For mechanical resonators, the most important source of dissipation is internal, like the amorphous nature of the material in our case. All amorphous materials are known to share low energy vibrational excitations [24],[25],[26],[27]. These properties of the materials have been explained based on density of tunneling defects in these devices [28]. To improve the quality factor of the nanomechanical resonator we need to make this structure out of materials which are single crystal, say single crystal Si. It is expected that such a structure would improve the quality factor of the mechanical resonators. Also, using a wet etching process instead of a dry etching would result in a smoother surface and would thus reduce the dissipation related to surface defects. The quality factor of our device was about 100,000 and was sufficient to be able to detect backaction effects of the SSET.

To cool down these mechanical resonators, with resonant frequencies of 10MHz, to their ground state we need milli Kelvin temperatures i.e. $\hbar\omega_{NR} << k_B T$. But these systems can have coherence times of the order of,

$$\tau = Q_0/\omega_{NR} \tag{3.5}$$

where, Q_0 is the quality factor and ω_{NR} is the resonant frequency of the mechanical beam. If the thermal state of the is resonator is $N_{th} = \frac{1}{2} + \left(e^{\frac{\hbar\omega_{NR}}{k_B T}} - 1\right)^{-1}$, the average resonator lifetime in one of these thermal states is,

$$\tau = \frac{Q_0}{\omega_{NR} N_{th}} \tag{3.6}$$

So if the "quantum manipulation time" is smaller than this time, observing quantum effects in these systems should be possible. What makes these systems interesting is that they are mechanical objects with 10^{10} degrees of freedom. It is fascinating to see how quantum mechanical effects manifest themselves in such systems as compared to atoms which have very few degrees of freedom.

3.3 Position Detection of NR using SSET

In our setup, the NR is 9μm long, 200nm wide and about 50 nm thick silicon nitride. It is coated with about 90nm of aluminum. The aluminum electrode on top provides a way of applying voltage to the NR and hence coupling it to the SSET. The NR acts as a gate for the SET and any motion of the NR can modulate the current through the SET. The thermal motion of the NR is related to its temperature T by equipartition of energy which states that the each degree of freedom has an energy equal to $\frac{1}{2}k_B T$.So

$$\frac{1}{2}kx^2 = \frac{1}{2}k_B T \tag{3.7}$$

where, k is the spring constant of the NR

k_B is the Boltzmann constant

Because of the capacitance between the voltage biased NR and the island of the SET, the charge on the island is given by,

$$q = C_{NR} V_{NR} \tag{3.8}$$

where, V_{NR} is the bias voltage applied to the beam and

C_{NR} is the capacitance between the SET and the resonator

Because of the thermal motion of the resonator the change in the charge seen by the SET is given by

$$\frac{dq}{dx} = \left(\frac{d}{dx} C_{NR}\right) V_{NR} \tag{3.9}$$

$$\delta q = \left(\frac{d}{dx} C_{NR}\right) V_{NR} \delta x \tag{3.10}$$

$$= \left(\frac{d}{dx} C_{NR}\right) V_{NR} \sqrt{\frac{k_b T}{k}} \tag{3.11}$$

Thus the charge induced on the island of the SSET, by the motion of the NR, can give the information about the temperature of the NR.

For small amplitude motions, the current through the SSET is modulated as

$$\frac{dI_{DS}}{dx} = \frac{dI_{DS}}{dV_G} \frac{dV_G}{dq} \frac{dq}{dx} \tag{3.12}$$

$$= \frac{dI_{DS}}{dV_G} \frac{1}{C_G} \frac{dC_{NR}}{dx} V_{NR} \tag{3.13}$$

Recently, LaHaye et.al [15] measured the thermal noise of a NR down to 50mK. The measurement amounted to a position resolution about 5 times above the quantum limit.

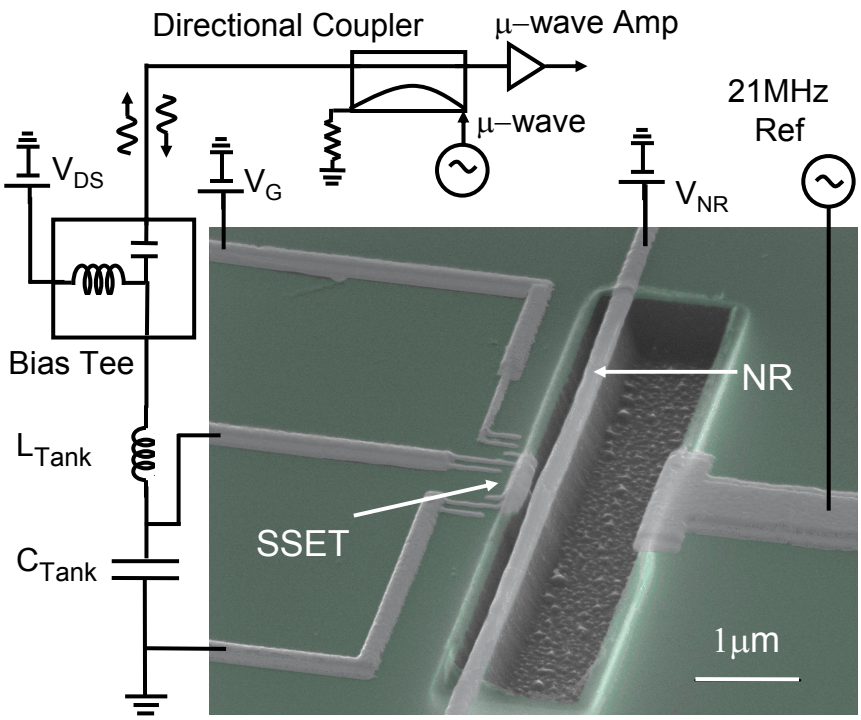

Figure 3.6: Simplified schematics of measurement using RFSET

3.4 Radio Frequency Single Electron Transistor

The single electron transistor, with typical junction resistance of 100kΩ and capacitance of 1fF, will have an intrinsic bandwidth of about one GHz. But cable capacitance (100pF)from device to the electronics restrict the usable bandwidth to tens of kHz.

One way to improve the bandwidth of the single electron transistor is to use a tank circuit close to the SET to transform the impedance at resonance of the tank to 50Ω [18]. A circuit diagram of this mode of operation,called the Radio Frequency Single electron transistor (RFSET) is shown in figure 3.6.

In RFSET, the SSET is embedded in a tank circuit made of L_{Tank} and C_{Tank}.

The resistance of the SSET, which depends on the bias conditions of the SSET, together with the tank circuit forms an LCR circuit. In the RFSET mode of detection, the SSET is DC biased using V_{DS} and V_G to a bias point where changes in the dynamic resistance of the SSET, with gate voltage, is maximum. A microwave signal, called carrier, corresponding to the resonant frequency of the tank circuit is sent down to the SSET. The reflection coefficient depends on the total impedance of the LCR tank circuit seen by the carrier i.e. the dynamic resistance of the SSET. The changes in the gate charge (resonator motion, motion of charges in substrate or any other signal on gates) changes the dynamic resistance and hence the reflection coefficient. The reflected wave, thus, carries the carrier frequency amplitude modulated at the frequency of the resonator motion(and/or other charge signals that is seen by the SSET). This mode of operation gives us the required bandwidth to detect the motion of the NR.

Chapter 4

Position Sensitivity and Backaction

Quantum mechanics stipulates that it is not possible to simultaneously measure the position and the momentum of an object to arbitrary precision. This precision is governed by the Heisenberg uncertainty principle,

$$\Delta x \times \Delta p \geq \frac{\hbar}{2} \tag{4.1}$$

where Δx and Δp are the uncertainty in the position and the momentum respectively and $2\pi\hbar$ is the Planck's constant. This principle does not restrict the accuracy to which we can measure the position or the momentum. It just puts limits on the product of these two, since any measurement of one would affect the subsequent measurements. For instance it is possible to do position measurements to arbitrary precision by doing one very strong measurement or by doing stroboscopic measurements [32]. We are interested in doing position measurements very close to the limits posed by quantum mechanics and exploring how various contributions of noise come into play when doing continuous position measurements. There has been a lot of interest in doing very sensitive position measurements. For instance,

1. The Laser Interferometer Gravitational-Wave Observatory (LIGO) [1], for instance, is involved in putting a lower limit on the stochastic gravitational background waves and also the power laws that their energy densities might follow. This information would provide a way of determining the source of

these gravitational bursts. LIGO involves km long Fabry Perot interferometers which can sensitively detect these gravitational bursts.

2. Single Electron transistors have been used recently to readout the motion of a radio frequency mechanical resonator [15] [19].

In our detection scheme, we detect the motion of the resonator by looking for changes in the current or the dynamic resistance of the SSET due to charges tunneling through the SSET. The thermal motion of the resonator is expected to have a position spectral density given by,

$$S_x(\omega)^{th} = \frac{4k_B T\omega_{NR}}{m_{eff}Q_{NR}} \frac{1}{\left(\left(\omega^2 - \omega_{NR}^2\right)^2 + \left(\frac{\omega\omega_{NR}}{Q_{NR}}\right)^2\right)} \tag{4.2}$$

where,

T is the temperature of the resonator

Q_{NR} is the quality factor of the resonator

ω_{NR} is the resonant frequency of the resonator

m_{eff} is the effective mass of the resonator and

k_B is the Boltzmann constant

The integrated response of the resonator noise power is a measure of the resonator position variance and thus, the temperature by equipartition theorem.

$$P_{NR} \propto \int S_x(\omega)\,\frac{d\omega}{2\pi} = \langle x^2 \rangle \tag{4.3}$$

$$= \frac{k_B T}{k} \tag{4.4}$$

The ultimate limit to the resolution of position detection of the resonator is limited due to the forward coupled noise of the detector and the backaction noise

due to the detector. How close we get to the quantum limit of position detection depends on the contributions of these two noise sources. Each of these effects is dominant in a different regime of coupling.

4.1 Forward Coupled Noise

Forward coupled noise is the noise floor of the measurement system. In an ideal case it would be the noise floor of the first stage of the amplifier. In our detection scheme that would be the shot noise of the SSET. If the followup amplifiers after the first stage are not sensitive enough, the forward coupled noise is determined by the overall detection system.

4.1.1 Shot Noise

The shot noise comes from the stochastic tunneling of the charge carriers though the device. The shot noise provides a way to study the correlations, internal energy scales and counting statistics of the device [39]. In a SSET, this noise comes when the charge carriers, cooper pairs and quasiparticles hop on and off the island and this charge fluctuation is a function of both coulomb blockade effects and coherence due to Josephson effects. The current noise due to this stochastic motion of charge is given by,

$$S_I = e\eta I_{DS} \tag{4.5}$$

where,

η, called the Fano factor, depends on the type of transport mechanism and

typically is of the order of 1.

e is the electronic charge and

I_{DS} is the average current through the SSET

The current through the SSET is related to the position x by equation 3.13. This current shot noise translates into the position shot noise given by,

$$S_x = \frac{S_I}{(dI_{DS}/dx)^2} \tag{4.6}$$

The shot noise is the dominant source of noise at low couplings. To determine if the measurement system is shot noise limited we can do shot noise measurements as described in the next chapter. If the measurement system is shot noise limited, then the power measured in a given bandwidth should go to zero for zero current through the SSET. A non zero intercept of a plot of shot noise S_I against the current indicates that the measurement system is not ideal and is limited by amplifiers.

4.1.2 Noise floor of amplifier

If the noise temperature of the amplifier which follows the SSET is not good enough to read out the shot noise from the SSET, the position sensitivity in that case would be limited by the noise floor of this amplifier. In our measurement system we used a Berkshire[1] microwave amplifier with noise temperature of 2K, following the RFSET. This along with losses in the cables degrades the noise performance of the system and gives us a measurement noise temperature of about 5K. To determine the charge sensitivity (or noise), $\sqrt{S_q}$, of the measurement system, we perform a

[1] Berkshire model L-1.1-30H

measurement as described in the next chapter. This charge sensitivity is related to the position noise by the following equation.

$$S_q = \left(\frac{dC_{NR}}{dx}V_{NR}\right)^2 S_x \tag{4.7}$$

Again as with the shot noise, it is possible to improve the position noise by increasing the coupling of the resonator to the SSET.

4.2 Backaction

Backaction is the result of influence of the measurement system on the object. For a linear position detector for instance, position measurement of an object changes the momentum of the object and hence affects the subsequent position measurements. In our system, the backaction effects are the result of potential change of the island of the SSET as the charges tunnel through the island. Every charge that tunnels into or out of the island, changes the potential seen by the resonator. These potential "kicks" to the resonator change the motion of the resonator. They get stronger as we increase its coupling to the SSET.

Backaction effects of the measurement system have been theoretically studied extensively in the last few years. Mozyrsky et.al [20] studied the backaction effects of a normal state tunnel junction on a mechanical resonator. They found that the tunnel junction acts like a thermal bath for the resonator and has an effective temperature given by,

$$k_B T_{eff} \propto \frac{eV_{DS}}{4} \tag{4.8}$$

Similar results were obtained for a normal state SET coupled to a mechanical resonator [22] [21]. In this case they found the effective temperature of the SET to be,

$$k_B T_{eff} \propto \frac{eV_{DS}}{2} \tag{4.9}$$

Clerk et. al. [14] in their analysis of qubits coupled to SSETs found that it is possible to enhance or diminish the lifetime of the qubit state just by changing the bias conditions of the SSET. They found that by biasing the SSET at certain points around double Josephson quasiparticle peak (DJQP) it is possible to invert the population of the charge qubits which would imply "negative temperatures".

4.2.1 Linear response theory

The linear response theory approach to determine the backaction effects of the SSET is given in detail in ref [29]. I am presenting the results of that analysis here for completeness. A SSET, like a lot of other detectors, is a non equilibrium device with non Gaussian noise properties. But analyzing such a detector is made easier by the fact that in most systems (as is the case in our system), the coupling between the object and the detector is small. Because of this weak coupling the detector responds linearly to the changes in quantity being measured. In our system, for instance, the coupling between the SSET and the resonator is weak enough that the current through the SSET changes linearly with the motion of the resonator. Thus the interaction Hamiltonian between the SSET island charge, q, and the resonator

position is given by,

$$H_{int} = -A\hat{x} \cdot \hat{F} \tag{4.10}$$

where,

A is a dimensionless coupling constant and

$\hat{F}$ is the backaction force due the detector which is coupled to the motion of the resonator and has a spectral noise density that is given as,

$$S_F(\omega) = \int_{-\infty}^{\infty} dt e^{i\omega t} \langle \hat{F}(t)\hat{F}(0) \rangle \tag{4.11}$$

Assuming linear response of the SSET to resonator motion we can write the relation between the two as,

$$\hat{F}(t) = A \int_{-\infty}^{\infty} dt' \lambda \left(t - t'\right) \hat{x}(t') \tag{4.12}$$

where,

λ is the detector gain.

For lowest order perturbation in A, it is possible to describe the resonator-SSET system in terms of classical Langevin equation as given below [30],

$$m\ddot{x} = -m\omega_{NR}^2 x(t) - m\gamma_{bath}\dot{x}(t) + \delta f_0(t) + f_{avg} + \delta f_{avg}(t) \tag{4.13}$$

where,

m is the mass of the resonator

γ_{bath} is the damping of the resonator due to the thermal bath (intrinsic damping)

δf_0 is the fluctuating force due to this equilibrium bath and

f_{avg} and δf_{avg} are the average backaction force and the fluctuation in it respectively

The fluctuations in the equilibrium bath force can be described by the fluctuation dissipation theorem,

$$S_{\delta f0}(\omega) = m\gamma_{bath}\hbar\omega \coth\left(\frac{\hbar\omega}{2k_B T_{bath}}\right) \tag{4.14}$$

where,

T_{bath} is the temperature of the equilibrium bath

γ_{bath} is the damping due to this bath

The average backaction force f_{avg} can be written as a sum of two forces viz,

1. The conservative force that is in phase with the motion of the resonator. This force is responsible for renormalization of the resonant frequency and can be written as,

$$f_{cons} = -\int_{-\infty}^{\infty} dt' \Delta k\,(t-t')\,x(t') \tag{4.15}$$

2. The damping force which is out of phase with the motion of the resonator and contributes to the damping of the resonator.

$$f_{damp}\,(t) = -m\int_{-\infty}^{\infty} dt' \gamma\,(t-t')\,\dot{x}\,(t') \tag{4.16}$$

Using Kubo relations,

$$\lambda(t) \quad = \quad \frac{i}{\hbar}\theta(t)\langle[F(t), F(0)]\rangle \tag{4.17}$$

$$
\begin{aligned}
m\gamma(\omega) &= A^2\left(\frac{\Im[\lambda(\omega)]}{\omega}\right) && (4.18)\\
&= \frac{A^2}{\hbar}\left(\frac{S_F(\omega)-S_F(-\omega)}{2\omega}\right) && (4.19)\\
\Delta k &= A^2\Re[\lambda(\omega)] && (4.20)
\end{aligned}
$$

The detector is a non-equilibrium device and in general is not related to damping but the fluctuation dissipation theorem can be still be used to describe this system, with an effective temperature and damping, at each frequency, ω.

$$
\coth\left(\frac{\hbar\omega}{2k_B T_{eff}(\omega)}\right) = \frac{S_{\delta f}(\omega)}{m\gamma\hbar\omega} \tag{4.21}
$$

where

T_{eff} and γ are effective temperature and damping due to the device at each frequency.

The detector system in this case can be described by a single effective temperature because of the fact that the mechanical resonator responds only to forces within a very small bandwidth, which is determined by its quality factor. The SSET thus looks like a bath with an effective temperature and damping.

For the resonator SSET system, the backaction force is given by,

$$
\begin{aligned}
\Delta F &\approx \frac{eV_{NR}}{C_\Sigma}\frac{dC_{NR}}{dx} && (4.22)\\
&= 2N\frac{E_c}{d} && (4.23)\\
&= 2E_C V_{NR}\frac{dC_{NR}}{dx} && (4.24)
\end{aligned}
$$

where, $N = \frac{V_{NR}C_{NR}}{e}$

If $S_q(\omega)$ denotes the charge noise spectrum of the SSET, the damping and the effective temperature associated with the SSET is given by,

$$\gamma_{SSET} = \frac{(\Delta F)^2}{2\hbar m\omega_{NR}}(S_q(\omega_{NR}) - S_q(-\omega_{NR})) \tag{4.25}$$

$$T_{SSET} = \frac{(\Delta F)^2}{4k_B m\gamma_{SSET}}(S_q(\omega_{NR}) + S_q(-\omega_{NR})) \tag{4.26}$$

Note that the charge noise spectrum is considered only around the resonant frequency of the NR since this is the part that would be contributing to its damping. The damping due to the SSET comes from the asymmetric part of the noise and the effective temperature comes from the symmetric part of the noise. In the low frequency limit i.e. $\omega_{NR} << \Gamma, E_J/\hbar$ the force noise due to backaction can be written as,

$$S_F(\omega_{NR}) = 2m\gamma_{SSET}k_B T_{SSET} \tag{4.27}$$

where

Γ is the quasiparticle tunneling rate.

This force noise within the bandwidth of the resonator produces mechanical noise spectra given by,

$$S_x^{BA}(\omega_{NR}) = \frac{S_F}{k^2}\frac{\omega_{NR}^4}{\left(\omega_{NR}^2 - \omega^2\right)^2 + \omega^2\gamma_{NR}^2} \tag{4.28}$$

Since the resonator is now connected to two baths, its temperature and the damping would be given by,

$$T_{NR} = \frac{\gamma_{bath}T_{bath} + \gamma_{SSET}T_{SSET}}{\gamma_{NR}} \tag{4.29}$$

$$\gamma_{NR} = \gamma_{bath} + \gamma_{SSET} \tag{4.30}$$

The effective temperature and the damping due the SSET depends on the bias conditions of the SSET. We will concentrate on backaction effects close to resonances called Double Josephson Quasiparticle Peak(DJQP) and Josephson Quasiparticle Peak(JQP).

DJQP

Figure 4.1 shows schematically the cycle involved in the DJQP process. It is a four step process and each step has energies involved which determine the rate of the process and thus the effective temperature and the damping of the SSET when biased close to this resonance.

- A cooper pair tunnels onto the island from junction 1.

$$\delta_A = 4E_C\left(1 - N\right) - eV_{DS} \tag{4.31}$$

- A quasiparticle (a virtual particle with charge of 1 electron) tunnels out of junction 2.

$$E_a = 2E_C\left(3/2 - N\right) + eV_{DS}/2 \tag{4.32}$$

- A cooper pair tunnels out of island through junction 2.

$$\delta_B = 4E_C N - eV_{DS} \tag{4.33}$$

- A quasiparticle tunnels onto island through junction 1.

$$E_b = 2E_C\left(1/2 + N\right) + eV_{DS}/2 \tag{4.34}$$

Each quasiparticle tunneling is characterized by a quasiparticle decay rate $\Gamma_a(\Gamma_b)$ which depends on energy $E_a(E_b)$ and the IV characteristics of the SSET and each copper pair resonance is characterized by a detuning energy $\delta_A(\delta_B)$. This detuning energy is the measure of how far the bias point is from the resonance. N is the normalized charge on the island of the SSET and depends on the gate voltage. If the junctions of the SSET are symmetric then the two quasiparticle rates are similar. The energy scales involved in this process determine the effective temperature and the damping of the SSET when it is biased close to DJQP.

$$T_{SSET} = \frac{[(\hbar\Gamma)^2 + 4\delta_A^2][(\hbar\Gamma)^2 + 4\delta_B^2]}{16k_B[\delta_A + \delta_B][(\hbar\Gamma)^2 + 4\delta_A\delta_B]} \tag{4.35}$$

$$\gamma_{SSET} = \frac{2\Delta F^2(\delta_A + \delta_A)}{mE_j^2\Gamma} \left(\frac{\left((\hbar\Gamma)^2 + 4\delta_A^2\right)\left((\hbar\Gamma)^2 + 4\delta_A^2\right)\left((\hbar\Gamma)^2 + 4\delta_A\delta_B\right)}{\left((\hbar\Gamma)^2 + 2\delta_A^2 + 2\delta_B^2\right)} \right) \tag{4.36}$$

where,

ΔF is the coupling parameter given by equation 4.24 and

E_J is Josephson coupling energy

JQP

The Josephson quasiparticle current process is shown in figure 4.2. This process involves a single cooper pair tunneling onto the island through one junction followed by tunneling out of two quasiparticles from the other junction. Assuming the process where the cooper pair tunnels through first junction and the quasiparticles tunnel out through the second one, we can write the energies involved in this

process as,

$$\delta = 4E_C(1-N) - eV_{DS} \tag{4.37}$$

$$E_a = 2E_C(3/2-N) + eV_{DS}/2 \tag{4.38}$$

$$E_b = 2E_C(1/2-N) + eV_{DS}/2 \tag{4.39}$$

Note that a similar set of equations can be written down for JQP process wherein the cooper pair tunnels out through the second junction and two quasiparticles tunnel onto the island through the first junction. When the SSET is biased close to the JQP, the effective temperature and the damping due to the SSET is given by,

$$T_{SSET} = \frac{(\hbar\Gamma_a)^2 + 4\delta^2}{16k_B\delta} \tag{4.40}$$

$$\gamma_{SSET} = 16\Delta F^2\delta\frac{E_j^2\Gamma_a}{m\Gamma_b^2}\left(\frac{4\delta^2 + c_1(\hbar\Gamma_a)^2 + c_2E_j^2}{\left(4\delta^2 + (\hbar\Gamma_a)^2 + c_3E_j^2\right)^3}\right) \tag{4.41}$$

where

$$c_1 = 1 + 4\frac{\Gamma_b}{\Gamma_a} + 8\left(\frac{\Gamma_b}{\Gamma_a}\right)^2 \tag{4.42}$$

$$c_2 = 1 + 4\frac{\Gamma_b}{\Gamma_a} + 4\left(\frac{\Gamma_b}{\Gamma_a}\right)^2 \tag{4.43}$$

$$c_3 = 2 + \frac{\Gamma_b}{\Gamma_a} \tag{4.44}$$

Note that the δ can be negative depending on the bias conditions of the SSET (see equation 4.37). This implies that depending on the bias conditions of the SSET it is possible to have negative damping and negative effective temperatures. As is obvious from the equations above, the temperature and the damping of the SSET are sensitive functions of the bias point. In our measurements we intend to

1. Explore the effect of backaction as the coupling between the SSET and the NR is increased with bias point of SSET fixed.

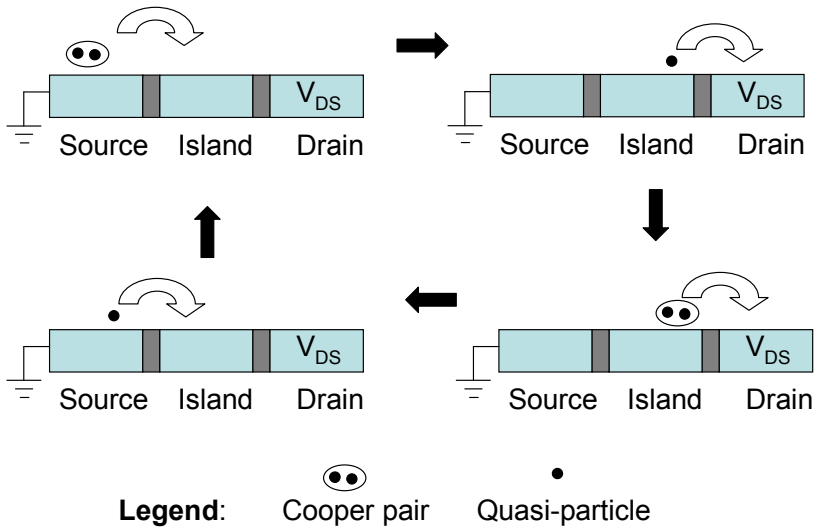

Figure 4.1: Schematics of DJQP process

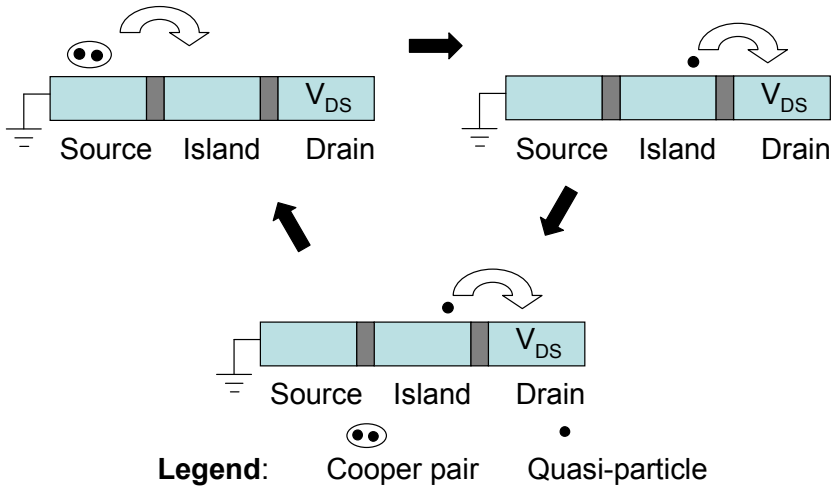

Figure 4.2: Schematics of JQP process

2. Evaluate how changing the bias point of the SSET, at fixed coupling, changes the resonator properties.

3. Look at how the resonator behaves when we bias the SSET in regions where negative damping and effective temperature of the SSET are expected.

4.3 Position Sensitivity

The spectral noise density contributions from both the forward coupled noise, S_x, and the backaction noise, S_x^{BA}, contribute to the position resolution of the system.

$$S_{xtotal} = S_x + S_x^{BA} \tag{4.45}$$

The position resolution of the SSET is then given by,

$$\Delta x_{RMS} = \sqrt{(S_x + S_x^{BA})\,\frac{\gamma_{NR}}{2}} \tag{4.46}$$

Figure 4.3 shows a representative plot of position resolution of the device as a function of the coupling voltage. This plot was produced using the above equation and parameters of our device. At low couplings the forward coupled noise dominates. The contributions from the backaction are negligible. As the coupling is increased, the position resolution improves because the forward coupled position noise decreases (see equation 4.6 or 4.7). At intermediate couplings, both the forward coupled and the backaction noise are significant. For optimal position measurement, the coupling voltage should be such that the contributions from the forward coupled and the backaction noise are equal. This point corresponds to coupling voltage

of about 0.5V in this figure. As the coupling is increased further, the backaction effects are dominant. Beyond certain coupling voltage the mechanical resonator is completely loaded by the SSET and the position resolution saturates.

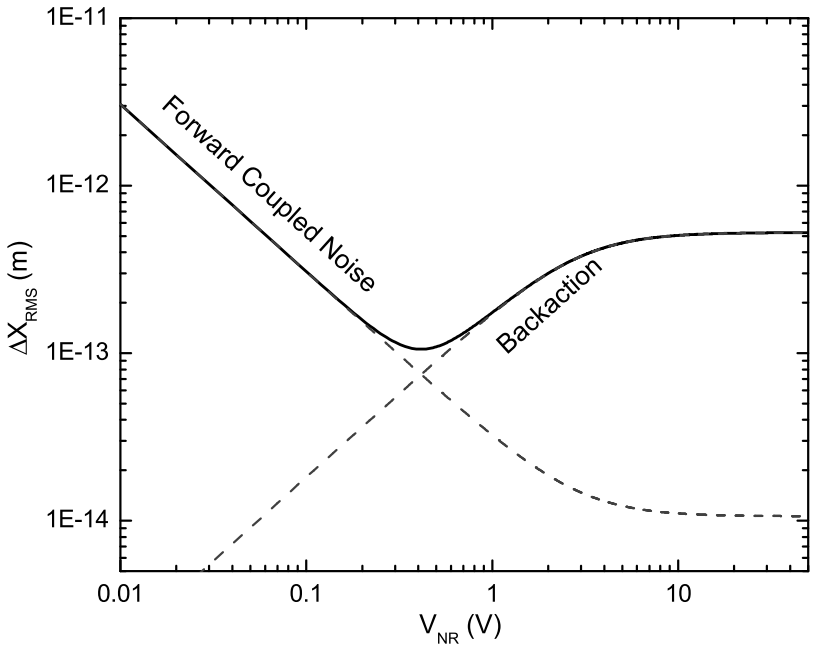

Figure 4.3: Position resolution of the device as a function of coupling voltage

Chapter 5

Methods

5.1 Resonator Characterization

5.1.1 Frequency and the quality factor

The frequency of the resonator is determined by the magnetomotive technique and is found to be $f_0 = 21.866030MHz$ at 0.5 Tesla. The circuit diagram for this measurement is shown in fig 5.1. This technique is based on the effect of Lorentz force. In presence of magnetic field, if a current is passed through the nanomechanical resonator, the resonator experiences the Lorentz force given by,

$$\vec{F} = L\vec{I}_{RF}(\omega) \times \vec{B} \tag{5.1}$$

where I_{RF} is the RF current flowing through the resonator, B is the strength of the magnetic field and L is the length of the nanoresonator.

When the driving current and thus the force oscillates at the resonant frequency the amplitude of the resonator becomes large and is recorded by the potential produced by the Lorentz force. Figure 5.2 shows the response of the amplitude and phase of the resonator as function of the drive frequency at magnetic fields of 6T.

The response of the resonator as a function of drive frequency can also give us information about the quality factor of the NR. The quality factor of the resonator

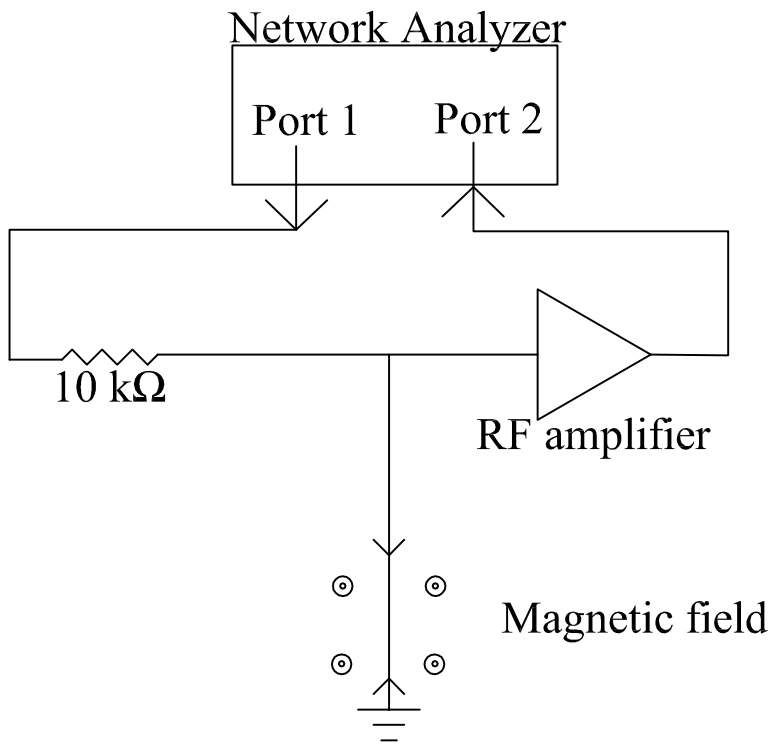

Figure 5.1: Circuit diagram for magnetomotive measurement

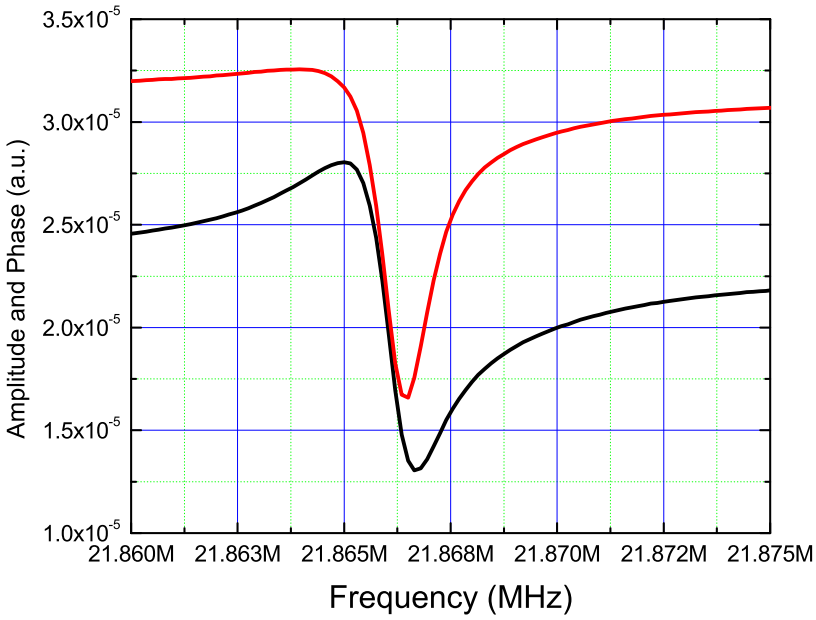

Figure 5.2: Amplitude (red line) and phase (black line) of the resonator as a function of frequency of current through the NR at a magnetic field of 6T

measured by this method is a combined effect of dissipation in resistive elements due to induced eddy currents i.e. loading by the external circuit in addition to the intrinsic dissipation. The electromechanical resistance of the beam is given by [37]

$$R_m = \frac{\zeta L^2 B^2 Q_0}{\omega_{NR} m} \tag{5.2}$$

where,

Q_0 is the intrinsic quality factor of the resonator

ω_{NR} is the resonant frequency of the NR,

ζ depends on the mode shape of resonator and is of order of unity and

m is the mass of the resonator

The dissipation mechanism because of this resistance is additive to the intrinsic dissipation Q_0^{-1}. So the total dissipation of the resonator $1/Q_L$ due to these two mechanisms is given by [37],

$$\frac{1}{Q_L} = \frac{1}{Q_0} + \frac{R_m \Re(Z_{ext})}{Q_0 Z_{ext}^2} \tag{5.3}$$

$$= \frac{1}{Q_0} + \frac{\zeta L^2 B^2 \Re(Z_{ext})}{\omega_0 m Z_{ext}^2} \tag{5.4}$$

where Z_{ext} is the total impedance of the measurement circuit.

To estimate the intrinsic quality factor of the resonator we measure the response of the resonator at different magnetic fields. The data is then fit with least square fit to obtain the quality factor at each magnetic field. Figure 5.3 shows the inverse of quality factor plotted as a function of the square of magnetic field. We estimate the intrinsic quality factor, Q_0 of the resonator by extrapolating the quality factor to zero magnetic field. This is calculated to be $1.20 \times 10^5 \pm 4 \times 10^3$.

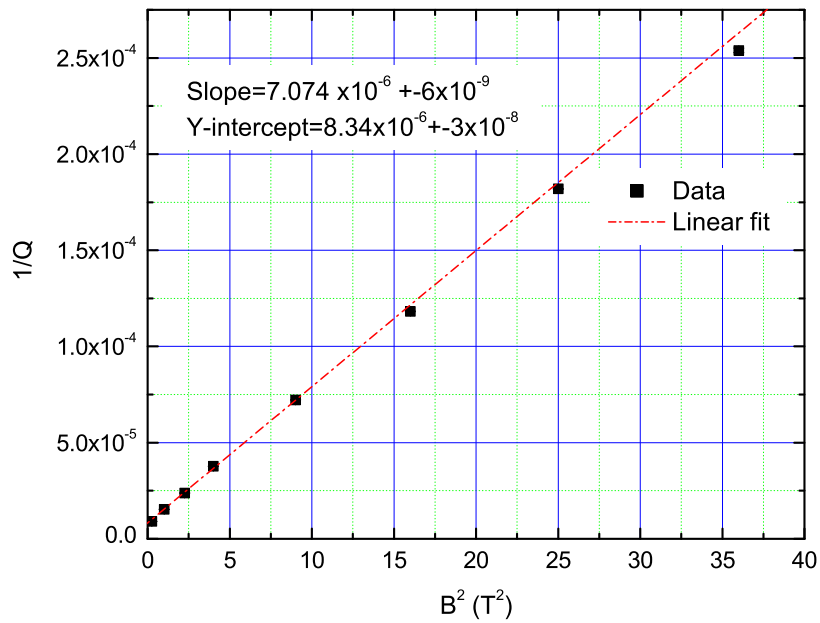

Figure 5.3: Quality factor of the resonator as a function of the magnetic field

5.1.2 Spring constant

The spring constant of the resonator can be estimated and cross checked in the following ways.

From the spring theory,

$$\omega = \sqrt{\frac{k}{m}} \tag{5.5}$$

Since we know the resonant frequency and the dimensions of the resonator it is quite straight forward to calculate the spring constant of the beam. For our device, the dimension of the resonator are $L = 9.5\mu m$, $w = 200nm$, $t_{Al} = 90nm$ and $t_{SiN} = 50nm$. Using these values and the density of Al(2.7gm/cc) and the SiN (3.0gm/cc) we calculate the mass of the resonator to be about $0.7 \times 10^{-}15kg$. Using this value of the mass and the resonant frequency we estimate the spring constant,k,

to be about 13.5 N/m. The calculation is just an approximation since we have no way of knowing if there is silicon attached to the bottom of the resonator, which makes mass uncertain.

Another way of estimating the value of spring constant is using the magnetomotive method. Using equation 5.4 and assuming $Z_{ext} = 50\Omega$ we can write,

$$\frac{1}{Q_L} = \frac{1}{Q_0} + \frac{\zeta l^2 B^2}{50\omega_0 m} \tag{5.6}$$

$$\frac{dQ_L^{-1}}{dB^2} = \frac{\zeta l^2 \omega_0}{50k} \tag{5.7}$$

This gives us a way to estimate the spring constant of the resonator using the slope of the plot shown in figure 5.3. Using the slope and other known values we calculate the spring constant to be 24. In this method, we assume that the external impedance is 50Ω. The actual impedance calculation would involve a complete circuit analysis for this measurement.

Another independent way of verifying the value of k estimated from above method is to drive the resonator and monitor the amplitude of the resonator. The circuit diagram for this measurement is shown in figure 5.4. For drive frequencies far away from the resonant frequency, the change in charge seen by the SSET is given by,

$$\delta q_{bkgnd} = C_{GNR} \delta V_{NR} \tag{5.8}$$

where,

C_{GNR} is the capacitance between NR gate and SSET island.

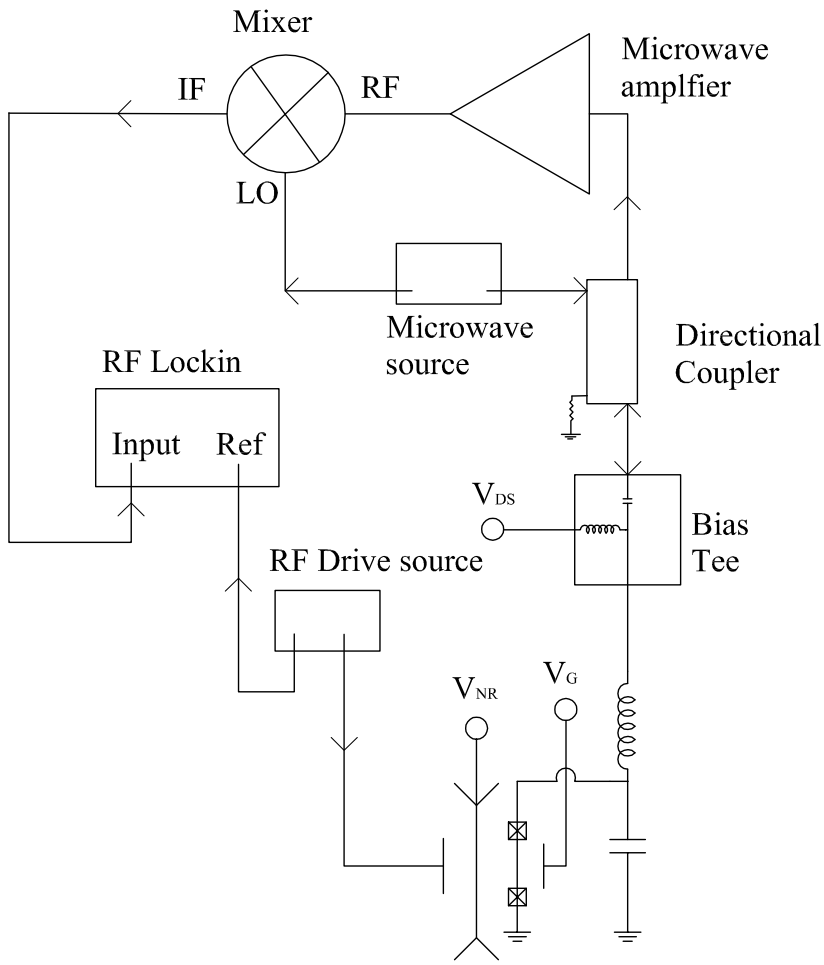

Figure 5.4: Simplified circuit diagram to drive the beam and measure its response

When the drive frequency is the same as the resonant frequency, the force applied by the drive signal is given by,

$$\delta F = \frac{C_{GB} V_{NR} \delta V_{NR}}{d_{GB}} \tag{5.9}$$

where

C_{GB} is the capacitance between NR gate and the NR and

d_{GB} is the distance between NR gate and the NR

The corresponding amplitude δx and the change in charge seen by SSET,δq_{res} are respectively given by,

$$\delta x = \frac{\delta F Q_0}{k} \tag{5.10}$$

$$\delta q_{res} = \frac{C_{NR} V_{NR} \delta x}{d} \tag{5.11}$$

$$= \frac{C_{NR} C_{GB} V_{NR}^2 Q_0 \delta V_{NR}}{d d_{GB} k} \tag{5.12}$$

where, d is the distance between the NR and the SSET

Figure 5.5 shows the data obtained by driving the resonator with $V_{NR} = 0.6V$. The plot also shows the harmonic oscillator fit. We use this fitting routine to obtain the resonant frequency, quality factor, amplitude and the background. For this data, we get $f_{res} = 21.890192MHz$, $Q = 67316 \pm 1688$, $Amplitude = 141.7\mu V$ and $background = 100\mu V$. Using,

$$\frac{\delta q_{res}}{\delta q_{bkgnd}} = \frac{Amplitude}{background} \sim 1.4$$

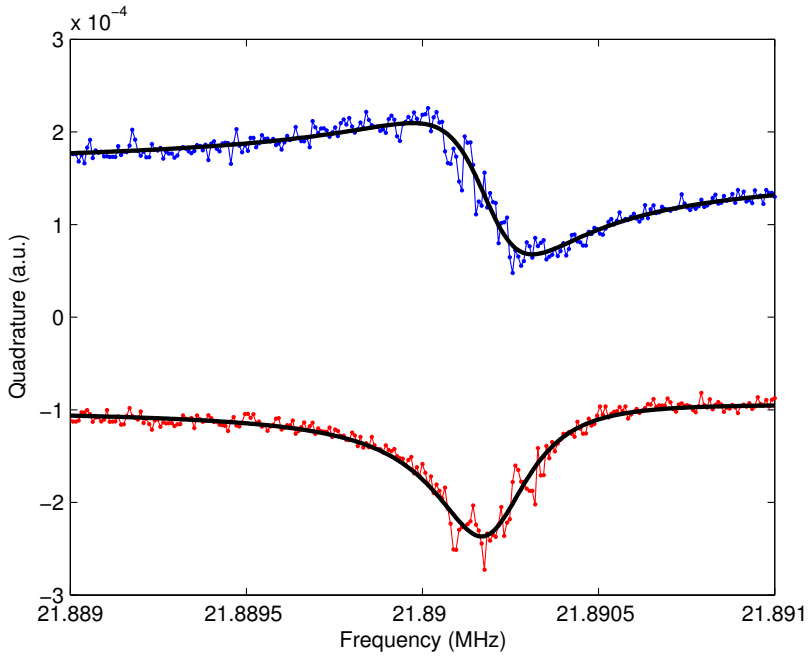

Figure 5.5: Response of the resonator as a function of drive frequency

and assuming $C_{GB} \approx C_{GNR}$ and using $C_{NR} = 36aF$ (see next section), we obtain the spring constant to be about 6. In this method we make the assumption that $C_{GB} \approx C_{GNR}$. We do not have an independent way of calculating the C_{GB}. This can introduce uncertainties in the calculation of the spring constant.

Since we do not have an accurate way of determining the spring constant, for all the further calculation we assume a spring constant value of 10.

5.2 SET Parameter Characterization

The parameters of the SET can be calculated from IV curves of the SET.

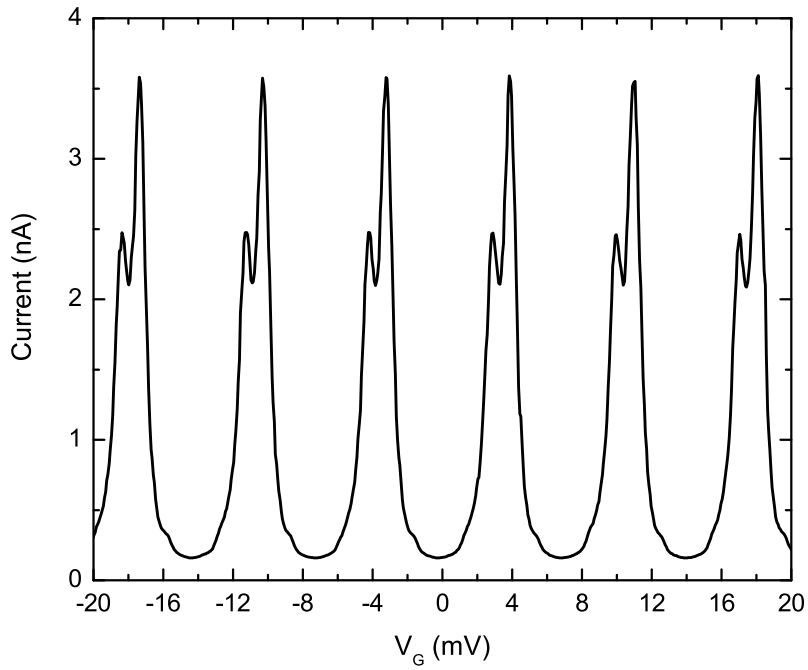

Figure 5.6: Current modulation of the SSET as a function of the SSET gate voltage

5.2.1 Capacitance of the device

The SET gate capacitance can be calculated from the gate modulation of the current. The periodicity of this coulomb blockade is given by $\Delta V_G = e/C_{GSET}$. Figure 5.6 shows the modulation of current through the SET as a function of SSET gate voltage. The number of peaks in each modulation depend on the V_{DS} bias. For instance, in figure 5.6 the SSET is biased very close to the JQP resonance and the double peak comes from the two JQP resonances.

The capacitance between the gate of the NR and the island, C_{GNR}, and between the NR and the island of SSET, C_{NR}, are calculated in a similar fashion by applying voltage to the NR gate and the NR respectively and monitoring the

modulation of the SSET current. The modulation curves for these two are shown in figures 5.7 and 5.8 respectively. The values of the various capacitances of the device are shown in table 5.1

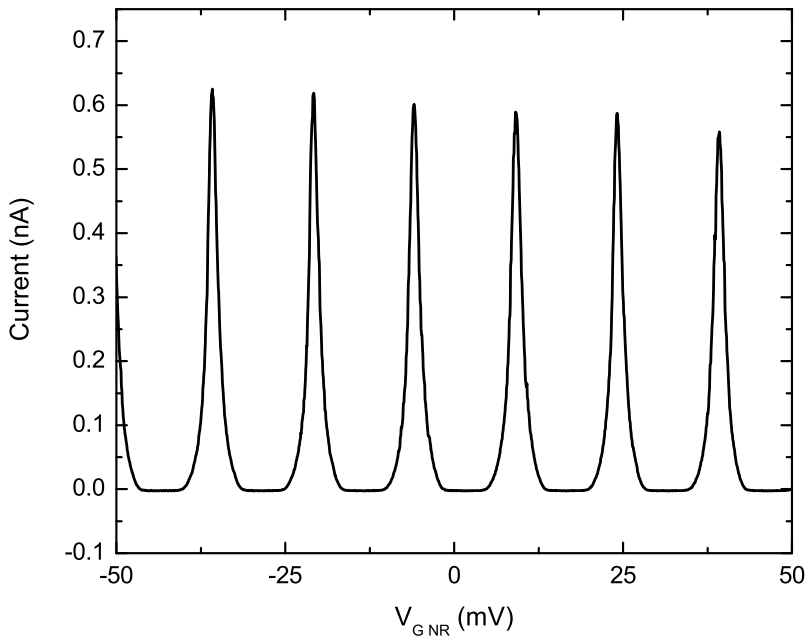

Figure 5.7: Current modulation of the SSET as a function of the NR gate voltage

The junction capacitance is calculated from the slopes of current feature in the $I_{DS}V_{DS}V_G$ map as shown in figure 5.9. This is an effect of the fact that the junction capacitance determines the energy required for transport of the charge carriers though the SSET. For detailed derivation of this, see reference [34] and references therein.

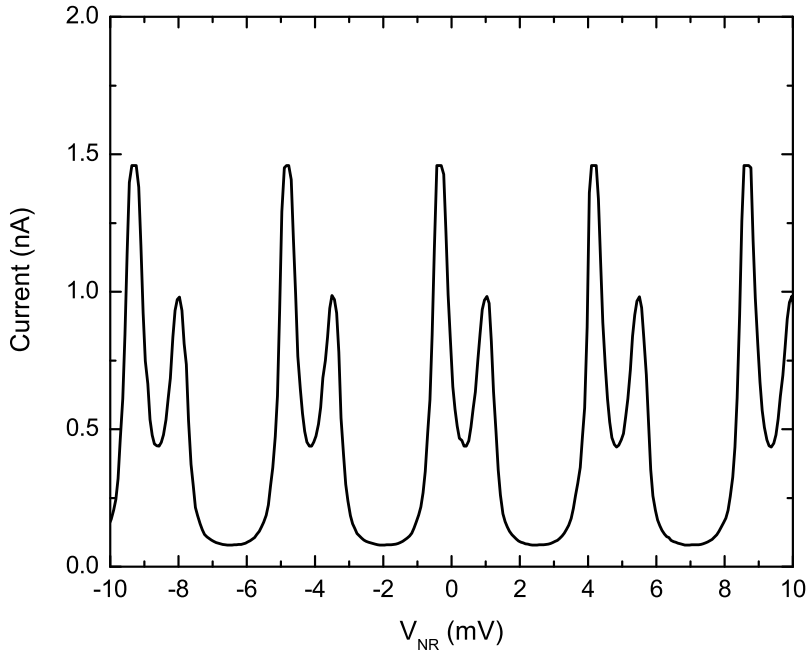

Figure 5.8: Current modulation of the SSET as a function of the NR voltage

5.2.2 Charging energy of the SSET

The charging energy, E_C can be calculated from the position of the DJQP and the crossing of JQP peaks from the origin. The peak of the DJQP is located at $eV_{DS} = 2E_C$ and the JQP crossing is at $eV_{DS} = 4E_C$. The charging energy of the SET can also be calculated from the value of the total capacitance $C_\Sigma = C_{J1} + C_{J2} + C_{GSSET} + C_{GNR} + C_{NR}$. The charging energy is related to the total capacitance of the SET by the following equation.

$$E_C = \frac{e^2}{2C_\Sigma} \tag{5.13}$$

The charging energy from these methods was calculated to be $175\mu eV \pm 4\mu eV$.

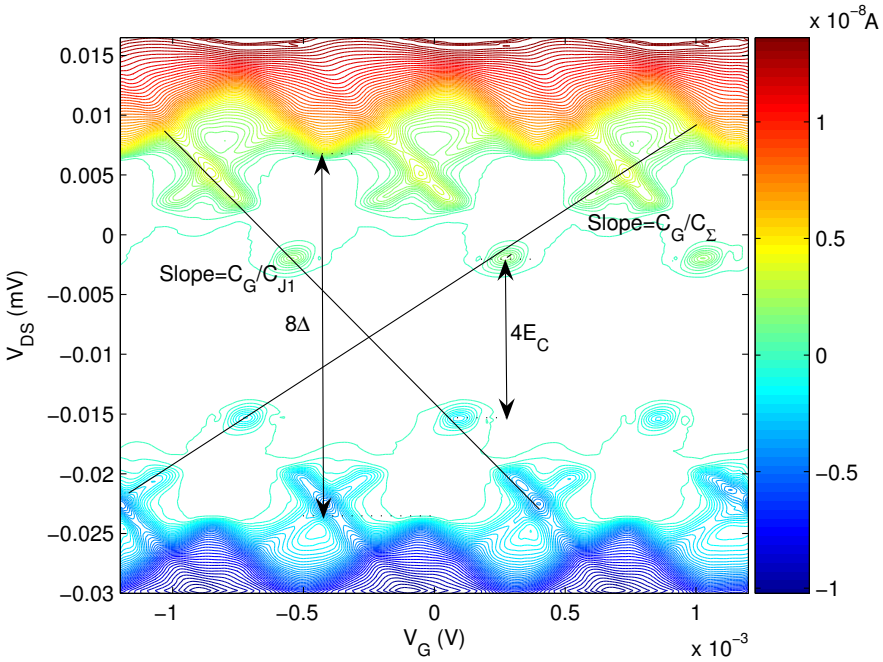

Figure 5.9: Current map of the SSET as a function of drain source voltage and gate voltage

Capacitance	Symbol	Value
Between SET and SSET gate	$C_G SET$	$22.6 \pm 0.6aF$
Between SET and NR gate	C_{GNR}	$10.7 \pm 0.1aF$
Between SET and NR	C_{NR}	$33.6 \pm 1aF$
Junction 1 of SSET	C_{J1}	$181 \pm 9aF$
Junction 2 of SSET	C_{J2}	$199 \pm 20aF$
Total Capacitance	C_Σ	449 ± 30

Table 5.1: Capacitance values of the device

5.2.3 Superconducting gap of the SSET

Since the material used for making the SSET is aluminum which is superconducting below 1.2K, the current through the SSET is suppressed for $eV_{DS} < 4\Delta$ due to the superconducting gap(Δ) of the island and the lead of the SSET. The current for $eV_{DS} < 4\Delta$ is primarily due to the resonant processes that are unique to the superconducting SETs. The current rises at $eV_{DS} = 4\Delta$ rapidly due to the onset of quasiparticle current. We use the position of this onset current to calculate the superconducting gap Δ (See figure 5.9).

5.2.4 Resistance of the SSET

The junction resistance of the SSET is calculated from the slope of I_{DS} against V_{DS} at $e|V_{DS}| >> 4\Delta$ as shown in figure 5.10.

5.2.5 Estimates of Josephson energy of the junctions

The Josephson energy for each junction is given by

$$E_J = \frac{R_Q \Delta}{8R_J} F(E_c/\Delta) \tag{5.14}$$

where, R_Q is the resistance quantum and the function F(x) describes the renormalization of E_J over the usual Ambegaokar-Baratoff value due to the finite value of E_C. In physical terms, the charging energy lowers the energy of the virtual state involved in a Josephson tunneling event, thus enhancing E_J. For detailed discussion of this effect see Ref. [35]. Using this analytical form, we obtain $F(x) = 1.26$ for our device and $E_{J1} = 13\mu V$ and $E_{J2} = 17\mu V$.

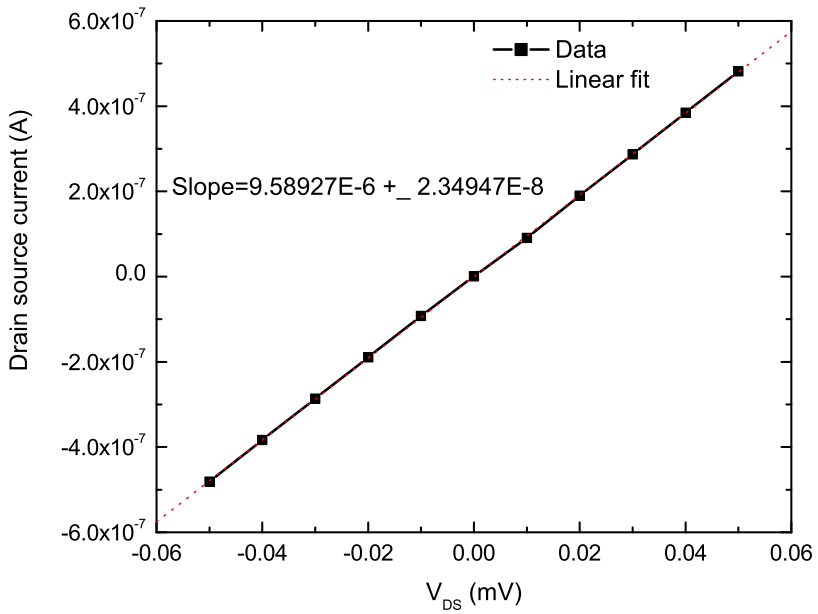

Figure 5.10: Plot of drain source current against the drain source voltage. The slope of the plot at V_{DS} much larger than the 4Δ gives the value of $1/R_{\Sigma}$.

5.3 Characterize RFSET

The RFSET is characterized by the following parameters.

5.3.1 Center frequency and bandwidth

To determine the center frequency and the bandwidth of the tank circuit we measure the noise spectra of the circuit with no current flowing through the SSET. Figure 5.11 shows the simplified circuit for doing this measurement. This includes the effect of the Berkshire and the Minicircuits amplifier. We then adjust the $V_{DS} \sim 20mV$ such that $0.2\mu A$ of current flows through the SSET. The shot noise because of this current through the SSET is amplified by the tank circuit and the noise spectra is then recorded. The two spectra are shown in figure 5.12. Figure 5.13 shows the difference between the two spectra. We can use this spectra to estimate the center frequency and the bandwidth of the tank circuit of RFSET. For our device we found the center frequency to be about 1.12GHz and the bandwidth to be about 100MHz. This gives a quality factor of about 10 for the tank circuit.

5.3.2 Gain and noise temperature

The gain of the RFSET measurement circuit can be calculated by doing shot noise measurement. In this measurement, we send a current though the SET and look at the shot noise that is amplified by the RFSET. This noise, P_N, is related to the gain and the bandwidth by equation [38]

$$P_N = G\Delta f(k_B T_n + 2e\eta I_{DS}) \tag{5.15}$$

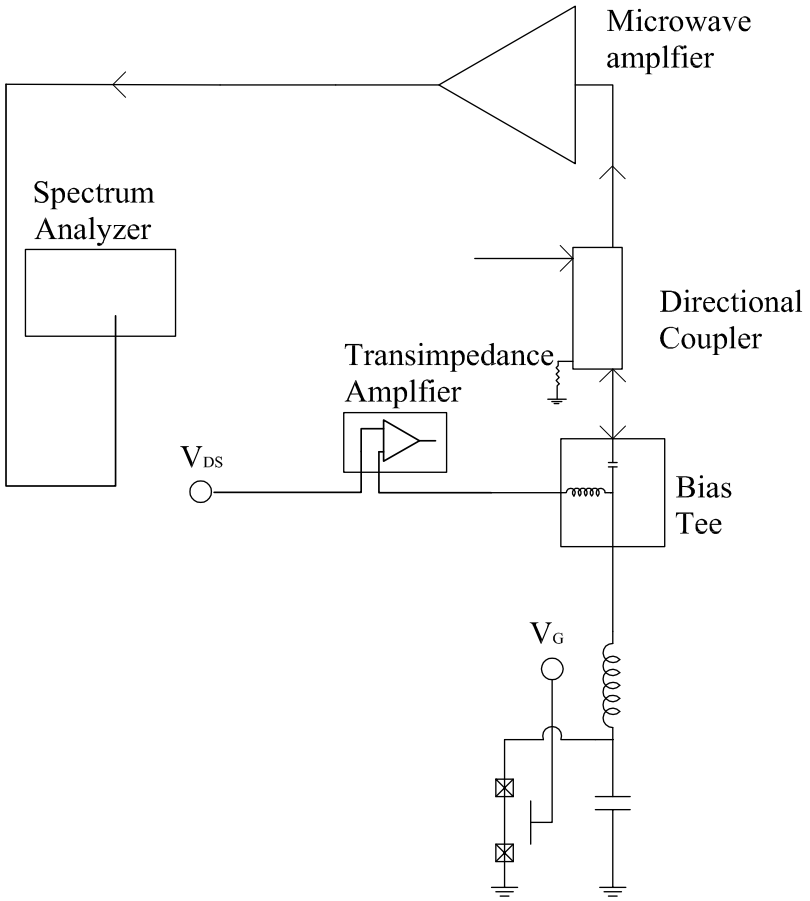

Figure 5.11: Simplified circuit for measuring frequency, bandwidth, gain and noise temperature of the measurement system

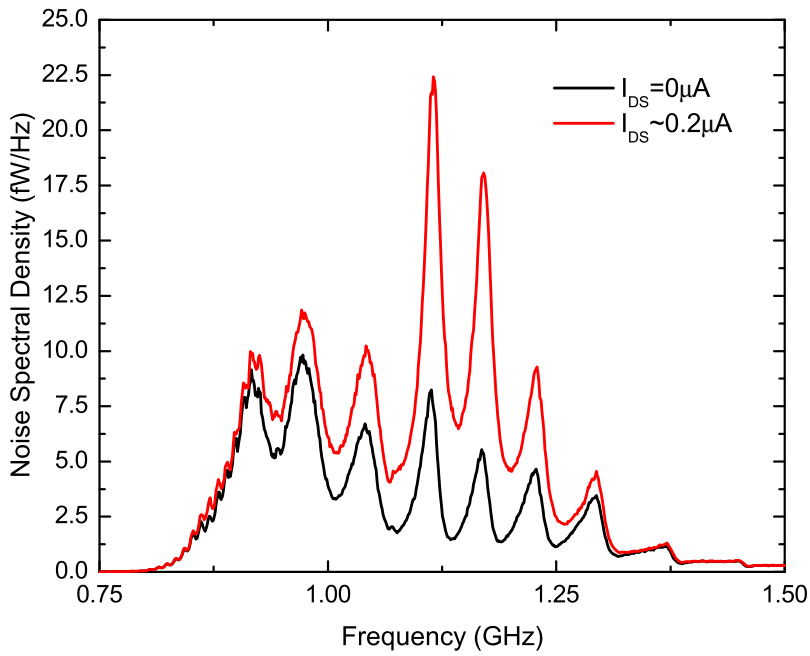

Figure 5.12: Plot of noise spectra with zero current and $0.2\mu A$ through the SSET.

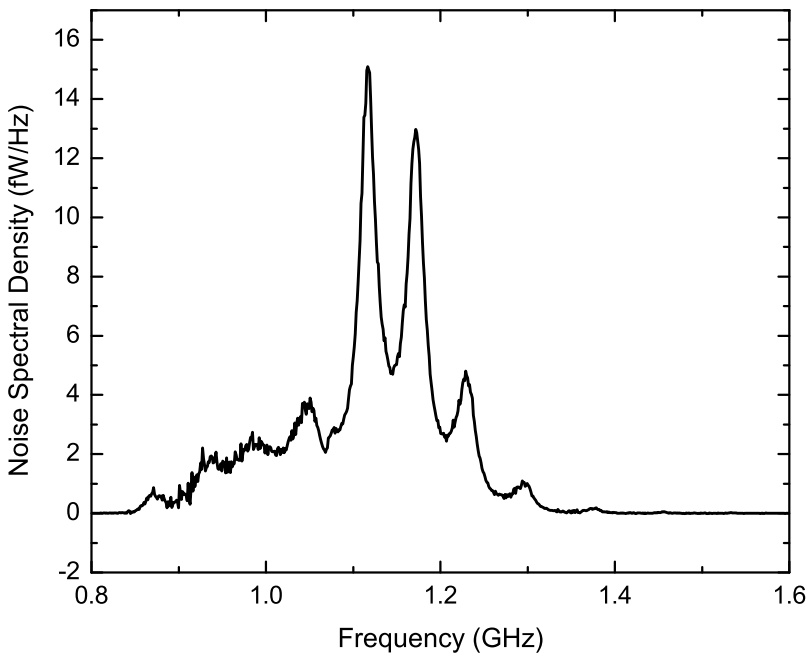

Figure 5.13: Plot of noise spectra shot noise of the RFSET

where, G is the gain of the system

Δf is the measurement bandwidth

k_B is the Boltzmann constant

T_n is the noise temperature of the system

e is the electronic charge

η is the constant determined by the transport mechanism and

I_{DS} is the current through the SSET.

Figure 5.11 shows the simplified circuit used to perform this measurement.

Figure 5.14 shows the plot of noise as a function of the current through the SSET. We use the slope and y-intercept of this plot to determine gain and the noise temperature of the RFSET system. For our device, we find the gain to be around

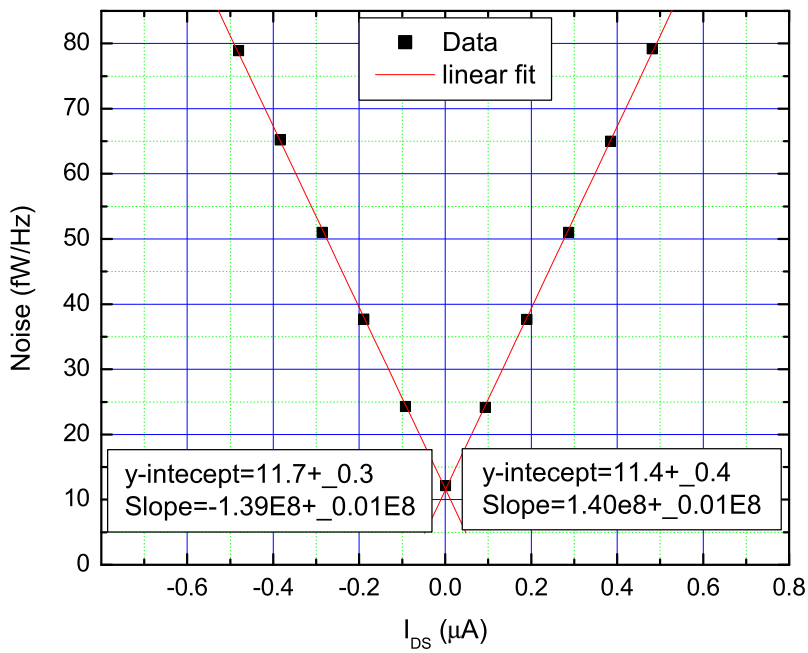

Figure 5.14: Plot of noise as a function of current through the RFSET

82dB with noise temperature of about 5K.

5.3.3 Reference signal calibration

We use a reference signal to calibrate all the signals that come out of the devices. We send a charge signal to the gate of the SET which can be calibrated using Bessel function calibration [36]. In this calibration technique we look for the drain source voltage where the coulomb blockade is approximately sinusoidal. Figure 5.15 shows the typical coulomb blockade curve and the bias point which is used to do the calibration.

The bias point for this measurement is the point of maximum sensitivity. We increase the amplitude of the input sinusoidal signal of a fixed frequency sent to the

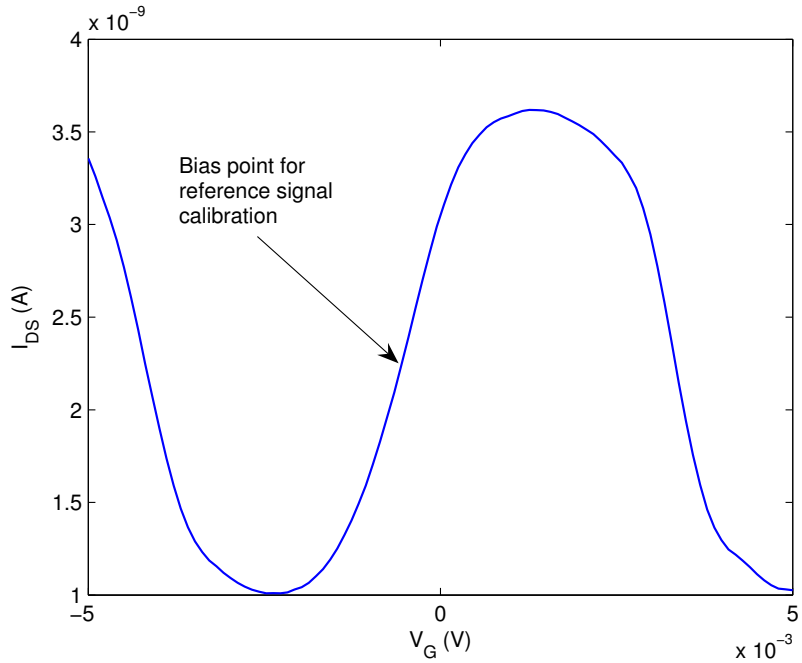

Figure 5.15: Typical coulomb blockade that is suitable for reference signal calibration

gate and monitor this signal after amplification by the RFSET using a RF lockin amplifier. The plot of output amplitude as a function of the amplitude of the input signal is the Bessel function of first kind [35]. By fitting the output amplitude we should be able to extract the amplitude of the signal at the source which would correspond to 1e at the SSET. The circuit for this measurement is shown in figure 5.16. Figure 5.17 shows the typical output of the measurement and the Bessel function fit to the data. For our device we found that the amplitude of $0.51V_{RMS}$ at source corresponds to 1e at the SSET.

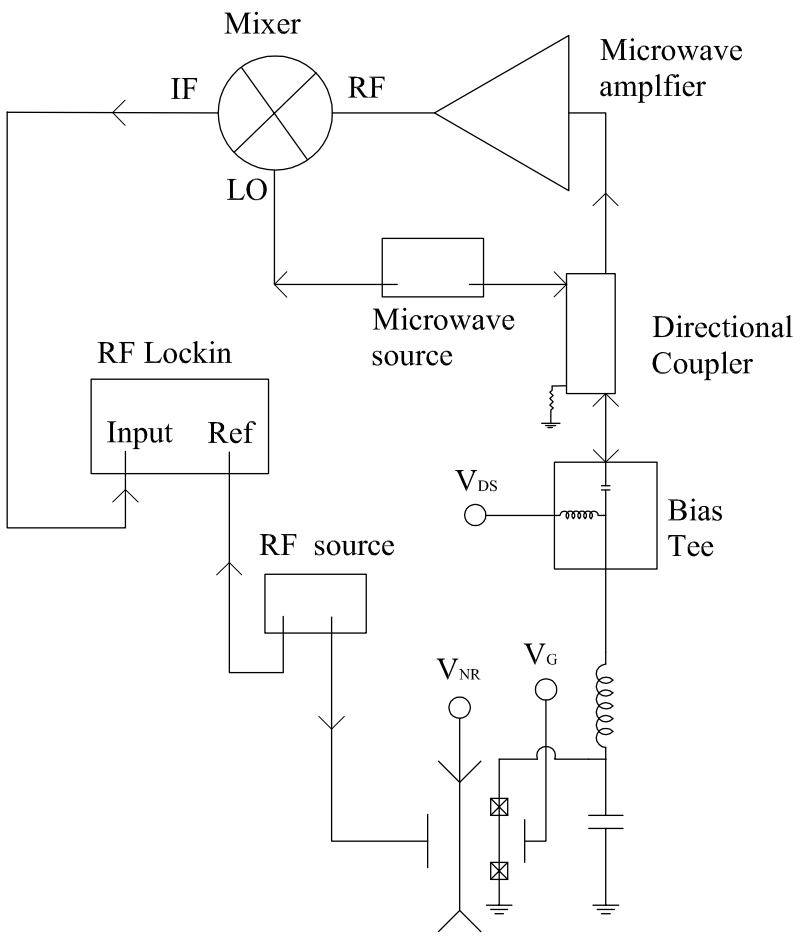

Figure 5.16: Circuit diagram for Bessel function calibration of the gate charge signal figure7.

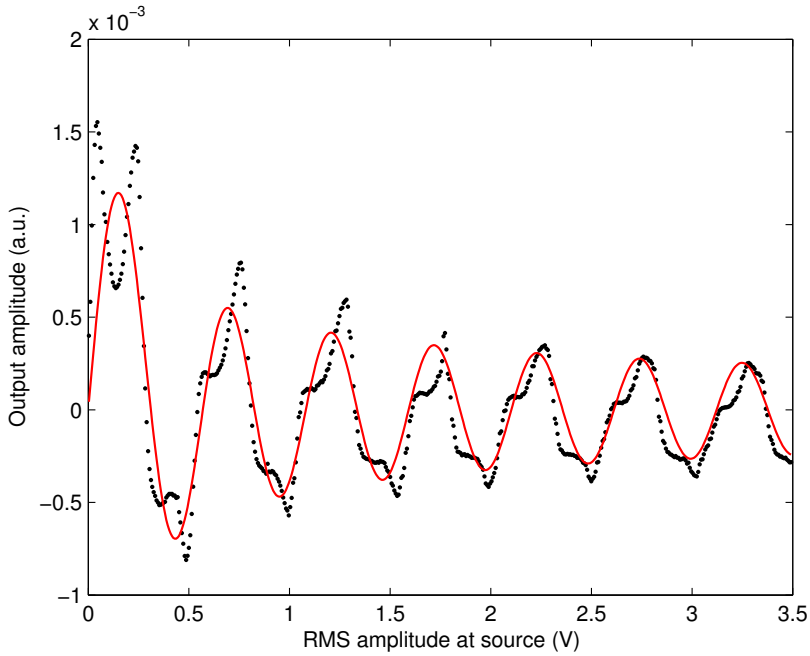

Figure 5.17: Plot of output amplitude as a function of RMS amplitude at the source. The red lines shows the Bessel fit to the data

5.3.4 Sensitivity

The sensitivity of the RFSET determines the how fast and accurately a measurement of charge can be done. Figure 5.18 shows the simplified circuit for doing the charge sensitivity measurements. To measure the charge sensitivity of the RF-SET, we bias the SSET at point of good gain and send the microwave signal to the SSET. To the gate of the NR we send a signal whose amplitude is calibrated as mentioned in the previous section. We then amplify the reflected microwave and observe it on spectrum analyzer. We look at the power in the sideband and the noise level around this sideband. Using these values, the measurement bandwidth and the amount of charge signal being sent to the SSET, we can calculate the charge

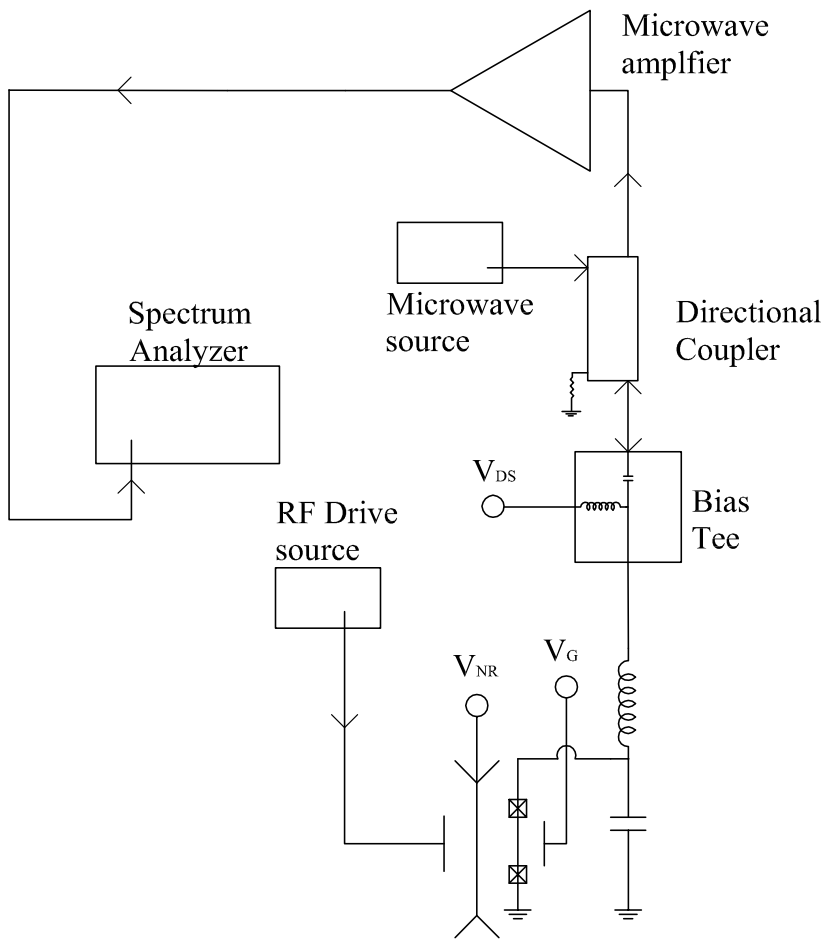

Figure 5.18: Simplified circuit to measure the charge sensitivity of the RFSET

sensitivity of the RFSET as [38],

$$\sqrt{S_q} = \delta q \sqrt{\frac{Noise}{Power}} \tag{5.16}$$

where,

δq is the amount of charge signal, in units of e_{RMS}, sent to the SSET

$Noise$ is the noise around the sideband in Watts/Hz

$Power$ is the power in the sideband in Watts

By optimizing the bias point of the SSET and the carrier amplitude we calculate the charge sensitivity to be $S_q = 3.3 \times 10^{-5} e_{RMS}/\sqrt{Hz}$.

5.4 Method for Backaction Measurement

As mentioned in the previous chapter, the backaction effect of the SSET manifests itself as an additional thermal bath to which the NR is connected. In essence, the SSET and NR system can be depicted as if the NR is connected to two independent thermal baths viz.

1. The thermal bath due of the environment (i.e. everything other than the SSET). The temperature of this bath is controlled by the dilution refrigerator temperature. The damping due to this bath is the intrinsic damping of the resonator.

2. The "non-equilibrium" bath of the SSET. It is possible to define a effective temperature for this non-equilibrium device. The effective temperature and the damping due to this bath is governed by the bias conditions of the SSET.

Since the resonator is now coupled to an additional bath i.e. the SSET, this bath must have some effect on the NR. This additional damping and temperature change the parameters of the resonator. To monitor the backaction effects of the SSET on the resonator, we look for changes in the resonator parameters as we change the SSET bath. We have looked for backaction effects of the SSET in the following two ways.

- Look for changes in the resonant frequency, damping and temperature of the NR as we increase the coupling between the resonator and the SSET while keeping the bias point of the SSET constant. In this case, the properties of the resonator should be determined by the environment bath at low couplings between the resonator and the SSET, while at stronger coupling the parameters of the resonator would be determined predominantly by the SSET bath.

- Look for changes in the resonant frequency, damping and temperature of the NR as we change the bias conditions of the SSET, while the coupling is constant.

5.4.1 Measuring spectra for the backaction

The simplified circuit for doing this backaction measurement is shown in figure 5.19. In the measurement, the SSET is DC biased by applying a drain source voltage, V_{DS}, and gate voltage, V_G. The coupling between the SSET and the resonator can be adjusted by changing the resonator voltage, V_{NR}. We use a current feedback system to hold the bias point of the SSET fixed against charge motion in

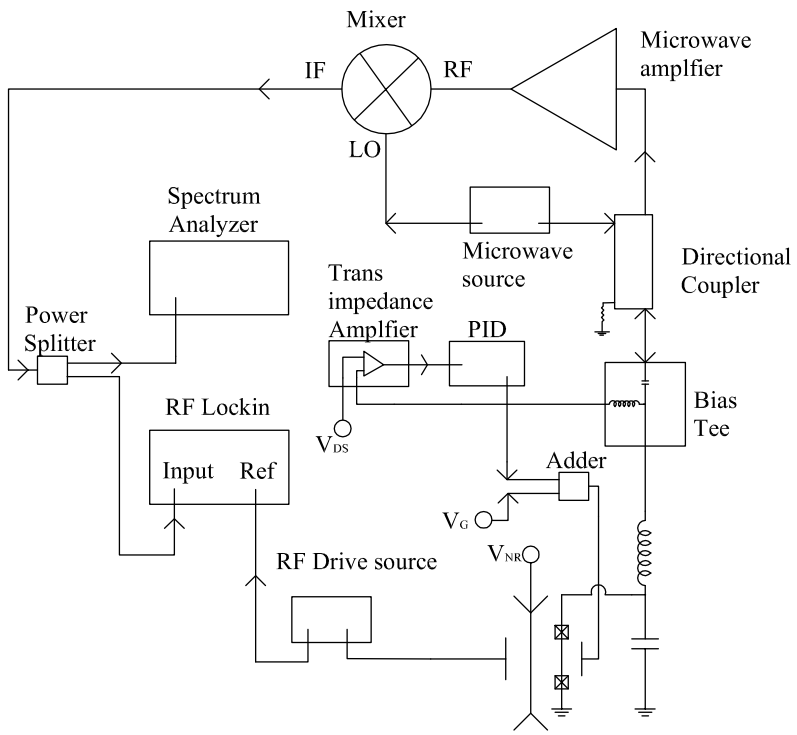

Figure 5.19: Circuit diagram for measuring the spectra

the substrate. In this scheme, we continously monitor the current through the SSET using a transimpedance amplifier and the measured current is fed into the feedback controller which outputs a gate signal depending on the error. This gate signal is added into the V_G using an adder circuit and sent to the gate of the SSET to keep the current through the SSET fixed. To obtain the mechanical noise spectra we send a microwave signal at the tank resonance of the RFSET to the device. The reflected microwave signal is modulated by the motion of the resonator. This reflected microwave is amplified and mixed down using the microwave source. The resulting spectra is then observed on the spectrum analyzer. The typical mechanical noise spectra observed on the spectrum analyzer is shown in figure 5.20. This spectra is then fitted with a Lorentzian to obtain the resonant frequency, the quality factor and the power under this curve. To monitor the gain of the system, during the measurement we also send a known amount of signal to the resonator gate. This signal also modulates the reflected microwave signal. We continously monitor this signal, after mixing down, using a RF lock-in amplifier. Since the gate signal has been calibrated, we know the equivalent charge it corresponds to at the SSET island. This technique is described in section 5.3.3 . To nullify any effects of change in gain affecting the calculation of power under the spectra we normalize the spectra using this signal. Since the calibration signal is known in units of electronic charge, the power units are converted into e^2/Hz.

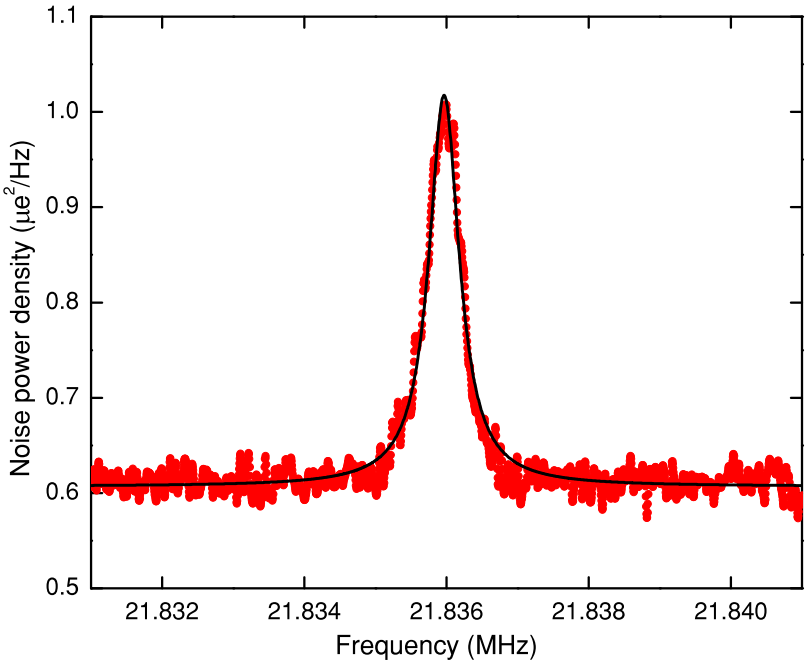

Figure 5.20: Mechanical noise spectrum and the Lorentzian fitting

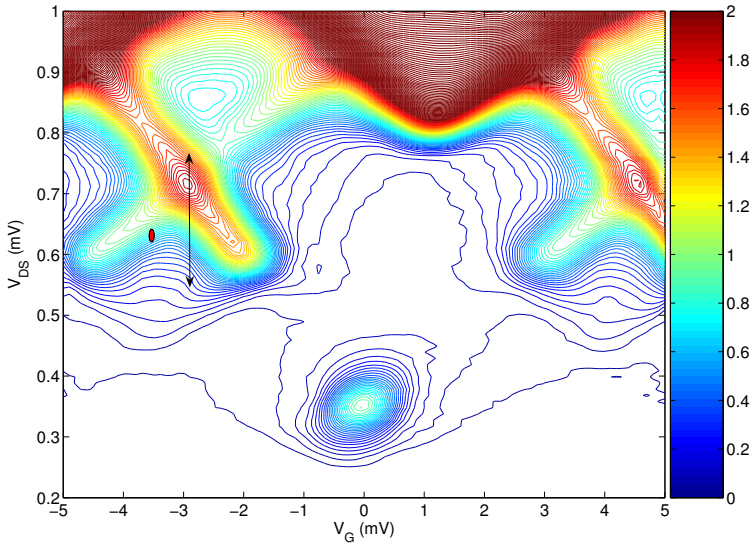

Figure 5.21: Amplitude of the microwave for optimal working of RFSET and for measuring backaction

5.5 Optimizing the RFSET for backaction measurements

For optimizing the functioning of the RFSET as a position detector, the amplitude of the microwave incident on the SSET should be roughly the size of the features in the $I - V_{DS} - V_G$ map as shown by the double headed arrow in figure 5.21. But that size of amplitude of microwave would sweep the SSET between bias points having different backaction effects. To be able to probe regions of SSET bias with similar backaction effects, we reduced the microwave amplitude by about 25dB. This amplitude is shown as the small red ellipse. This kept the bias point from sweeping different regions of backaction while keeping the RFSET sensitivity at reasonable levels. With this reduced microwave amplitude, the RFSET sensitivity was about $400\mu e_{RMS}/\sqrt{Hz}$.

Chapter 6

Results and Future Work

This chapter describes the experiments and results obtained during this doctoral research. The experiments to evaluate the effect are roughly done in three steps. First we determine the effect of the equilibrium (intrinsic) bath i.e. the behavior of the resonator in absence of backaction. Then we determine how the resonator changes as the coupling between the non-equilibrium bath, SSET, and the NR is changed. Then we keep the coupling between the SSET and the resonator the same but change the properties of the non-equilibrium bath and see how that affects the behavior of the NR. Unless specifically mentioned all the measurements are done near JQP resonances.

6.1 Effects of the intrinsic bath

To separate the effects of the intrinsic or the equilibrium bath on the NR, we measure the properties of the resonator at the lowest coupling between the resonator and the SSET i.e. $V_{NR} = 1V$.

6.1.1 Frequency

As a first step towards studying the backaction effects of the resonator, we biased the SSET at different points near JQP and DJQP and looked at the me-

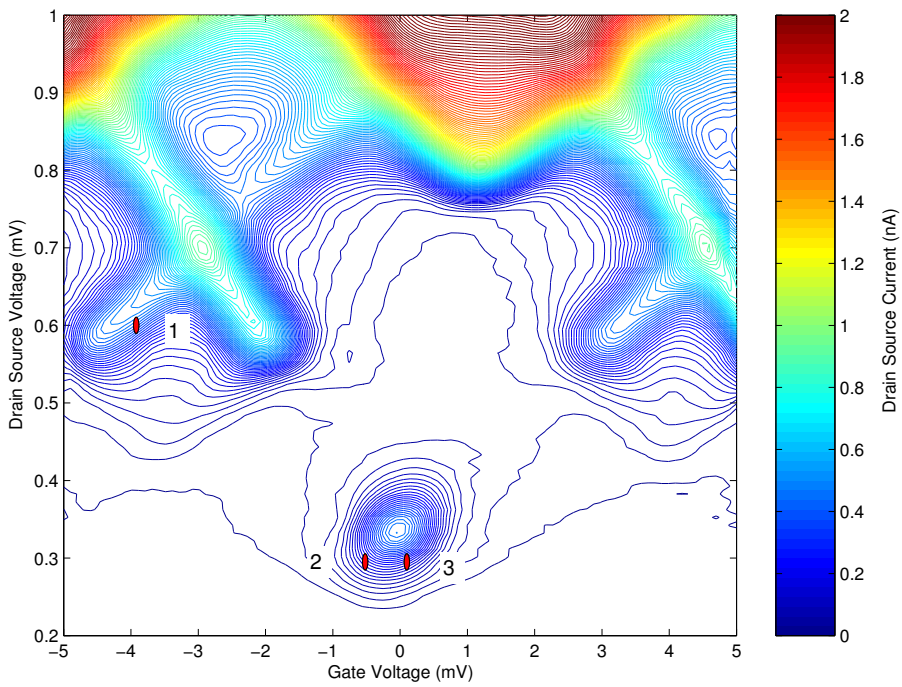

Figure 6.1: $I - V_{DS} - V_G$ map showing the bias point for evaluating the effect of coupling between the SSET and NR. Point 1 is near one of the JQP resonance and 2 and 3 are near DJQP

chanical frequency response. These bias points are shown on the $I - V_{DS} - V_G$ map shown in figure 6.1

Figure 6.2 shows the results of these frequency measurements at different dilution refrigerator temperatures. It is quite clear that the resonant frequency of the resonator is changing very little with the bias indicating negligible backaction effects of the SSET. The frequency of the resonator has a log dependence on temperature as shown in figure 6.3. This log dependence of the frequency on temperature has been a known phenomenon in glassy materials [27].

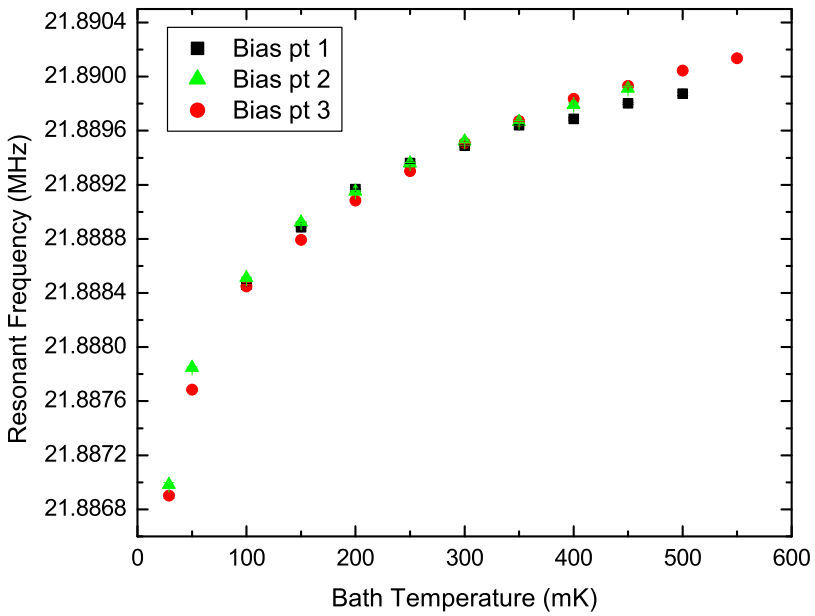

Figure 6.2: Plot of the resonant frequency as a function of bath temperature with SSET biased at different points at a coupling voltage, $V_{NR} = 1V$

.

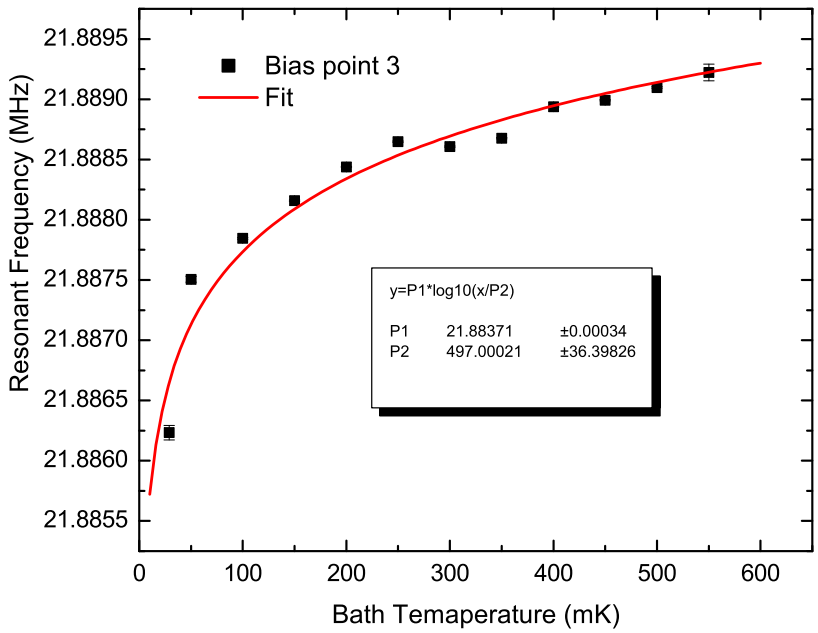

Figure 6.3: Intrinsic frequency of the resonator

6.1.2 Damping

The glassy nature of the material of the resonator is also evident in the damping of the resonator at $V_{NR} = 1V$. Figure 6.4 shows the damping of the resonator as a function of the fridge temperature for three different bias points. The scatter in the data of the damping does not indicate a dependence on the bias conditions of the SSET but is possibly due to the low signal to noise ratio at this coupling voltage. To improve the signal to noise ratio we average the spectra for up to 3 hours. If the resonant frequency of the NR has some Allan variance i.e. drift in resonant frequency with time , this would show up in the spectra as a lower Q of the resonator. For the calculation of resonant frequency and the integrated response of power spectra this does not produce an error as the average values of these quantities

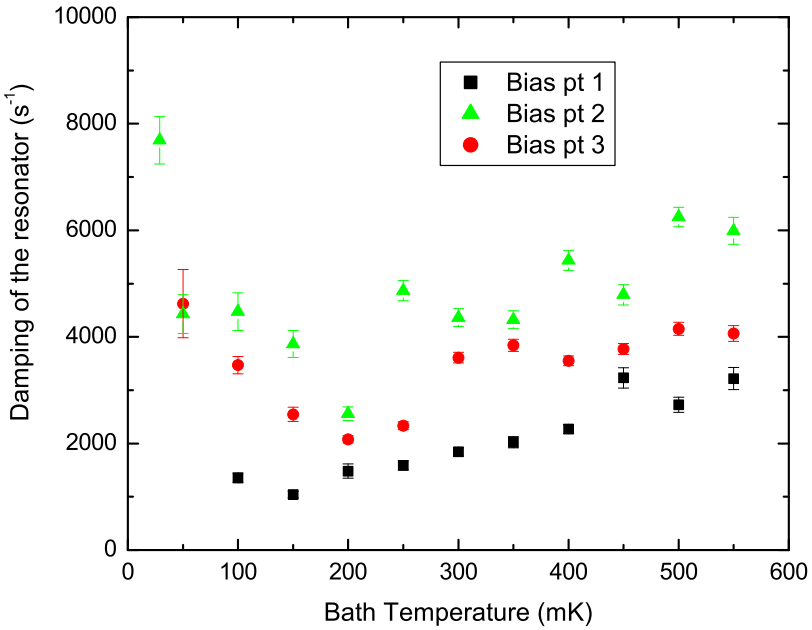

Figure 6.4: Intrinsic damping of the resonator

are not affected. Since the damping values evaluated at this coupling are not very reliable, for further calculations, we will use the intrinsic quality factor of 120000 obtained by magnetomotive technique.

6.1.3 Temperature of the resonator

At low couplings between the SSET and the resonator, it is expected that the resonator power would just linearly follow the temperature of the dilution refrigerator according to the equipartition theorem. Figure 6.5 shows the plot of power i.e. integrated response of the mechanical spectra as a function of dilution refrigerator temperature. As is evident from the figure, the plot is linear plot passing through the origin. Also the powers are independent of the bias point of the SSET. This

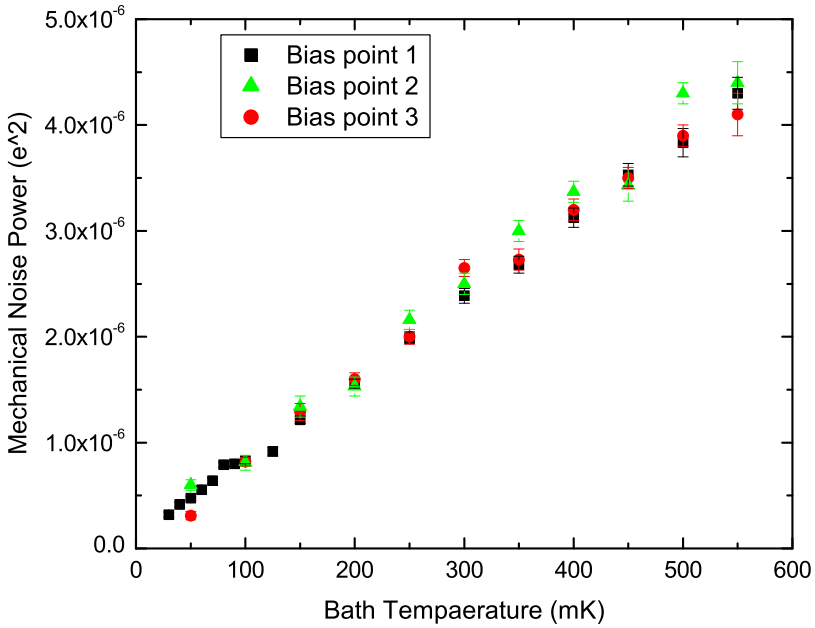

Figure 6.5: Power of the resonator

indicates that the system is indeed following the equipartition theorem at coupling voltage of 1V and we can use the power values in this measurement as a temperature calibration for measurements at higher coupling.

6.2 Effect of coupling the NR to SSET

In this set of measurements we look at the mechanical noise of the resonator as a function of the temperature for different coupling voltages. The SSET bias is fixed at $eV_{DS} = 3.4E_C$ and $\delta q_G = C_G V_G = 0.078e$ from the JQP resonance, for this measurement (bias point 1 in figure 6.1). At each coupling voltage we measure the mechanical noise from the resonator and fit it to a Lorentzian to obtain the resonant frequency, damping and the integrated response of the mechanical spectra.

We use the power value obtained at coupling of 1V as the temperature calibration to convert the integrated response obtained into temperature. After changing the coupling voltage each time we wait about 2 days at 4K for the charge noise to settle down. Using the equations 4.40 and 4.41 , we can calculate the effective temperature, for our bias point, to be about $T_{SSET} = 220mK$ and we expect the quality factor to be $Q_{SSET} = 14 \times 10^5/V_{NR}^2$.

6.2.1 Effect on the resonant frequency

As the coupling between the SSET and the resonator is increased the electrostatic force changes the spring constant of the resonator. This change in stiffness changes the resonant frequency of the resonator. This electrostatic effect is much larger than the changes in the resonant frequency introduced by the backaction effect. The plot of change in frequency as a function of the coupling voltage is shown in figure 6.6. Because of the electrostatic softening of the mechanical resonator the change in the spring constant is given by,

$$\Delta k = -\frac{d^2 C_{NR}}{dx^2} V_{NR} \tag{6.1}$$

which produces a change in frequency given by

$$\frac{\Delta\omega_{NR}}{\omega_{NR}} = -\frac{V_{NR}^2}{2k}\frac{d^2 C_{NR}}{dx^2} \tag{6.2}$$

Using the estimated value of the spring constant in chapter 4 and Femlab simulation to estimate $\frac{d^2 C_{NR}}{dx^2} = 0.004aF/nm^2$, we expect the frequency shift to be about $\frac{\Delta\omega_{NR}}{\omega_{NR}} = -2 \times 10^{-4} \times V_{NR}^2$. The slope of the plot gives the actual frequency shift

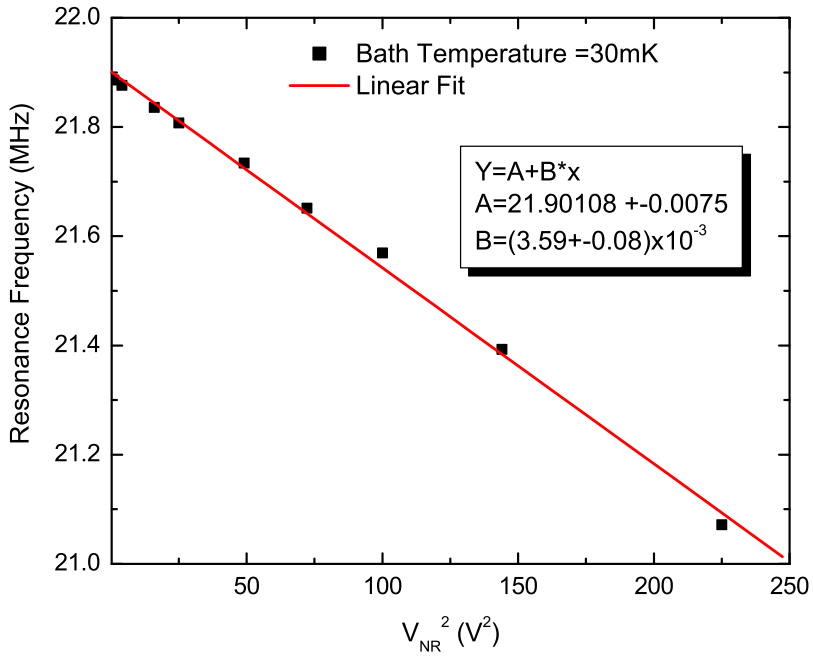

Figure 6.6: Plot of resonant frequency of the resonator as a function of the coupling voltage

to be $-1.6 \times 10^{-4} \times V_{NR}^2$. Also the quadratic dependence of the frequency shift on the coupling voltage indicates that the resonator is indeed mechanical and not some spurious electrical signal.

6.2.2 Effect on the damping of the resonator

The damping of the resonator is due to two different thermal baths. One is the equilibrium bath from the environment and second is due to the non-equilibrium bath of the SSET. The damping of the resonator at low couplings to the SSET is dominated by the intrinsic damping of the resonator. This damping due to the equilibrium bath is independent of the coupling voltage. The damping contribution from the SSET on the other hand has a quadratic dependence on the coupling voltage. So we should expect the damping of the resonator to be entirely due to the equilibrium bath at low couplings and move asymptotically towards the damping due to the SSET as the coupling is increased. We use the damping of the resonator at the lowest coupling, $V_{NR} = 1V$, to be the intrinsic coupling of the resonator. Figure 6.7 shows the theoretical damping that is expected from the SSET. Also shown is the intrinsic damping (at base temperature), which should not change with coupling voltage and the total damping of the resonator. Figure 6.8 shows the damping of the resonator as a function of coupling voltage for different dilution refrigerator temperature. The data show

1. The damping of resonator at low couplings is saturated to fixed value. This saturation value of damping is dependent on the temperature of the dilution

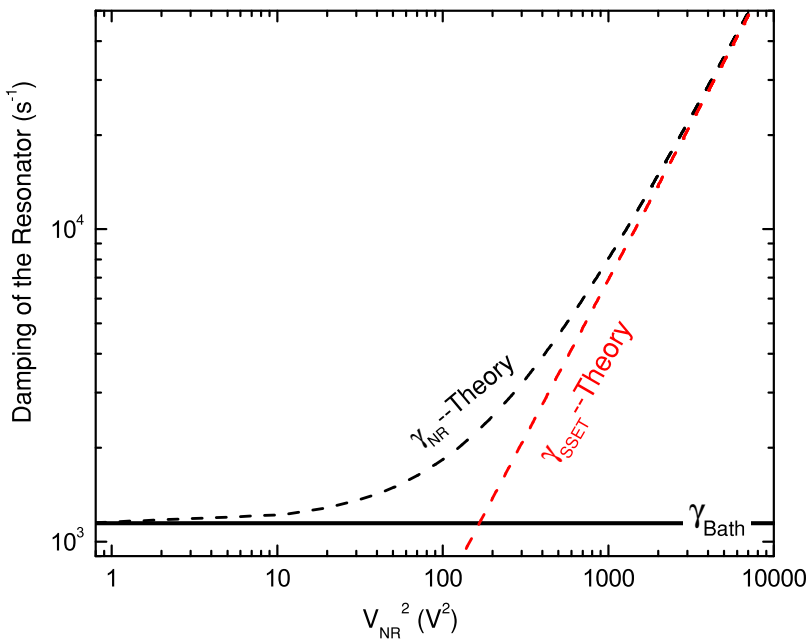

Figure 6.7: Expected damping of the SSET as a function of the coupling voltage

refrigerator. This is due to the glassy nature of the material and is from the thermal bath.

2. The damping of the resonator at strong couplings asymptotically shows a V_{NR}^2 behavior, irrespective of the temperature. This behavior is expected if the SSET is coupled to another bath, SSET in this case, electrostatically.

3. The damping from the SSET is about 14 times higher that what is expected from the theory. This discrepancy is under investigation but it could be the result of a)The discrepancy observed between theory and measured values of the current. b)The result of higher order processes which have been ignored in the theoretical calculations, or contribution from both of these.

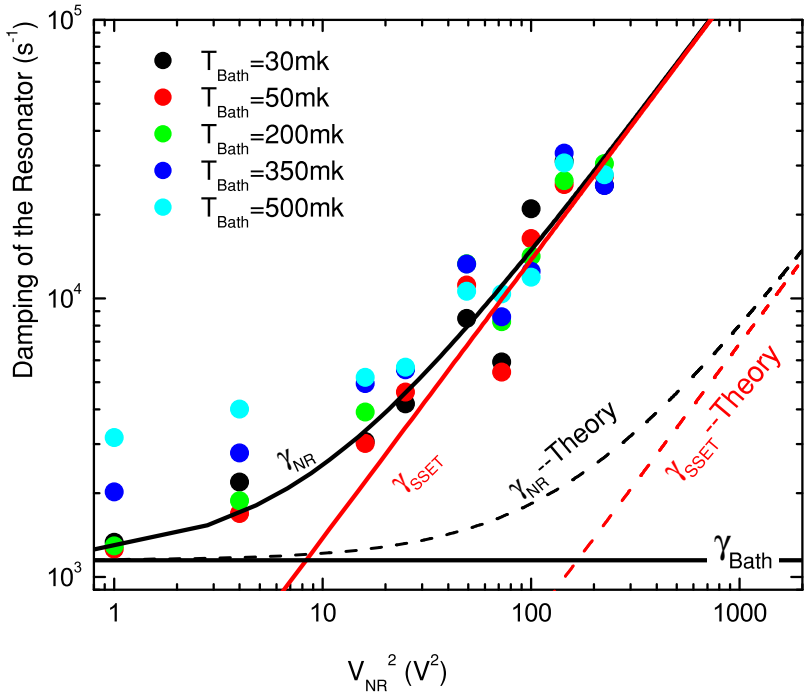

Figure 6.8: Damping of the NR as a function of the coupling voltage. Note that damping due to the bath has temperature dependence and we have shown just one of those γ_{Bath} lines for clarity

6.2.3 Effect on the temperature of the resonator

To evaluate the backaction effect of the SSET on the resonator, we looked at the temperature of the resonator as function of the dilution refrigerator temperature for different couplings. At each temperature of the dilution refrigerator and coupling, we measure the noise spectra of the resonator and measure the power under the curve. We then convert this power into units of e^2/Hz using the calibration signal that is sent to the gate of SSET (see chapter 4 for details). We then use the data taken at the coupling of 1V to calibrate this noise power into temperature. Figure

6.9 shows the effect of backaction of the SST on the temperature of the resonator. At low couplings between the NR and the SSET the temperature of the resonator

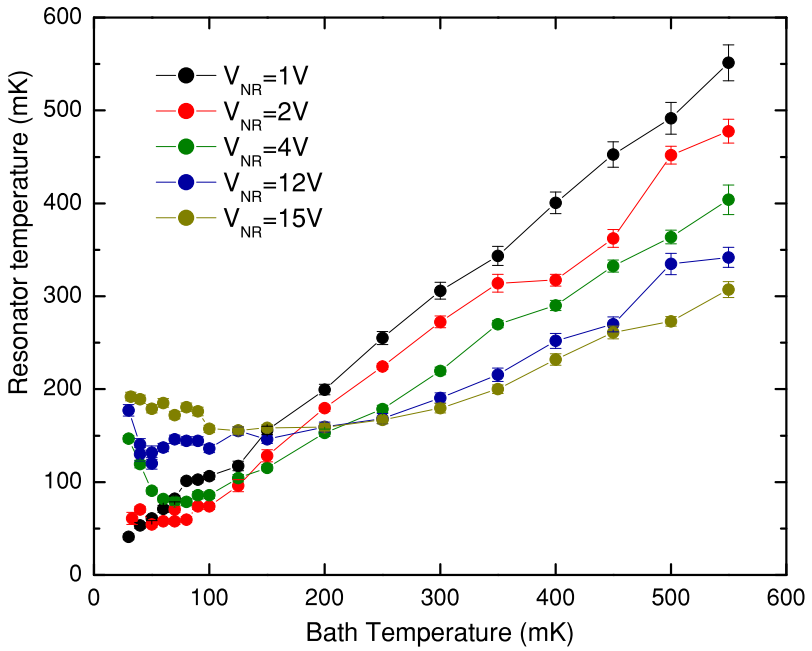

Figure 6.9: Temperature of the resonator as function of bath temperature for different couplings

follows the temperature of the dilution refrigerator . At higher couplings, the NR is coupled strongly to the SSET and it is expected that the NR would be clamped at the effective temperature of the resonator. From the figure 6.9 it is quite clear that as the coupling is increased, back-action effects are modifying the properties of the resonator. For dilution refrigerator temperatures below 200mK, the temperature of the resonator increases with coupling voltage and ultimately saturates to about 200mK at the highest coupling voltage. For bath temperatures above 200mK, we see the counter-intuitive effect of cooling as we increase the coupling between an

noisy device, SSET, and the NR. The fact that backaction effects become obvious at lower temperature at lower couplings is related to the fact that the damping of the resonator is lower at lower temperatures making SSET effects the dominant source.

6.3 Effect of Changing the SSET Bias Point

To further study the backaction effects of the SSET, we fix the coupling between the SSET and the NR and change the bias conditions of the SSET. Since the damping and the effective temperature of the SSET bath depend on the bias conditions, we expect to see the behavior of the NR altered as we move from one bias point to another. For these measurements we chose to arbitrarily bias the SSET at $V_{DS} = 4E_C - 100\mu eV$ and the gate voltage of the SSET is varied such that we sweep across the two JQP resonances. During this set of measurements, the temperature of the fridge was kept at the base temperature $\sim 30mK$ and the coupling voltage was fixed at $V_{NR} = 5V$. Figure 6.10 shows the measured current as we change the gate voltage to move across the two JQP resonances. The difference in the current peaks indicates the asymmetry in the junction resistances. The figure also shows the current expected from the theory [33][29]. It is clear that the measured value of current is significantly different from the theory. This behavior has been observed in other work [40] and the origin of this discrepancy is not known.

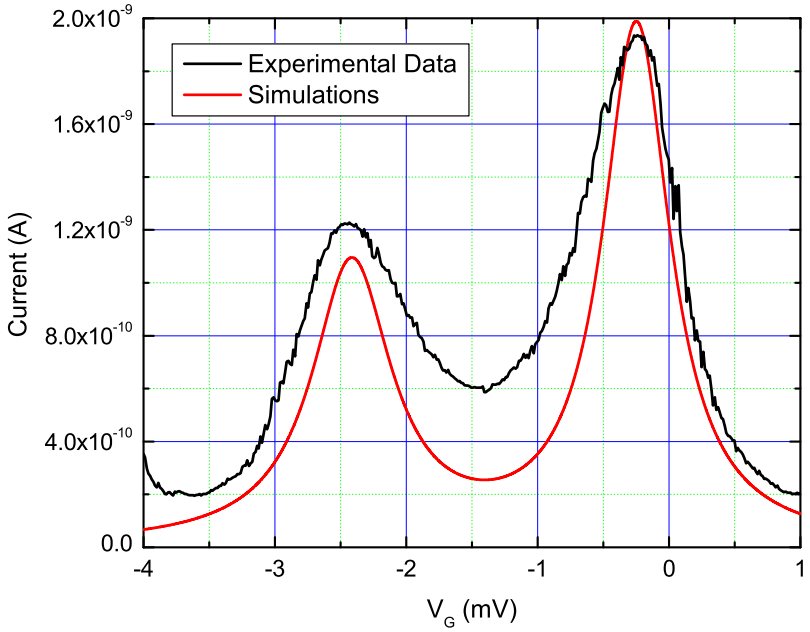

Figure 6.10: The measured value and theoretical prediction for the current as we sweep across the two JQP peaks

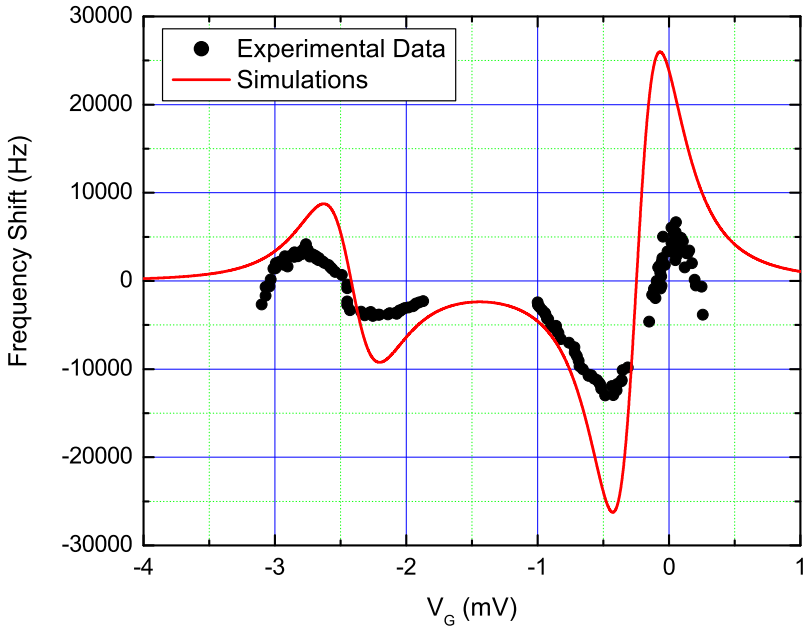

Figure 6.11: The measured value and theoretical prediction for the frequency shift as we sweep across the two JQP peaks

6.3.1 Effect on resonant frequency

Figure 6.11 shows the shift in frequency of the resonator as we sweep the gate voltage of the SSET across the two JQP resonances. The figure also shows the shift in frequency expected from the theoretical considerations [33][29]. To produce the data for shift in resonant frequency we arbitrarily chose a fixed frequency value and subtracted it from the resonant frequency data. The measured values qualitatively agree with the theory. The rounding of the experimental data is due to the averaging effect of changes in bias point. The bias point of the SSET is changing both due to the charge fluctuations and due to the microwave being applied for operation of the RFSET.

6.3.2 Effect on the damping of the NR

Figure 6.13 shows the total damping of the resonator as we sweep the gate voltage across the two JQP resonances. For certain bias conditions of the SSET, it is possible for the damping and the effective temperature of the SSET to be negative (see equations 4.40 and 4.41). Figure 6.12 shows the region where the damping and the effective temperature are positive. When the bias point is in between the two JQP resonances, the measured value of the damping qualitatively follow the behavior expected from the theory. Again the damping we observe experimentally is 14 times higher than expected. The simulation for the damping shown in figure 6.13 is obtained by multiplying the factor 14 to the theoretical values[33][29] of the SSET damping. For the region beyond the two JQP peaks (the dark yellow region),

the damping and effective temperature are negative. In this region, the damping obtained experimentally deviates significantly from the theoretical values[33][29].

To understand this behavior, we need to look at the actual interaction between the SSET and NR. At any particular bias point of the SSET, the motion of the resonator causes the current or the dynamic resistance of the SSET to change. This happens because of the shifts in bias point of the SSET as the resonator moves. If the motion of the resonator is small enough, the response of the SSET is linear. For large amplitude of motion of the resonator, the bias point of the SSET can shift between points of negative and positive damping. When the SSET is biased in a negative damping region, the resonator is being driven by the SSET. In this regime, the SSET is dumping energy continously into the resonator which increases its amplitude. For large enough amplitude of the resonator, the linear response assumption is no longer valid and the theory breaks down. The resonator amplitude continues to grow until the amplitude is large enough that it changes bias point of the SSET to positive damping regime for part of the oscillation cycle. To evaluate the negative damping regime of the SSET theoretically we need to consider the evolution of this system in the strong coupling regime. Also note that since we can only measure the width of the resonance to determine the damping of the resonator, the experimentally determined values of damping would always be positive, even if the resonator was being driven. Figure 6.14 shows the absolute value of damping calculated theoretically along with the experimental data.

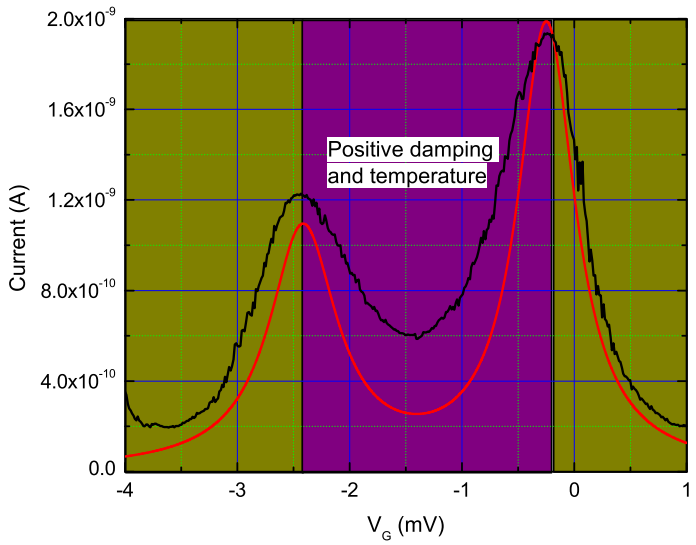

Figure 6.12: Plot of current as a function of gate voltage showing regions of positive and negative damping

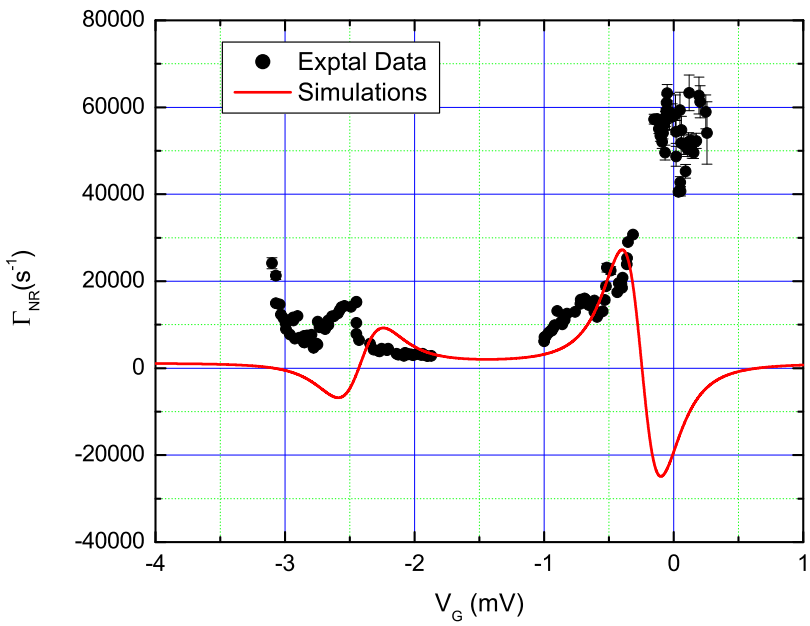

Figure 6.13: The measured value and theoretical prediction for the damping of the resonator as we sweep across the two JQP peaks

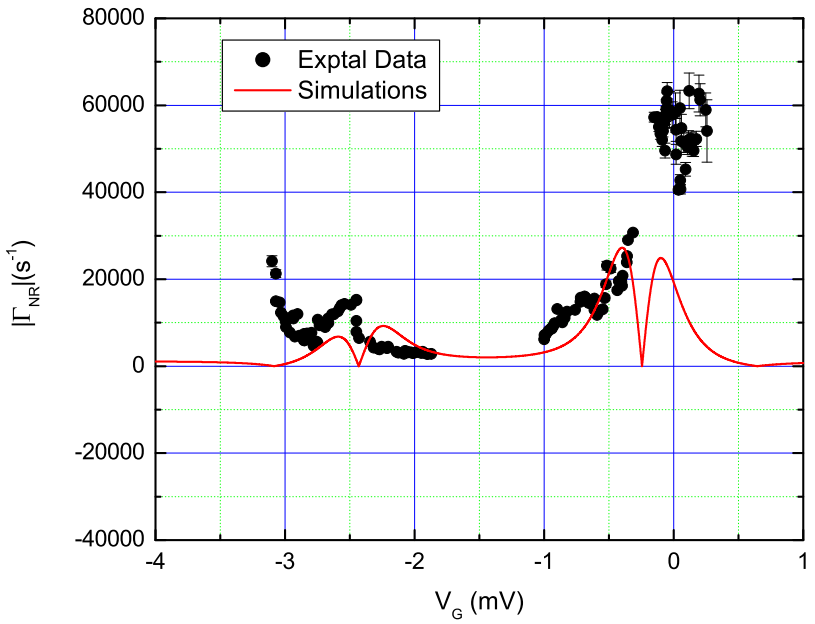

Figure 6.14: The measured value and theoretical prediction for the absolute value of damping of the resonator as we sweep across the two JQP peaks

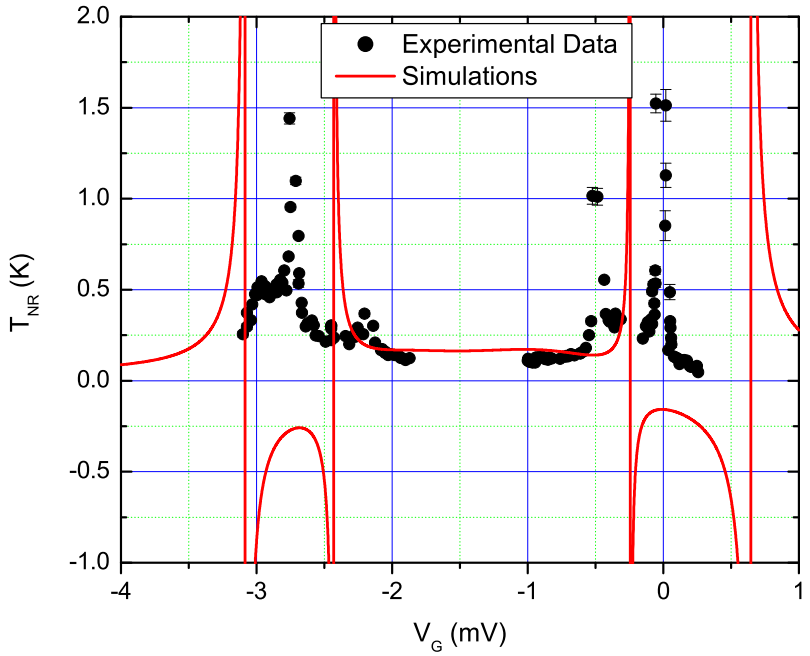

Figure 6.15: The measured value and theoretical prediction for the temperature of the resonator as we sweep across the two JQP peaks

6.3.3 Effect on the Temperature of the NR

Figure 6.15 shows the temperature of the resonator as a function of the gate voltage. For the region between the two JQP resonances, the temperature of the resonator more or less saturates, as expected, as we move away from the peaks. In the experimental data, there are two peaks near each JQP resonance. Again during measurements we can measure only the power under the mechanical spectrum which would always be positive. The negative temperature of the resonator shown by the simulations just imply that the resonator is being driven by the SSET. Using equation 4.29, we expect the spikes in the resonator temperature when the intrinsic

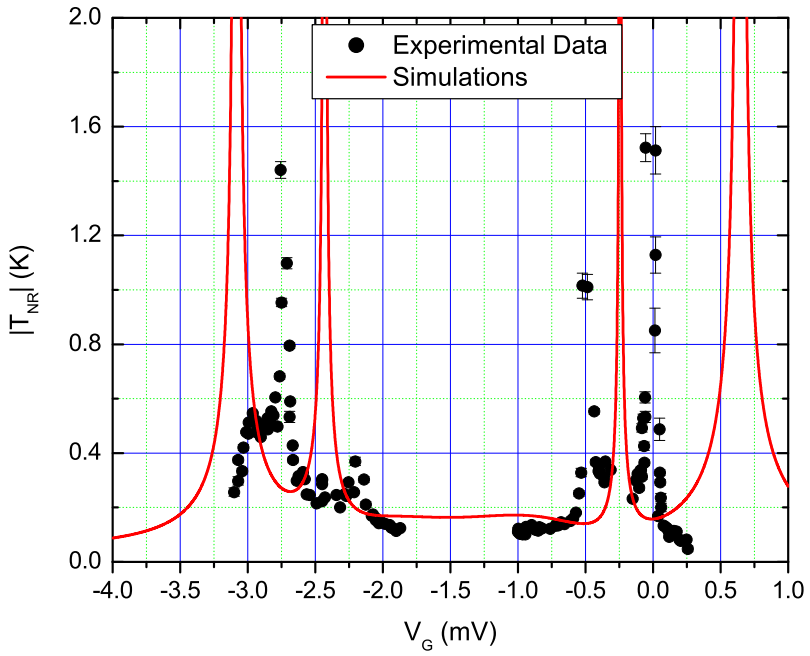

Figure 6.16: The measured value and theoretical prediction for the absolute value of temperature of the resonator as we sweep across the two JQP peaks

damping of the resonator is canceled by the negative damping due to the SSET. We suspect that the position of the spikes deviate from what is predicted by the theory due to the fact that the damping of the SSET does not quite follow the expected behavior. Again since we can only measure the integrated response i.e. area under the curve, experimental determination of temperature always gives positive values. Figure 6.16 shows the absolute value of calculated temperature of the resonator as a function of the gate voltage along with the experimental values.

6.4 Backaction Effects near DJQP

We also briefly looked at the behavior of the resonator when the SSET is biased near the DJQP. Studying the device at DJQP was difficult because of the following two reasons.

1. The backaction effects are stronger at DJQP as compared to JQP by a factor given by $(\Gamma/E_J)^4 \sim 100$ where Γ is the quasiparticle decay rate and E_J is the Josephson energy. To improve the signal to noise ratio of the mechanical spectra, we had to increase the coupling between the SSET and the NR. But for these bias voltages on the NR, if the SSET is biased near DJQP, the interaction is already in the strong coupling regime where the linear response theory breaks down.

2. Near DJQP, the regions of strongest backaction effects are also the regions where the gain of the RFSET are minimal. This makes probing these regions difficult.

Nevertheless, we were able to probe the region around the DJQP resonance to see if the behavior was consistent with what is expected from the theory. Figure 6.17 shows the $I - V_{DS} - V_G$ map around DJQP and the four bias points where we looked at mechanical spectra of the resonator. Points 1 and 2 are in the region where the SSET has negative damping and temperature. The spectra at these bias points show driven response with very high quality factors. Points 3 and 4 are in the region of positive damping and effective temperature of the SSET. At these bias points we see damped response of the resonator. The gain of the RFSET at points 1 and 2 is zero. This makes it difficult to calculate the temperature of the resonator when SSET is biased at these points. The ordinate of the spectra are therefore in raw power units and is not normalized to charge units. Although it is possible to normalize spectra for points 3 and 4, we have plotted the raw spectra for comparison with spectra obtained at points 1 and 2.

6.5 Effect of NR motion on the SSET

The interaction between the NR and the SSET changes the properties of the $I - V_{DS} - V_G$ curves. The effect of the motion of the resonator on the SSET can be observed by looking at the $I - V_{DS} - V_G$ curves of the SSET at different coupling voltages.

Figure 6.18 shows the $I - V_{DS} - V_G$ map of the SSET near JQP for different coupling voltages. At zero coupling voltage, the $I - V_{DS} - V_G$ map shows the two JQP resonances crossing each other at $V_{DS} \sim 0.7mV$. This map is smooth with no

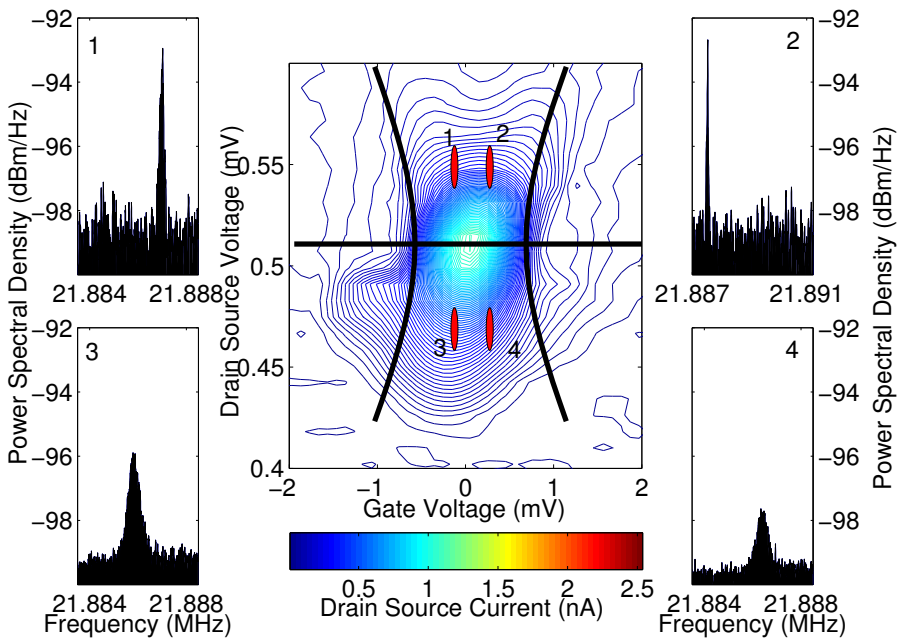

Figure 6.17: Backaction effects on NR with SSET biased near DJQP resonance distortions. As we increase the coupling we start seeing a few effects.

- At $V_{DS} \sim 0.8V$ we see the distortion of the JQP resonance. The slope of this distortion is roughly twice that of the JQP resonance. The slopes of the resonances indicate the electrostatic energy required for the current transport mechanism (see section 5.2). Thus the distortion of the $I - V_{DS} - V_G$ map might indicate that, at larger couplings between the SSET and the NR, there are additional current transport mechanisms in the SSET which involve the motion of the resonator.

- Some unknown electromechanical features start appearing near the JQP resonances. These resonances are not predicted by the theory. If the SSET is biased in this region, we see a mechanical response with quality factors as high a 600000.

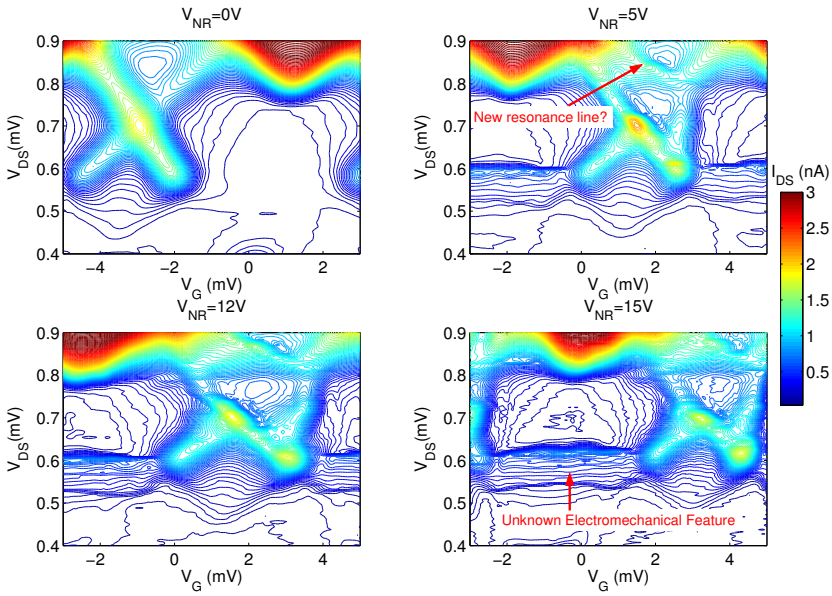

Figure 6.18: Distortion of the IV curve near JQP resonance due to coupling to the NR

The study of these features is of interest and should be pursued in the near future.

A similar distortion of the $I - V_{DS} - V_G$ curves near the DJQP is also observed as shown in figure 6.19. The first subplot shows the $I - V_{DS} - V_G$ curve of the SSET near the DJQP with the NR grounded. The plot has a pink shaded region which indicates the region of bias where the SSET damping and effective temperature are negative. In the rest of the area the damping and effective temperature are positive. The black solid lines indicate the approximate boundary between the regimes of positive and negative damping of the SSET. As the coupling between the SSET and the resonator is increased, the DJQP resonance distorts along this boundary. For coupling voltages above $V_{NR} = 2V$, the current in the negative damping region above the DJQP resonance (i.e. for $V_{DS} > 0.125mV$ in the figure) reduces to zero.

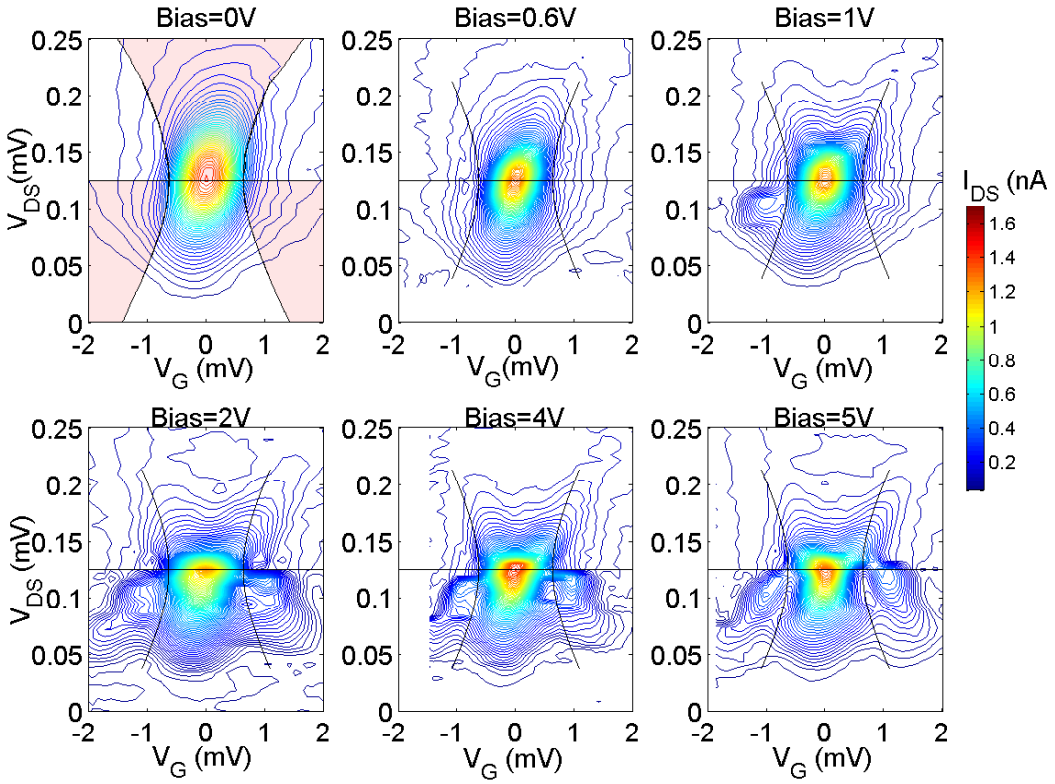

Figure 6.19: Distortion of the IV curve near DJQP resonance due to coupling to the NR

To see if these and other unexpected features in the $I - V_{DS} - V_G$ curves are in any way related to high electric fields near the NR and the SSET, we grounded the NR and applied a voltage to the NR gate to simulate the electric field generated between the NR and the SSET and measured the $I - V_{DS} - V_G$ curves of the SSET. We do not see any distortion of the $I - V_{DS} - V_G$ curves of the type seen when the NR is voltage biased. This leads us to believe that the distortion of the $I - V_{DS} - V_G$ curves is due to the motion of the resonator.

6.6 Limits of our device

One measure of the quality of a linear amplifier is how close it get to the limits placed by quantum mechanics. For continuous linear position detection, this limit is given by,

$$S_x S_F \geq \frac{\hbar}{2} \tag{6.3}$$

where

S_x is the forward coupled position noise

S_F is the backaction force noise

For a shot noise limited measurement the forward coupled noise is given by,

$$S_x = \frac{S_I}{(dI_{DS}/dx)^2} \tag{6.4}$$

where

dI_{DS}/dx is given by equation 3.12 and

$S_I = 2eI_{DS}$ is the current shot noise, in the worst case, for a bias point near

JQP [39].

Using derivative dI_{DS}/dV_G from our experimental data and $dC_{NR}/dx = 300pF/m$ from our Femlab simulations, we calculate, $dI_{DS}/dx = 12.5A/m$ at $V_{NR} = 1V$. Using these values and other known parameters we can calculate the position noise $\sqrt{S_x} = 1.4 \times 10^{-15} m/\sqrt{Hz}$ at our point of bias ($I_{DS} = 0.8nA$) and for coupling voltage $V_{NR} = 1V$.

In the low-frequency limit ($\omega_{NR} << \Gamma, E_J/\hbar$), the backaction force noise is frequency independent and is given by[30],

$$S_F(\omega_{NR}) = 2m\gamma_{SSET}k_B T_{SSET} \tag{6.5}$$

Using the experimentally obtained values of $\gamma_{SSET} = \omega_{NR}/\left(10^6 V_{NR}^2\right)$ and $T_{SSET} \sim 200mK$,we calculate $\sqrt{S_F} = 0.64 \times 10^{-18} N/\sqrt{Hz}$ at$V_{NR} = 1V$. Using these value of S_x and S_F, we find that for our device,

$$\sqrt{S_x S_F} = 15\frac{\hbar}{2}$$

On the other hand if we use the theoretical value for damping of the SSET, we get $\sqrt{S_F} = 0.2 \times 10^{-18} N/\sqrt{Hz}$ giving us,

$$\sqrt{S_x S_F} = 4\frac{\hbar}{2}$$

For our measurements, because of the limitations of the preamplifier noise floor and the reduced microwave operation of the RFSET, our charge sensitivity was $\sqrt{S_q} = 170\mu e/\sqrt{Hz}$. This gives a position noise,

$$\sqrt{S_x} \quad = \quad \sqrt{\frac{1}{2}\frac{S_q}{\left(V_{NR}\frac{dC_{NR}}{dx}\right)}} \tag{6.6}$$

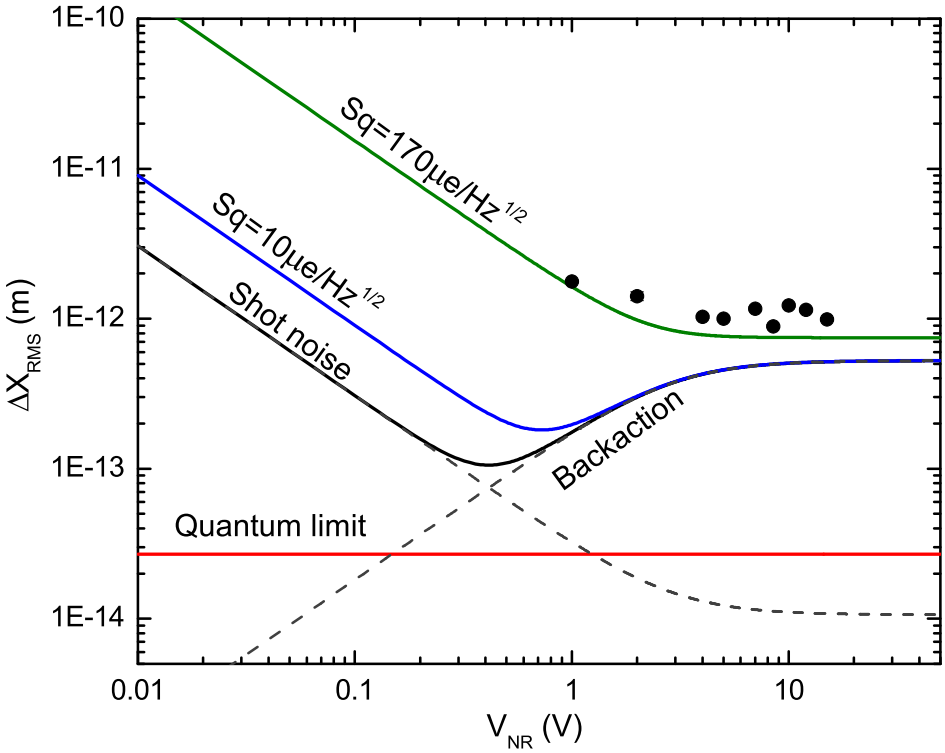

Figure 6.20: Position resolution of the device as a function of the coupling voltage

$$= \quad 64.5 \times 10^{-15} m/\sqrt{Hz}$$

Figure 6.20 shows the plot of position resolution as a function of the coupling voltage. For a shot noise limited detection scheme (black line), the coupling voltage of about 0.4V is the optimal value for position measurements. At this coupling voltage the measurement is about 3.9 times away from the quantum limit on position resolution (red line). The blue and the green line shows the position resolution of the detection scheme when the RFSET sensitivity is $10\mu e/\sqrt{Hz}$ and $170\mu e/\sqrt{Hz}$ respectively. The black solid circles are the actual data points for the measurement.

6.7 Conclusion

As part of this research, we have been able to observe the backaction effects of the SSET on a NR. For a NR with large enough quality factor, a non equilibrium device has been indeed shown to be equivalent to a thermal bath. In fact, it is possible to cool the NR by coupling it to this non-equilibrium device. We have been able to demonstrate that we can cool the NR from 500mK to about 280mK using the SSET. Also, assuming a worst case scenario for current shot noise and experimentally obtained values for backaction force, we have been able to show that our device is 15 times away from the limit $\sqrt{S_x S_F} \geq \frac{\hbar}{2}$ and 4 times away from the quantum limit on position resolution.

6.8 Future Work

To conclude this thesis we discuss the things that this work was not able to resolve and some interesting physics that this research might lead to.

In our work we observed that the damping due the SSET is much stronger than what is expected from the theoretical considerations. It would be important to pinpoint the source of this extra damping. It could be that the source of this extra damping is the same as the source of additional current seen in the SSET near JQP resonance. The enhancement of current near the JQP resonances could be due to higher order transport processes like cotunneling[41],[42],[43],[44]. In the cotunneling process, the charge carriers can tunnel across both junctions from source to drain. This transport mechanism is significant unless junction resistances

are much larger than the quantum of resistance i.e.$R_J >> R_K$.

The backaction effect of the SSET can lead to population inversion in a two level system [14]. In our case the SSET drives the resonator when it is biased at certain points. The mechanism involved in this interaction is similar to that in lasers[45][46]. It would be interesting to look for the strong backaction effects in the SSET-NR system using a detection scheme that is linear in the regime of large amplitude motion of the NR. One way to do this is using a capacitive detection scheme [47]. We have started work on this measurement and hope to see a more quantitative description of SSET-NR system when the SSET is biased in negative damping regimes.

Appendix A

Theoretical Calculations

For the calculations in the thesis we have used the following values.

Notation	Value	Comments
C_1	$181aF \pm 9aF$	Junction capacitance of junction 1
C_2	$199aF \pm 20aF$	Junction capacitance of junction 2
C_{GNR}	$10.7aF \pm 0.1aF$	Capacitance between SSET and NR gate
C_{NR}	$33.6aF \pm 1aF$	Capacitance between SSET and resonator
C_G	$22.6aF \pm 0.6aF$	Capacitance between SSET and SSET gate
C_Σ	$449aF \pm 30aF$	Total device capacitance
R_Σ	$104k\Omega \pm 2k\Omega$	Total device resistance
E_C	$175\mu V \pm 4\mu V$	Coulomb blockade energy
Δ	$192.0\mu \pm 0.7\mu V$	Superconducting energy gap
E_{J1}	$13\mu V$	Josephson energy for junction 1
Γ_{a2}	$67\mu V$	1st quasiparticle tunneling rate through junction 2
Γ_{b2}	$32\mu V$	2nd quasiparticle tunneling rate through junction 2

Notation	Value	Comments
E_{J2}	$17\mu V$	Josephson energy for junction 2
Γ_{a1}	$50\mu V$	1st quasiparticle tunneling rate through junction 1
Γ_{b1}	$24\mu V$	2nd quasiparticle tunneling rate through junction 1
R_{j1}	$59.5k\Omega$	Resistance of junction 1
R_{j2}	$44.5k\Omega$	Resistance of junction 2
$\frac{dC_{NR}}{dx}$	$300pF/m$	Derivative of the coupling capacitance
k	$10N/m$	Spring constant
ΔF	$105fN$	Coupling strength ($V_{NR} = 1V$)
ω_{NR}	$2\pi \times 21.866MHz$	Resonator intrinsic frequency at 30mK
I_{DS}	$0.8nA$	Approximate source-drain current
$\frac{dI_{DS}}{dV_G}$	$940nA/V \pm 50nA/V$	Current/gate voltage response($V_{NR} = 1V$) near bias point
$\frac{dI_{DS}}{dx}$	$12.5A/m \pm 0.5A/m$	Current/displacement response($V_{NR} = 1V$)near bias point
T_{SSET}	$200mK$	Approximate experimental value of effective temperature of SSET bath

Notation	Value	Comments
Q_{SSET}	$(10^6)/V^2$	Approximate experimental value of resonator quality factor due to damping from SSET bath
Q_{Bath}	120000 ± 8000	Intrinsic resonator quality factor ($T_{Bath} = 100mK$and $V_{NR} = 1V$)

For the calculation of the changes in parameter of the resonator as we sweep across the two junction resistances, we used the following matlab programs. The program, JQP2.m, requires two inputs. One array of values for $d0$, which is gate charge, N, and a value for the coupling voltage, V. The program outputs current through SSET, Iset, frequency shift, Df, damping of the resonator, GammaNR and temperature of the NR, TNR, as a function of the d, which is the detuning in units of electronic charge ($1e \equiv 7.09mV$). To compare with the experimental values we multiply d with 7.09 to convert it into gate voltage in mV. The program was written by Dr. Olivier Buu and was modified by me. It also has inputs from Dr. Andrew Armour and Dr. Aashish Clerk.

```
%%%MATLAB Program: JQP2%%%%%%%%%%%%%%%%%%%%%%%%%%%%%%%%%

%%%%%%%%%%%%%%%%%%%%%%%%%%%%%%%%%%%%%%%%%%%%%%%%%%%%%%%%%

%   SET backaction at JQP
```

```
%   combine results for the 2 JQP resonances
%
%%%%%%%%%%%%%%%%%%%%%%%%%%%%%%%%%%%%%%%%%%%%%%%%%%%%%%%%%%%%

Ec=175e-6;      %eV charging E
A=1.05e-13;   %N/V  coupling const
A=V*A;         %N  coupling const
k=10;          %N/m    spring const
F0=21.866e6;     %Hz     Natural frequency
Q0=1.2e5;        % natural quality factor
T0=.03;         %K fridge temperature
Vds=1-1.07e-4/Ec/4; %Bias point/4Ec

%Fund consts
hbar=6.63e-34/2/pi;
h=6.63e-34;
kb=1.38e-23;
e=1.6e-19;

%First ridge
Ej=17.4e-6;
Ga=50.4e-6/4/Ec; %% decay rate of first quasiparticle
Gb=24.12e-6/4/Ec; %% decay rate of second quasiparticle
```

```
d=d0-(Vds-1);

JQP1;%% calls function JQP1 to calculate the
%%frequency shift, damping, current and the temperature
Df1=Df;Tset1=Tset;Iset1=Iset;Gamma1=Gamma;

%Second ridge
Ej=13.0e-6;
Ga=67.4e-6/4/Ec;  %% decay rate of first quasiparticle
Gb=32.3e-6/4/Ec; %% decay rate of second quasiparticle
d=-d0+(1-Vds);

JQP1; %% calls function JQP1 to calculate the
%%frequency shift, damping, current and the temperature
Df2=Df;Tset2=Tset;Iset2=Iset;Gamma2=Gamma;

%Combined results
Iset=Iset1+Iset2;%Current through the SET
Df=Df1+Df2;%total frequency shift of the NR
GammaNR=Gamma1+Gamma2+2*pi*F0/Q0; %Damping of the NR
TNR=(1./GammaNR).
*(Gamma1.*Tset1+Gamma2.*Tset2+T0*2*pi*F0/Q0);
%temperature of NR
```

```
Ts=(Gamma1.*Tset1+Gamma2.*Tset2)./(Gamma1+Gamma2);

%%effective temperature of SET

%%%%%%%%%%%%%%%%%%%%%%%%%%%%%%%%%%%%%%%%%%%%%%%%%%%%%%%%%%



%%%%%%%MATLAB Program: JQP1%%%%%%%%%%%%%%%%%%%%%%%%%%%%%%%

%%%%%%%%%%%%%%%%%%%%%%%%%%%%%%%%%%%%%%%%%%%%%%%%%%%%%%%%%%

%   SET backacion at JQP

%   AA Clerk notes equs 28a-c See ref[29]

%

%%%%%%%%%%%%%%%%%%%%%%%%%%%%%%%%%%%%%%%%%%%%%%%%%%%%%%%%%%

r=Gb/Ga;

c1=1+4*r+8*r^2;

c2=1+4*r+4*r^2;

c3=2+1/r;


%Damping


term1=16*A^2*hbar*((F0*2*pi)^2)/(e*Ej)^2/k/r;

term2=(4*(d*4*Ec/Ej).^2+c1*(Ga*4*Ec/Ej)^2+c2)

./(4*(d*4*Ec/Ej).^2+(Ga*4*Ec/Ej)^2+c3).^3;

Gamma=14*(d/Gb)*term1.*term2; %% w/Q. Factor 14 is

%%arbitrarily introduced to match the experimental values.
```

```
Df=-((F0)/(2*(2*pi*F0)^2)/14).*Gamma.
*(4*Ec*e*Gb/hbar).*(1+2*r).
*((4*(4*Ec.*d./Ej).^2)+(4*Ec*Ga/Ej)^2+c3)
./((4*(4*Ec.*d./Ej).^2)+c1.*(4*Ec*Ga/Ej)^2+c2);


%Temperature
term5=(1+4*(d/Ga).^2)./(d/Ga)/16;
term6=4*Ec*Ga*e/kb;
Tset=term5*term6;   %K


%current
%equation 26 in Aash cond-mat
Imax=2*e*(Ej*e)^2*(4*Ec*Ga*e/hbar)
/((4*Ec*Ga*e)^2+((Ej*e)^2*(2+Ga/Gb)));
Iset=2*e*(Ej*e)^2*(4*Ec*Ga*e/hbar)
./(4.*(4*Ec.*d*e).^2+(4*Ec*Ga*e)^2+(((Ej*e)^2)*(2+Ga/Gb)));
%%%%%%%%%%%%%%%%%%%%%%%%%%%%%%%%%%%%%%%%%%%%
```

Appendix B

Femlab Calculations

We used the Femlab software to calculate the capacitance and the derivatives. For this we modeled our device as a 2-D structure with nominal thickness and widths. The program gives capacitance per unit length for 2-D structure. We obtained the capacitance value by multiplying the output by the length of the island. We made the grid size smaller than the 1/100th of the feature size. We also tried smaller grid sizes but saw less than 1% change in the capacitance values. The program yielded the following values of capacitance

Distance between NR and SET island	C_{NR}
160nm	23.12aF
150nm	24.34aF
140nm	25.65aF
130nm	27.21aF
120nm	29.19aF
110nm	31.41aF
100nm	34.12aF
90nm	37.76aF
80nm	42.59aF
70nm	49.34aF

We used these values to calculate $\frac{d}{dx}C_{NR}$ and $\frac{d^2}{dx^2}C_{NR}$. The value of the C_{NR} obtained by this simulation is pretty close to the measured capacitance of about 34aF. Also the $\frac{d^2}{dx^2}C_{NR}$ calculated from the above table gives good estimate of the shift in resonant frequency of the NR due to electrostatic softening(see section 6.2.1). This gives us confidence in the calculated value of the $\frac{d}{dx}C_{NR}$.

BIBLIOGRAPHY

[1] B. Abbott et al., "Limits on Gravitational-Wave Emission from Selected Pulsars Using LIGO Data", Phys. Rev. Lett. 94, 181103 (2005)

[2] D Rugar, R Budakian, HJ Mamin, BW Chui, "Single spin detection by magnetic resonance force microscopy", Nature 430, 329 (2004)

[3] Ekinci KL, Huang XMH, Roukes ML, "Ultrasensitive nanoelectromechanical mass detection", Appl. Phys. Lett. 84 (22): 4469-4471 MAY 31 2004

[4] Y. T. Yang, C. Callegari, X. L. Feng, K. L. Ekinci, and M. L. Roukes,"Zeptogram-Scale Nanomechanical Mass Sensing", Nano Lett., 6 (4), 583 -586, 2006.

[5] Ekinci KL, Yang YT, Roukes ML. "Ultimate limits to inertial mass sensing based upon nanoelectromechanical systems", J OF Appl. Phys 95 (5): 2682-2689 MAR 1 2004

[6] K. L. Ekinci and M. L. Roukes, "Nanoelectromechanical systems", Rev. Sci. Instrum. 76, 061101 (2005)

[7] Sergey Savel'ev, Xuedong Hu, Franco Nori. "Quantum electromechanics: Qubits from buckling nanobars", cond-mat/0412521

[8] A. N. Cleland and M. R. Geller. "Superconducting Qubit Storage and Entanglement with Nanomechanical Resonators", Phys. Rev. Lett. 93, 070501 (2004)

[9] C. P. Sun, L. F. Wei, Yu-xi Liu, Franco Nori. "Quantum transducers: Integrating Transmission Lines and Nanomechanical Resonators via Charge Qubits",quant-ph/0504056

[10] E. K. Irish and K. Schwab, "Quantum measurement of a coupled nanomechanical resonatorCooper-pair box system" Phys. Rev. B 68, 155311 (2003)

[11] Shor, "P. Polynomial-time algorithms for prime factorization and discrete logarithms on a quantum computer", SIAM J. Comput. 26, 14841509 (1997).

[12] Lov K. Grover,"Quantum Mechanics Helps in Searching for a Needle in a Haystack", Phys. Rev. Lett. 79, 325328 (1997).

[13] Lieven M.K. Vandersypen, Matthias Steffen, Gregory Breyta, Costantino S. Yannon, Richard Cleve, and Isaac L. Chuang,"Experimental realization of

order-finding with a quantum computer", Phys. Rev. Lett., Volume 85, Number 25, pages 5452-5455 (2000)

[14] A. A. Clerk, S. M. Girvin, A. K. Nguyen, and A. D. Stone,"Resonant Cooper-Pair Tunneling: Quantum Noise and Measurement Characteristics", Phys. Rev. Lett. 89, 176804 (2002)

[15] M. D. LaHaye, O. Buu, B. Camarota and K. C. Schwab, "Approaching the Quantum Limit of a Nanomechanical Resonator ", Science, Vol 304, Issue 5667, 74-77 , 2 April 2004.

[16] Averin, D. V. and Likharev, K. K., "Coulomb blockade of tunneling and coherent oscillations in small tunnel junctions", J. Low Temp. Phys. 62, 345-372 (1986)

[17] Carlton M. Caves, Kip S. Thorne, Ronald W. P. Drever, Vernon D. Sandberg, and Mark Zimmermann ,"On the measurement of a weak classical force coupled to a quantum-mechanical oscillator. I. Issues of principle",Rev. Mod. Phys. 52, 341392 (1980).

[18] R.J. Schoelkopf, P. Wahlgren,A.A. Kozhevnikov, P. Delsing, and D.E. Prober,"The Radio-Frequency Single-Electron Transistor (RF-SET):A Fast and Ultrasensitive Electrometer", Science,Vol.280, p. 1238 (May 22, 1998)

[19] R. G. Knobel and A. N. Cleland,"Nanometre-scale displacement sensing using a single electron transistor",Nature 424, 291-293 (17 July 2003)

[20] D. Mozyrsky and I. Martin, "Quantum-Classical Transition Induced by Electrical Measurement" ,Phys. Rev. Lett. 89, 018301 (2002)

[21] D. Mozyrsky, I. Martin, and M. B. Hastings,"Quantum-Limited Sensitivity of Single-Electron-Transistor-Based Displacement Detectors", Phys. Rev. Lett. 92, 018303 (2004)

[22] A.D. Armour, M. P. Blencowe, Y. Zhang,"Classical dynamics of a nanomechanical resonator coupled to a single-electron transistor", Phys. Rev. B 69, 125313 (2004).

[23] T. A. Fulton and G. J. Dolan, "Observation of single-electron charging effects in small tunnel junctions", Phys. Rev. Lett. 59, 109112 (1987)

[24] R. C. Zeller and R. O. Pohl, "Thermal Conductivity and Specific Heat of Noncrystalline Solids", Phys. Rev. B 4, 20292041 (1971)

[25] J. F. Berret and M. Meissner, "How universal are the low temperature acoustic properties of glasses?", Zeitschrift fr Physik B Condensed Matter, 1988.

[26] K. A. Topp and D. G. Cahill, "Elastic properties of several amorphous solids and disordered crystals below 100 K", Z. Phys. B 101, 235 (1996)

[27] Xiao Liu, B. E. White, Jr., R. O. Pohl, E. Iwanizcko, K. M. Jones, A. H. Mahan, B. N. Nelson, R. S. Crandall S. VeprekAmorphous, "Solid without Low Energy Excitations", Phys. Rev. Lett. 78, 44184421 (1997)

[28] W. A. Phillips, "Tunneling states in amorphous solids", J. Low Temp. Phys. 7, 351 (1972).

[29] A. A. Clerk, S. Bennett, "Quantum nano-electromechanics with electrons, quasiparticles and Cooper pairs: effective bath descriptions and strong feedback effects", New J. Phys. 7, 238, 2005

[30] A.A. Clerk, "Quantum-limited position detection and amplification: A linear response perspective", Phys. Rev. B 70, 245306 (2004)

[31] A. N. Cleland and M. L. Roukes, "Noise processes in nanomechanical resonators", J. Appl. Phys. 92, 2758 (2002)

[32] Rusko Ruskov, Keith Schwab,and Alexander N. Korotkov, "Squeezing of a nanomechanical resonator by quantum nondemolition measurement and feedback" Phys. Rev. B 71, 235407 (2005)

[33] M P Blencowe, J Imbers and A D Armour, "Dynamics of a nanomechanical resonator coupled to a superconducting single-electron transistor", New J. Phys. 7 (2005) 236.

[34] Mathew LaHaye, "Radio Frequency Single Electron Transistor Displacement Detector", Ph.D. Dissertation, University of Maryland, 2005.

[35] P. Joyez, "The single Cooper pair transistor: a macroscopic quantum device", Ph.D. Thesis, Universit Paris 6, 1995.

[36] P. Wahlgren, "The radio-frequency single electron transistor and the horizon picture for tunnelling", Ph.D. dissertation, Chalmers University of Technology, Goteborg University, 1998.

[37] A.N.Cleland,M.L.Roukes,"External control of dissipation in a nanometer-scale radio frequency mechanical resonator" Sensors and Actuators,72(1999), 256-261.

[38] A. Aassime, D. Gunnarsson, K. Bladh, P. Delsing and R. Schoelkopf, "Radio-frequency single-electron transistor: Toward the shot-noise limit", App. Phys.s Lett., 79 (2001), Issue 24, pp. 4031-4033.

[39] M-S Choi, F. Plastina and R. Fazio,"Charge and current fluctuations in a superconducting single-electron transistor near a Cooper pair resonance", Phys. Rev. B 67, 045105 (2003).

[40] S. Pohlen, "The Superconducting Single Electron Transistor". Ph.D. Thesis, Harvard University, December 1999

[41] D. V. Averin and Yu. V. Nazarov,"Virtual electron diffusion during quantum tunneling of the electric charge", Phys. Rev. Lett. 65, 2446 (1990).

[42] L. J. Geerligs, D. V. Averin, and J. E. Mooij, "Observation of macroscopic quantum tunneling through the Coulomb energy barrier", Phys. Rev. Lett. 65, 3037 (1990).

[43] H. Schoeller and G. Schn,"Mesoscopic quantum transport: Resonant tunneling in the presence of a strong Coulomb interaction", Phys. Rev. B 50, 18 436 (1994).

[44] J. Knig, H. Schoeller, and G. Schn,"Resonant tunneling and Coulomb oscillations", Europhys. Lett. 31, 31 (1995).

[45] D.A. Rodrigues, J. Imbers, A.D. Armour, "Quantum dynamics of a resonator driven by a superconducting single-electron transistor: a solid-state analogue of the micromaser", cond-mat/0608166.

[46] Private communication with A.A.Clerk.

[47] P. A. Truitt, J. Hertzberg, C.C. Huang , K. Ekinci, K. C. Schwab, "Efficient and Sensitive Capacitive Detection of Nanomechanical Resonator Arrays", Submitted to Nano letters.